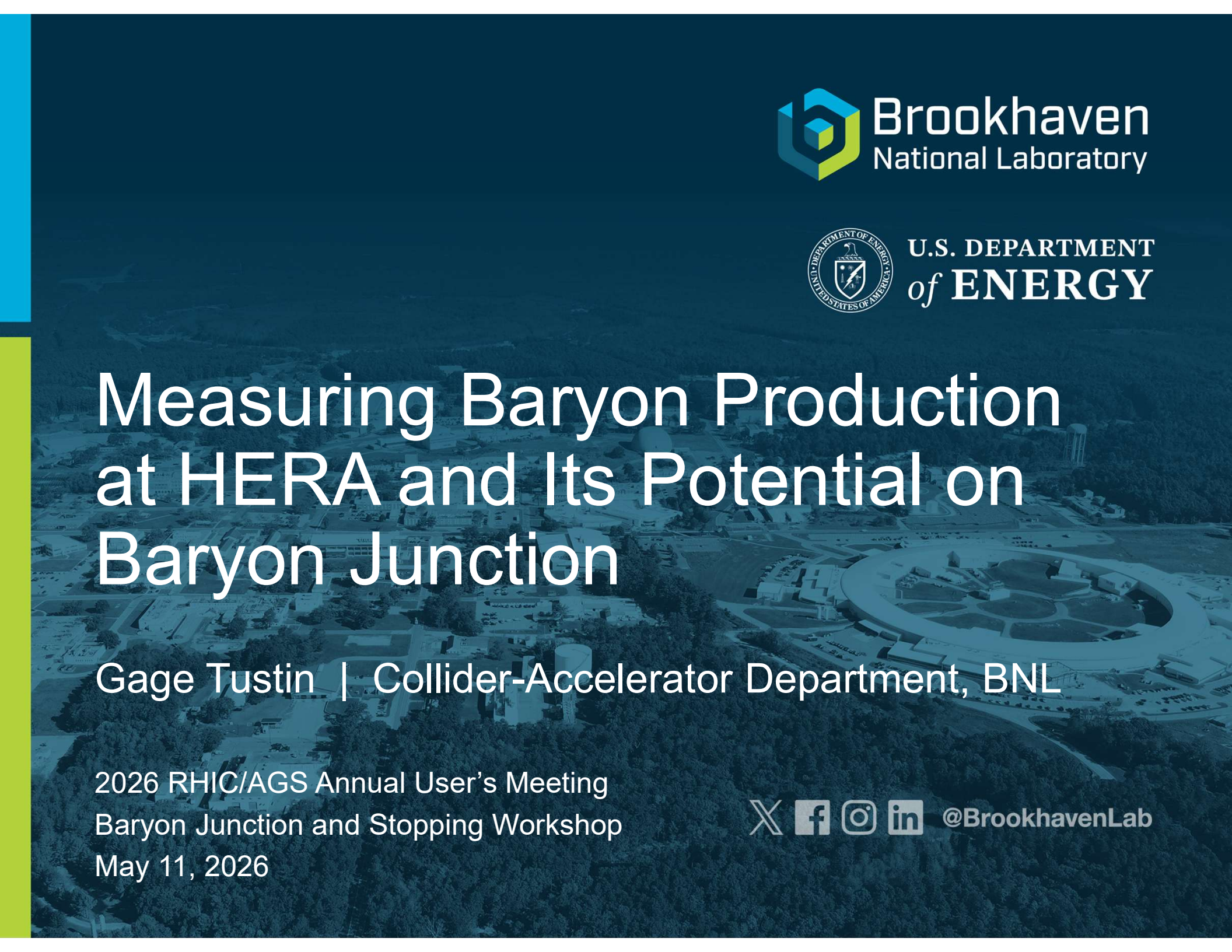

Brookhaven National Laboratory

U.S. DEPARTMENT of ENERGY

Measuring Baryon Production at HERA and Its Potential on Baryon Junction

Gage Tustin | Collider-Accelerator Department, BNL

2026 RHIC/AGS Annual User's Meeting
Baryon Junction and Stopping Workshop
May 11, 2026

@BrookhavenLab

Talk Outline

- Baryon Junction Motivation
- HERA Overview
- DIS Kinematics
- Baryon Production at HERA and Existing Results
- H1 Experiment at HERA
- Results of Current Ongoing Analysis (Not H1 Official Result Yet) Measuring Λ - $\overline{\Lambda}$ Baryon Asymmetry
- Conclusion

Brookhaven National Laboratory

Baryon Junction Motivation

- Baryon number is an empirically observed symmetry of nature, but how it is carried and transported is not well understood

Quark Model: Traditionally, baryon number is assigned to valence quarks carrying 1/3 of the baryon number (-1/3 for anti-quarks)

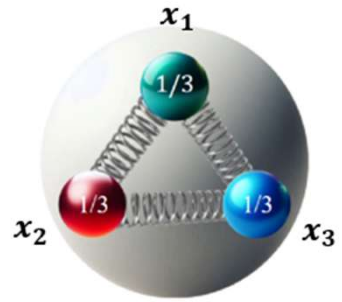

$$B(x_1, x_2, x_3) = \epsilon^{ijk} q(x_1)_i \; q(x_2)_j q(x_3)_k$$

Gluon/Baryon Junction Model: Y-shaped configuration of gluons connecting valence quarks carries baryon number, was proposed in the 1970's as a way of constructing a gauge invariant baryon state [1]

Local
Gauge Invariance

$$P(x_n, x) \equiv \mathcal{P} \exp\left(ig \int_{x_n}^{x} A_\mu dx^\mu\right)$$

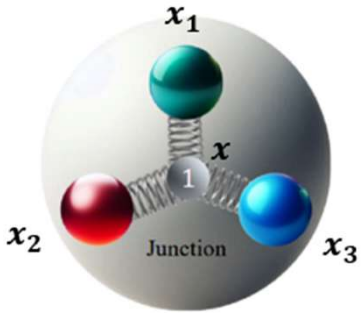

$$B(x_1, x_2, x_3, x) = \epsilon^{ijk} \; [P(x_1, x) \; q(x_1)]_i \; [P(x_2, x) \; q(x_2)]_j \; [P(x_3, x) \; q(x_3)]_k$$

Baryon Junction Motivation

- In relativistic heavy ion collisions baryon asymmetries have been observed at mid-rapidity (central region perpendicular to the collision axis), appears to be inconsistent with a pure valence quark model:
  - Au+Au colliding system here has net positive baryon number which should be reflected in final state as baryon number is conserved
  - Valence quarks carry a large momentum fraction of colliding partons and then require significant energy transfer to transport baryon number to mid-rapidity. Furthermore, at high energies valence quarks have less time to interact due to longitudinal length contractions
  - **Gluon junctions carry a much lower momentum fraction of colliding partons and can help explain these observations if they transport baryon number to the final state**

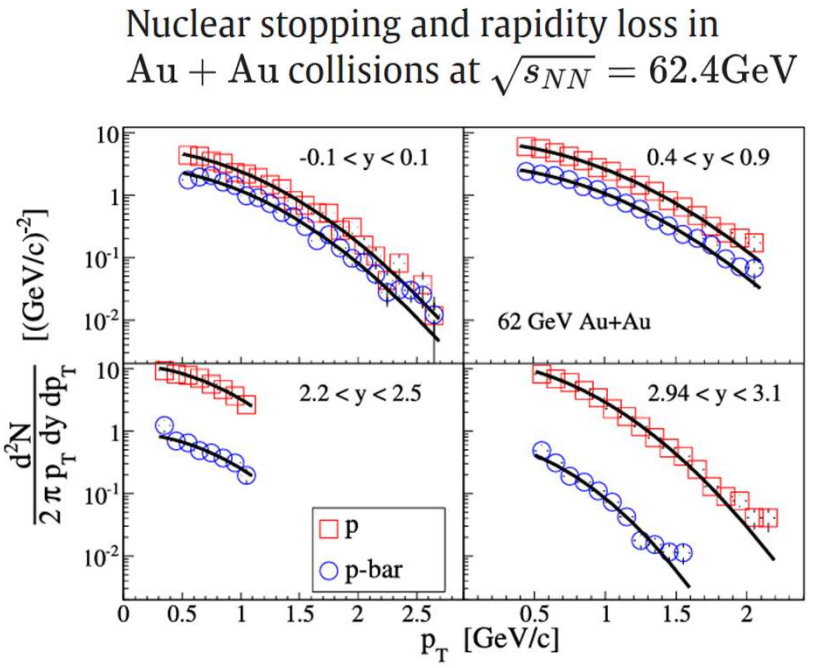

BRAHMS Result Published in 2009:
https://doi.org/10.1016/j.physletb.2009.05.049

$$m \ll |\mathbf{p}| \Rightarrow E \approx |\mathbf{p}| \Rightarrow \eta \approx y$$

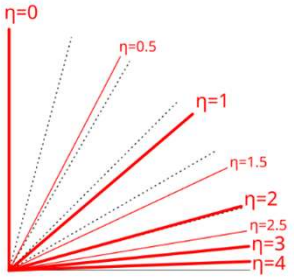

$$\eta \equiv -\ln\left[\tan\left(\frac{\theta}{2}\right)\right]$$

Baryon Junction Motivation

- Some interesting methods have been recently proposed by STAR studying charge vs baryon stopping in heavy ion collisions to search for baryon junction evidence [2]
- Looking forward to EIC, we should also be able to look for baryon junction signatures in electron-ion collisions [3]
- **Deep-inelastic *ep* scattering, as studied at HERA, can also be used to look for junctions [4,5]**

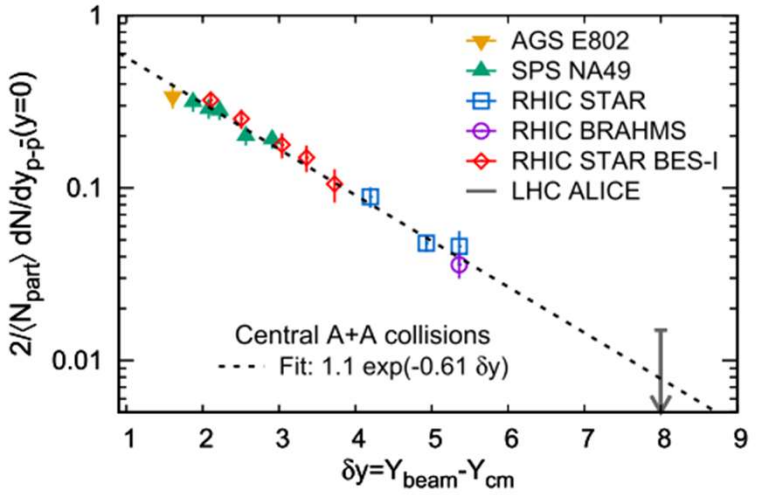

https://doi.org/10.1140/epjc/s10052-024-12834-2

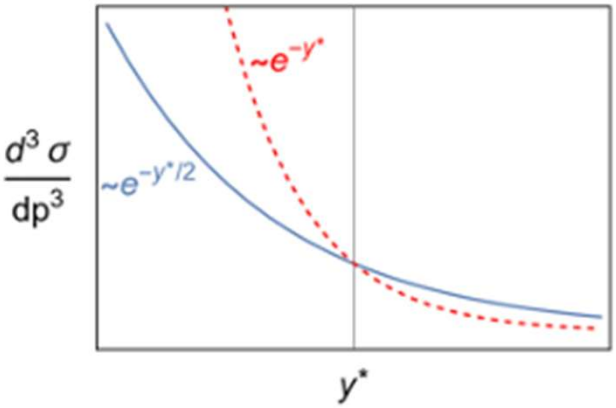

https://doi.org/10.1016/j.physletb.2024.138680

Baryon Junction Motivation

- Testing gluonic junctions in *ep* scattering initially seems tricky due to the electron coupling to charged quark constituents rather than directly to the gluons
- Basic idea is that the quark-antiquark component of the virtual photon in the *ep* scattering can interact with the proposed gluon junction and pull it into the hadronic final state to transfer baryon number
- At high energies, the purely gluonic exchange (therefore uncorrelated in proton flavor when valence quarks do not participate) is expected to dominate due to the higher Regge intercept [4]

Signatures of baryon junctions in semi-inclusive deep inelastic scattering

David Frenklakh [a b], Dmitri E. Kharzeev [a b c], Wenliang Li [b]

https://doi.org/10.1016/j.physletb.2024.138680

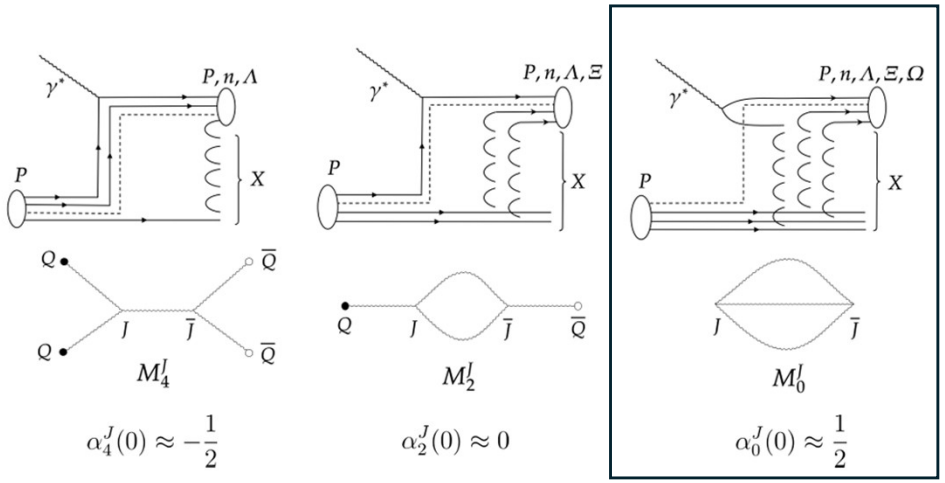

Purely gluonic exchange

Baryon Junction Motivation

- **David Frenklakh and Dmitri Kharzeev gave us a quick calculation based on their gluon junction framework in this publication and estimate a baryon asymmetry in DIS of 0.03±0.02 within the accessible kinematic range at HERA**
  - Based on a 3→3 Forward scattering in Regge Theory framework
  - Regge intercept for purely gluonic junction exchange cannot be calculated from first principles, but they estimated it from the Au-Au RHIC Beam Energy Scan data, hence the large uncertainty
- Not a precise estimate but gives us a ballpark expectation

Signatures of baryon junctions in semi-inclusive deep inelastic scattering

David Frenklakh [a b], Dmitri E. Kharzeev [a b c], Wenliang Li [b]

https://doi.org/10.1016/j.physletb.2024.138680

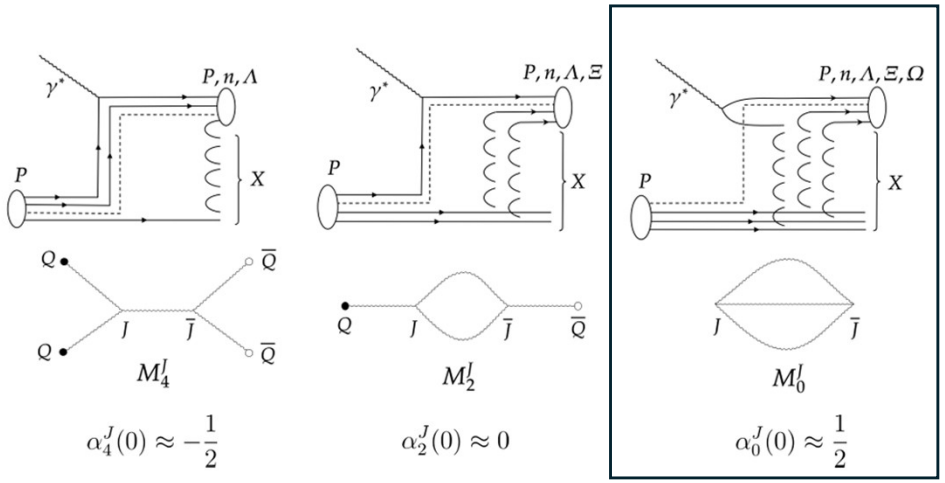

Purely gluonic exchange

HERA

- The only high energy *ep* collider accelerator ever operated
- Ran from 1992-2007 at DESY in Hamburg, Germany with nominal electron/positron energy of 27.6 GeV and proton energy of 920GeV ($\sqrt{s}$ = 319 GeV)
- Serviced four experiments
  - Hermes: Fixed target with electron beam
  - HERA-B: Fixed target with proton beam
  - ZEUS: General purpose hermetic detector
  - H1: General purpose hermetic detector
- **Delivered ~1fb^{-1} of total integrated luminosity to H1/ZEUS, perfect starting point to get a head start on what baryon junction signatures in EIC may look like**

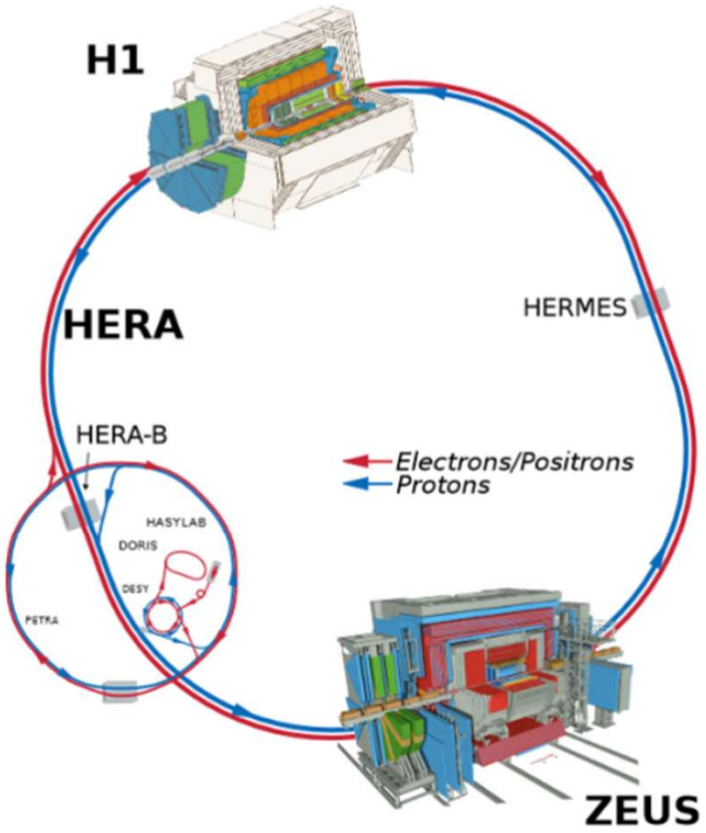

Hadron-Electron Ring Accelerator (HERA) complex, figure from [1]

Neutral Current Deep-Inelastic Scattering at HERA

- Kinematics of *ep* collisions can be completely described by four Lorentz scalars: Q^2, x, y, s
  - All can be written in terms of highlighted four momentums on the right
- Q^2 is the negative four momentum of the virtual photon squared (negative sign convention to keep quantity positive)
- x (also known as Bjorken- x) is the fractional momentum of the struck quark with respect to the proton's momentum
- **y is the inelasticity (not to be confused with y as rapidity which is standard in heavy ion physics)**, can be interpreted as the fractional energy lost by the electron in the scattering
- s is the center-of-mass energy of the colliding system squared
- W is the invariant mass of the hadronic final state (HFS) denoted X

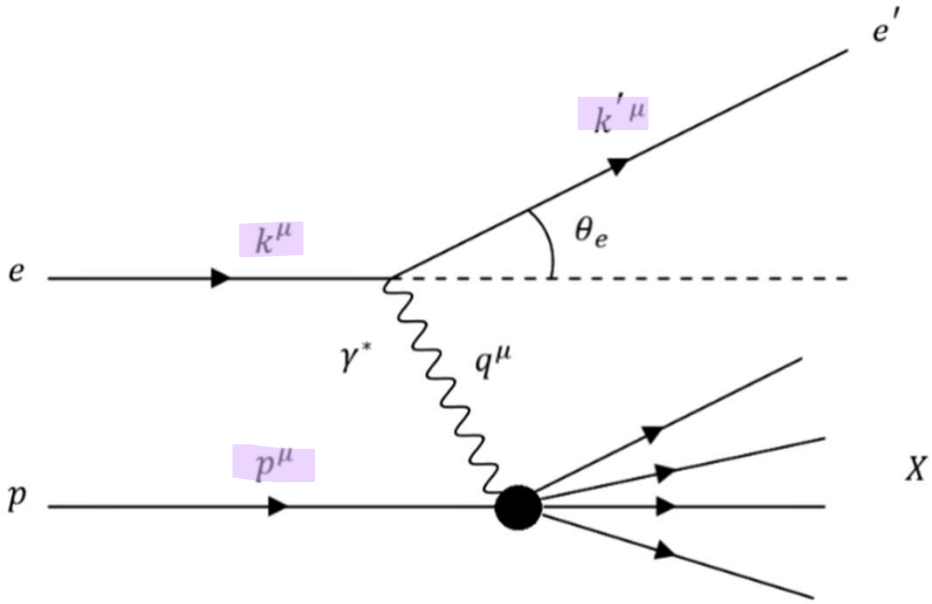

$$Q^2 \equiv -q^\mu q_\mu = -q^2 \qquad Q^2 = 4E_e E_e' \cos^2(\frac{\theta_e}{2})$$

$$y \equiv \frac{p^\mu q_\mu}{p^\nu k_\nu} \qquad y = 1 - \frac{E_e'}{E_e}\sin^2(\frac{\theta_e}{2})$$

$$x \equiv \frac{Q^2}{2p^\mu q_\mu} \qquad x = \frac{Q^2}{ys} = \frac{Q^2}{Q^2 + W^2 - m_p^2}$$

$$\boxed{Q^2 = xys}$$

$$W \equiv \sqrt{(q^\mu + p^\mu)^2} = \sqrt{ys - Q^2 + m_p^2}$$

Baryon Junction Search at HERA

- In DIS *ep* scattering you have one species providing baryon number, asymmetric colliding system → No forward/backward ambiguity
- Reduced complexity of observables and variables compared to ion-ion system
- Hermetic detectors (H1 and ZEUS) with large acceptance, tracking well understood within $|\eta| < 1.3$
- **Baryon production can be analyzed cleanly via Λ production**
  - For Λ, $c\tau \sim 7.8$ cm, so Λ produced at the primary DIS vertex can be observed at a resolvable secondary decay vertex, background greatly reduced by rejecting track primary vertex fitted tracks

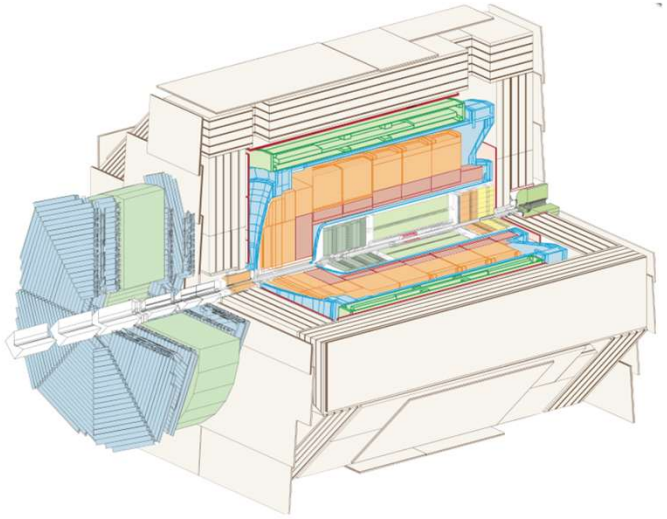

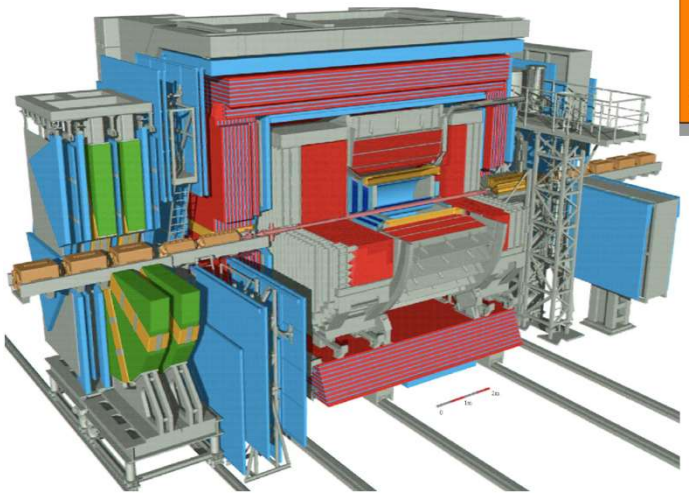

Existing Measurements

Strangeness Production at low Q^2 in Deep-Inelastic ep Scattering at HERA

https://doi.org/10.1140/epjc/s10052-009-0995-1

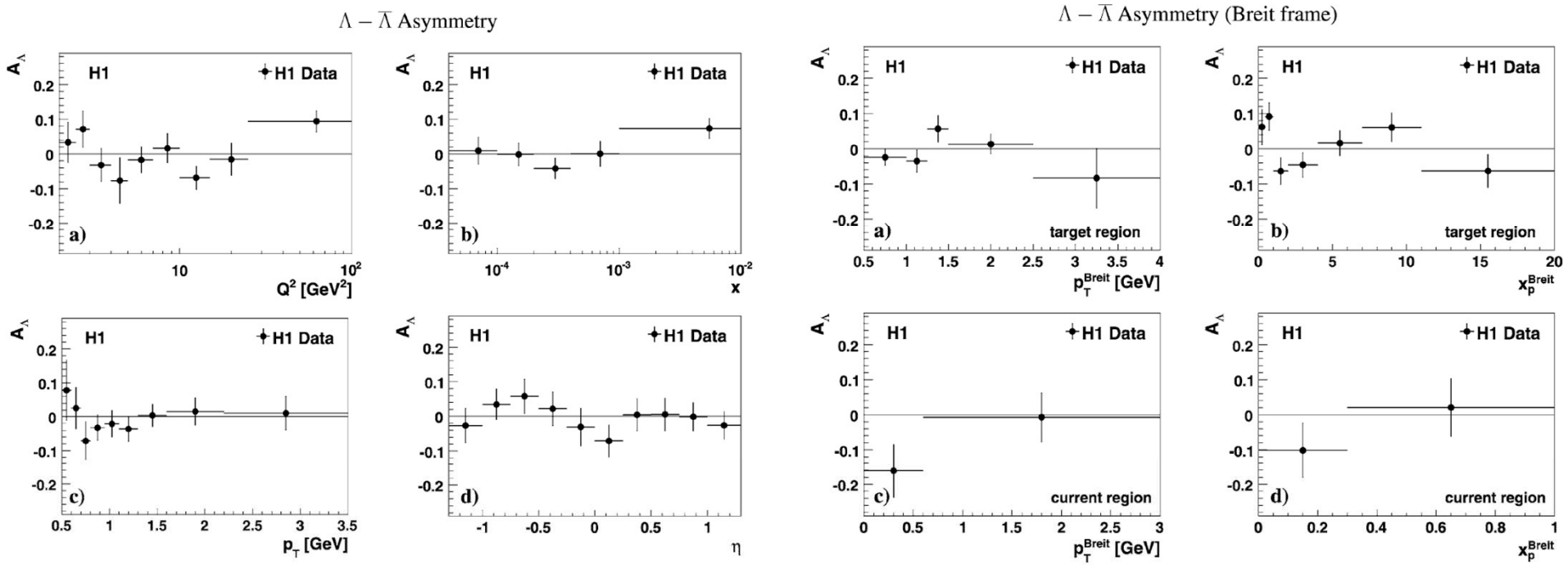

$$2 < Q^2[GeV^2] < 100, \quad 0.1 < y < 0.6$$
$$0.5 < p_T[GeV] < 3.5, \quad |\eta| < 1.3$$

- Consistent with zero, but high statistical uncertainty, ~ $\pm 10\%$
- **Not enough data to rule out an asymmetry on the order of a few percent**

HERA Running Summary

- Previous asymmetry measurement only uses 1999-2000 data
- HERA luminosity upgrade in 2000 → different scheme of beam separation and focusing within the detector material
- Introduced many background issues with freshly installed components from proton-gas interactions, largely sorted out by 2005 with higher CJC gains and improved charged particle track reconstruction, **~6x more data available in the 2005-2007 ($\sqrt{s}$ = 319 GeV) data set**

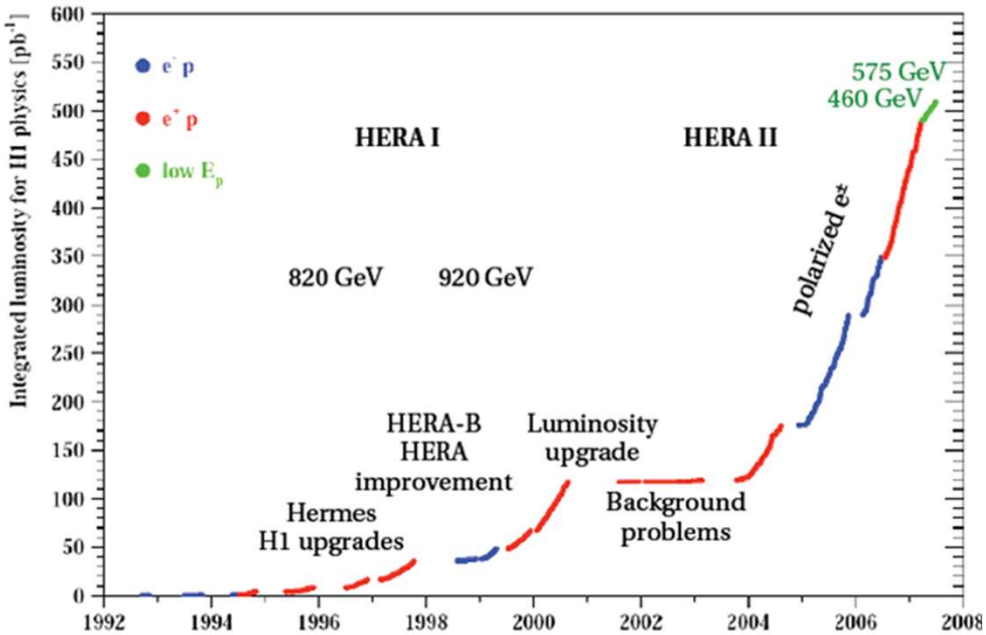

H1 Experiment and DPHEP

- **H1 leading efforts within DPHEP (Data Preservation in High Energy Physics) collaboration beginning in 2009, have updated full analysis software to retain full potential of experimental data (Level 4)**
  - Preserved full software stack and raw hit level data
- ZEUS between level 3 and 4, similar available statistics as H1
  - HERMES data still accessible but less advanced than H1 and ZEUS, HERA-B not accessible

Table 1. Data preservation levels defined by the DPHEP study group

Level	Preservation Model	Use Case
1	Provide additional documentation	Publication related info search
2	Preserve the data in a simplified format	Outreach, simple training analyses
3	Preserve the analysis level software and data format	Full scientific analyses, based on the existing reconstruction
4	Preserve the simulation and reconstruction software as well as basic level data	Retain the full potential of the experimental data

https://doi.org/10.48550/arXiv.1205.4667

H1 Analysis in Progress – Our Team

Axel Drees

Professor – Stony Brook

Henry Klest

Assistant Physicist – ANL

Gage Tustin

Operations Coordinator - BNL

H1 Analysis in Progress

- **All results shown here are not yet official H1 Results**
- H1 referees have been assigned for reviewing the analysis, studies for improving systematic uncertainties are in progress
- This work was used to complete my MA degree at Stony Brook and what is presented is the state of the analysis as of finishing my degree last December and is documented in my thesis

H1 Experiment at HERA

- Focus on calorimetry and tracking
- PID from dE/dx in tracking detectors
- Tracking System:
  - Two central drift chambers (CJC1 and CJC2) for charged particle trajectories
  - Central Silicon Tracker (CST) – silicon tracking for resolving interaction vertices just outside beam pipe
  - Good resolution for charged particle tracks with $p_T > 0.12$ GeV

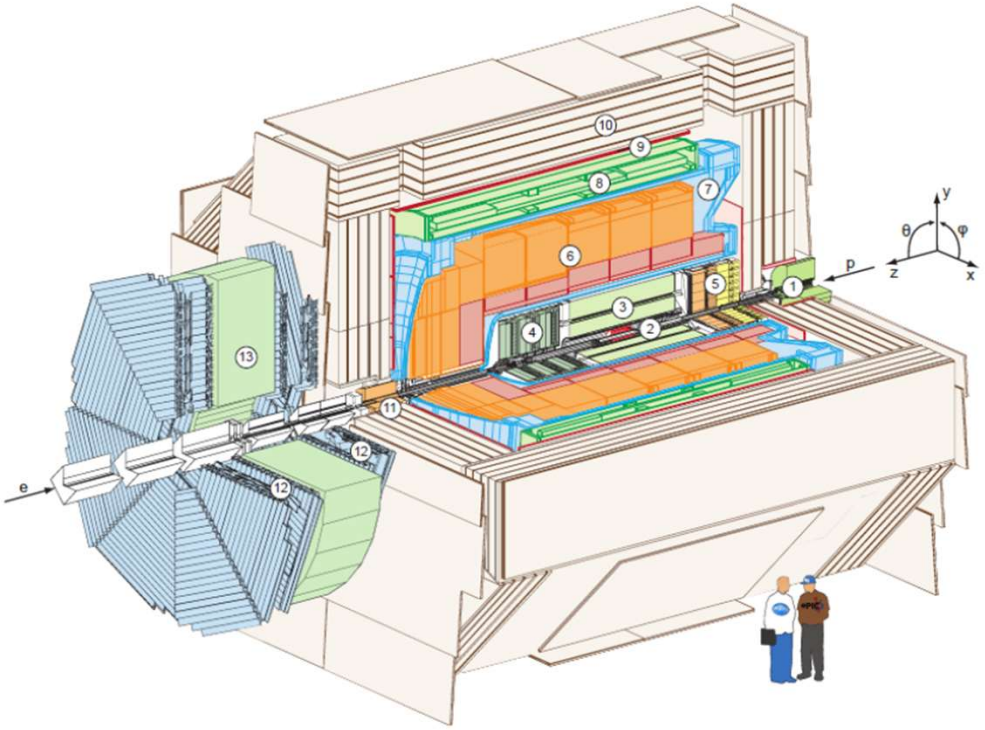

1. Beam pipe and beam magnets
2. Silicon tracking detector
3. Central tracking detector
4. Forward tracking detector
5. Spacal calorimeter (em and had)
6. Liquid Argon calorimeter (em and had)
7. Liquid Argon cryostat
8. Superconductiong coil
9. Muon chambers
10. Instrumented iron (streamer tube detectors)
11. Plug calorimeter
12. Forward muon detector
13. Muon toroid magnet

H1 Experiment at HERA

- SpaCal – calorimeter in backward direction for precise detection of scattered electron in lower Q^2 events ($5 < Q^2\ [\mathrm{GeV}^2] < 120$), consisting of long, thin scintillating fibers for precise position and energy measurement
  - Most statistics for baryon production exist in low Q^2 event range, limiting factor in how low we go based on SpaCal, new magnets for Luminosity upgrade required removal of inner SpaCal sections which causes issues trying to look at events with $Q^2 < 5\ \mathrm{GeV}^2$

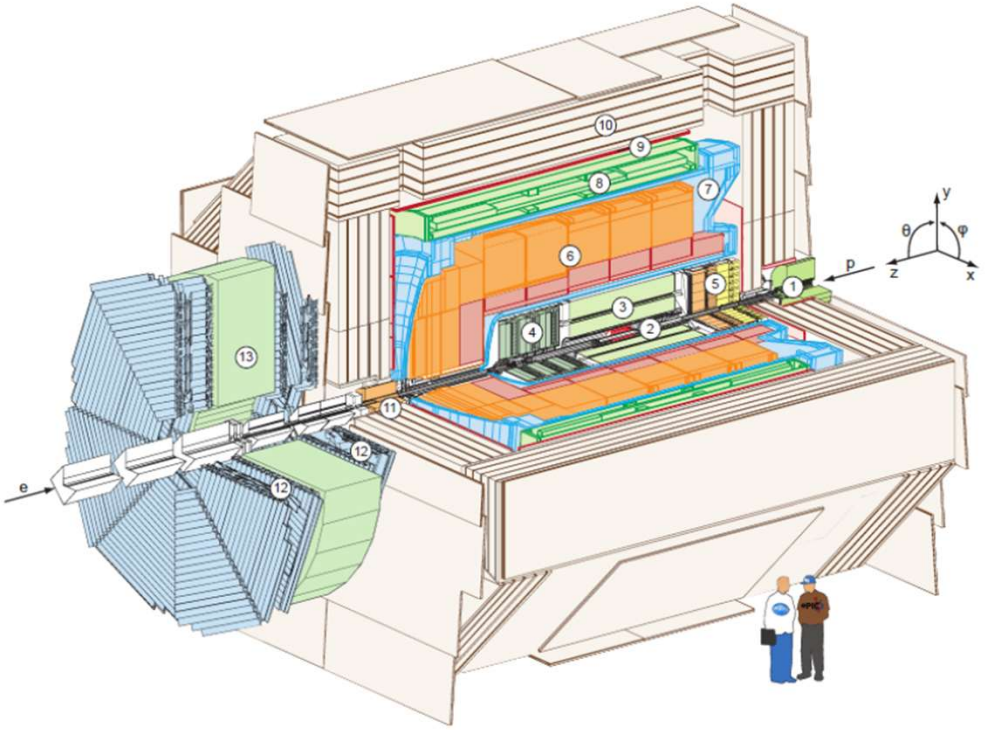

1. Beam pipe and beam magnets
2. Silicon tracking detector
3. Central tracking detector
4. Forward tracking detector
5. Spacal calorimeter (em and had)
6. Liquid Argon calorimeter (em and had)
7. Liquid Argon cryostat
8. Superconductiong coil
9. Muon chambers
10. Instrumented iron (streamer tube detectors)
11. Plug calorimeter
12. Forward muon detector
13. Muon toroid magnet

DIS Event Selections

$5 < Q^2\ [\mathrm{GeV}^2] < 100$

$0.1 < y < 0.6$

- $-30 < z_{VTX}\ [\mathrm{cm}] < 30$
- $35 < (E - p_z)\ [\mathrm{GeV}] < 70$
  - Reject events with missing FS particles, missing electron, detector issues
- s61 > 0 *Trigger that requires a track in the detector volume with a transverse momentum above some threshold (a Hadronic Final State), and a SpaCal energy deposit above some threshold (the DIS scattered electron)
  - p_T > 900 MeV
  - SpaCal energy deposit > 9 GeV
- SpaCal energy deposit > 11 GeV
- Scattered Electron Cluster Radius in SpaCal (Ecra) < 3.5cm

Λ Particle Selections

Λ BARYONS
($S = -1$, $I = 0$)
$\Lambda^0 = uds$

$$\Lambda \to p\pi^- \quad (63.90 \pm 0.5)\%$$

$c\tau = 7.845$ cm

Rough initial selections listed here, looking for secondary decay vertices separate from primary DIS vertex that is reconstructed from two oppositely charged tracks. The basic idea is **combinatorial background is reduced with PID and ensuring the secondary vertex is well separated from the primary.** Specifically, we require:

- p_T (p) >= 0.2 GeV
- p_T (π) >= 0.1 GeV (We strengthen this cut later)
- Track Length (π) >= 10 cm
- $p_{T,rel}$ (daughters w.r.t. Λ) < 0.15 GeV
- χ^2(fit of daughter tracks to secondary vertex) < 5
- Radial Distance of Secondary vertex from primary >= 1.5 cm

HERA II 2005-2007 e^+p/ e^-p $\Lambda + \bar{\Lambda}$ Cut Evolution

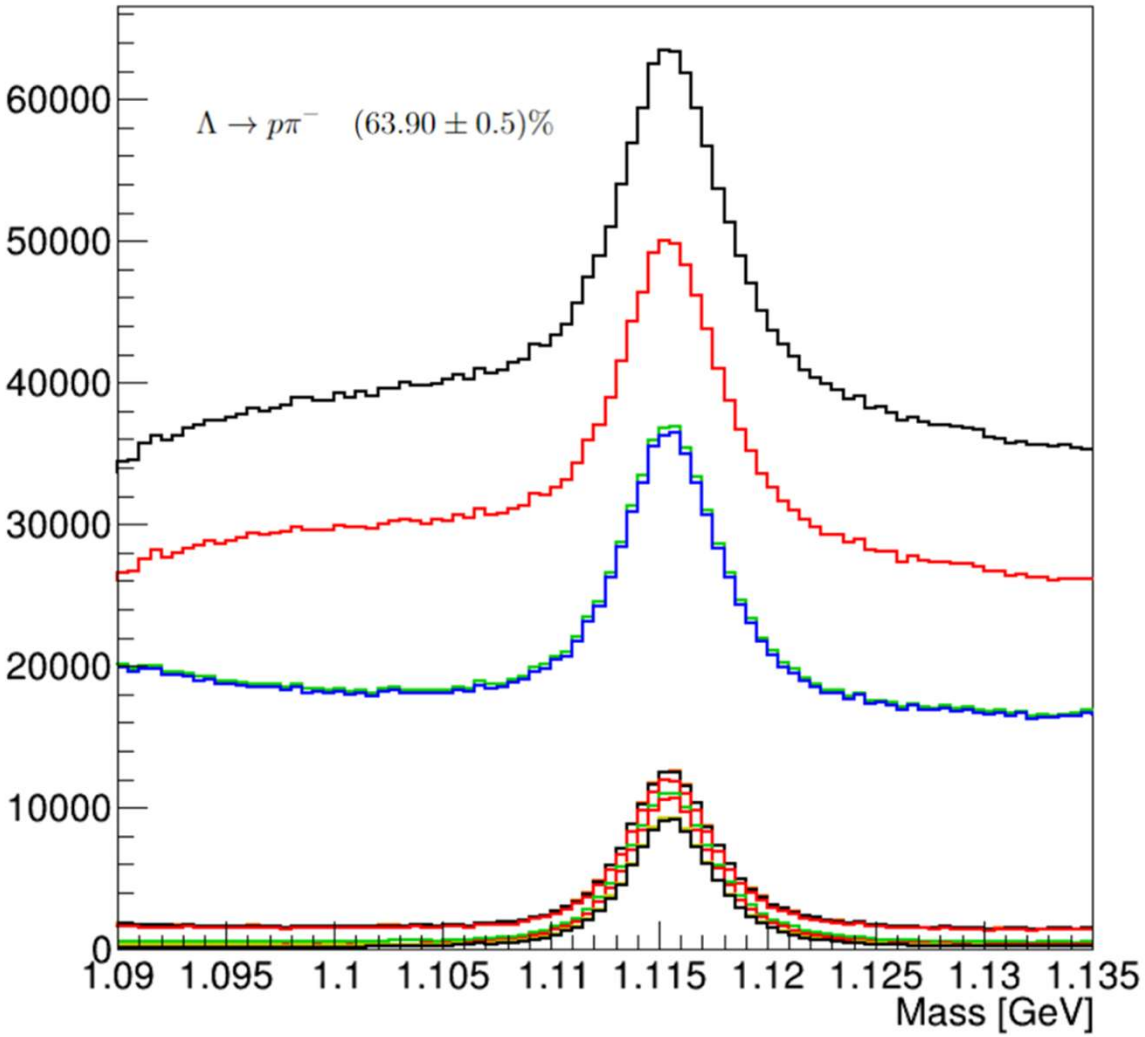

Cut 0 – Black: Starting point after selections on previous slide

Cut 1- Red: |η(Λ)| < 1.3

Cut 2- Green: 0.5 < p_T(Λ)[GeV] < 3.5

Cut 3- Blue: Track Start Radius < 35cm

Cut 4- Orange: Reject Primary Vertex Fitted Tracks

Cut 5- Black: Rejecting Tracks with Multiple Secondary Vertex Hypotheses (Keep Candidate with best Chi2 vertex fit)

Cut 6- Red: p_T (π) > 0.12 GeV

Cut 7- Green: $L_{\frac{dE}{dx}}(\mathrm{p}) > 0.001$

Cut 8- Blue: $L_{\frac{dE}{dx}}(\pi) > 0.001$

Cut 9- Magenta: $|S_{dca}$ (p)| > 0.2

Cut 10- Red: $|S_{dca}$ (π)| > 0.2

$$S_{dca} = \frac{d_{ca}}{\delta d_{ca}}$$

Cut 11- Yellow: M(π+π) < 0.465 GeV ||
M(π+π) > 0.530 GeV

Cut 12- Black: M(e^++ e^-) > 0.05 GeV

Peak Extractions

Composite PDF 1: Two body phase space shape

$$\underbrace{\frac{\Gamma(\frac{\nu+1}{2})}{\sqrt{\pi\nu}\Gamma\frac{\nu}{2}}(1+\frac{(\frac{m_\Lambda-\mu}{\sigma})^2}{\nu})^{-\frac{\nu+1}{2}}}_{\text{T-Distribution}} + \underbrace{(m_\Lambda - m_\pi - m_p)^{a_0} e^{(a_1(m_\Lambda - m_\pi - m_p))}}_{\text{BG PDF 1}}$$

Composite PDF 2: 4th order Polynomial, used for systematic uncertainty in the BG shape

$$\underbrace{\frac{\Gamma(\frac{\nu+1}{2})}{\sqrt{\pi\nu}\Gamma\frac{\nu}{2}}(1+\frac{(\frac{m_\Lambda-\mu}{\sigma})^2}{\nu})^{-\frac{\nu+1}{2}}}_{\text{T-Distribution}} + \underbrace{[b_0 + b_1 m_\Lambda + b_2 m_\Lambda^2 + b_3 m_\Lambda^3 + b_4 m_\Lambda^4]}_{\text{BG PDF 2}}$$

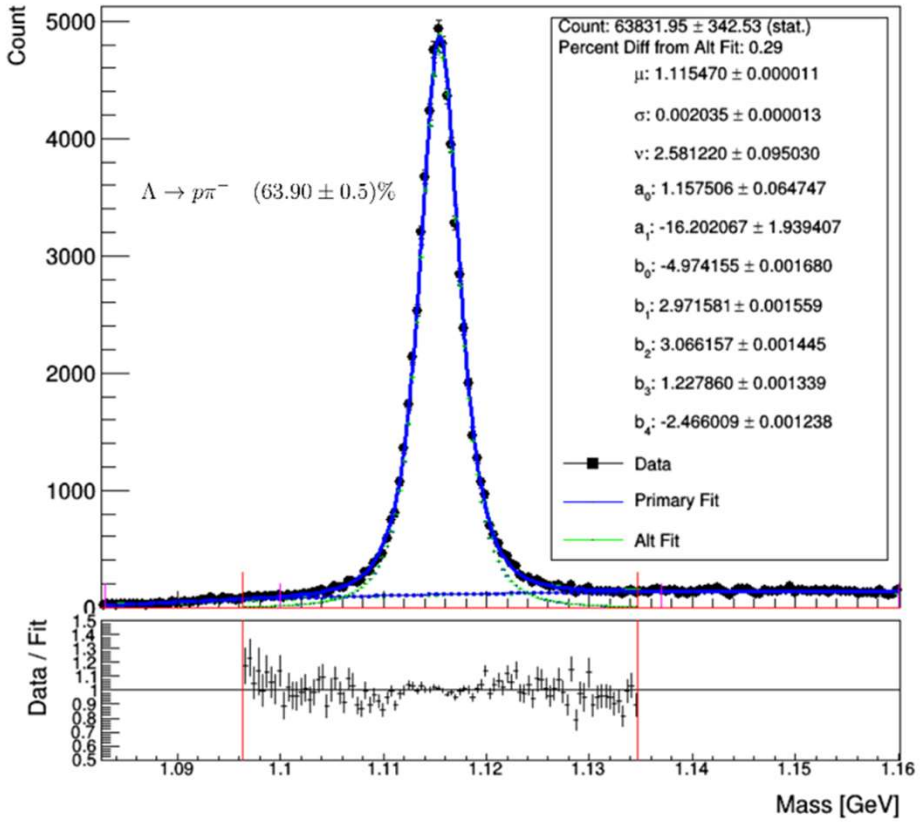

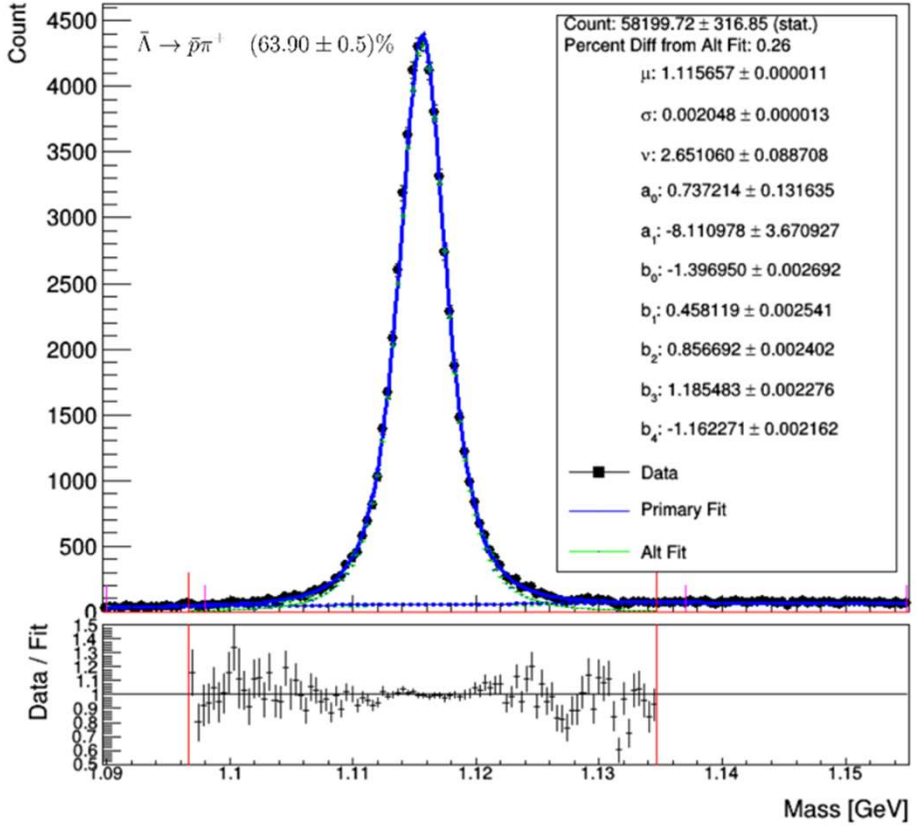

Cross Section Definitions

- Full normalized count of V^0 (particles identified in secondary decay vertex) defined in terms of this cross section within the detector's visible range:

$$5 < Q^2[\mathrm{GeV}^2] < 100 \qquad 0.1 < y < 0.6$$
$$0.5 < p_T(V^0)[\mathrm{GeV}] < 3.5 \qquad -1.3 < \eta(V^0) < 1.3$$

$$\sigma_{vis}(ep \to e'V^0X) = \frac{N}{\mathcal{L} \cdot \epsilon \cdot BR \cdot (1 + \delta_{QED})}$$

$$\epsilon = \epsilon_{rec} \cdot \epsilon_{trig} \qquad \epsilon_{rec} = \frac{N_{rec}^{MC}}{N_{gen}^{MC}} \qquad 1 + \delta_{QED} = \frac{N_{gen}(V^0)^{rad}}{N_{gen}(V^0)^{non-rad}} \cdot \frac{\mathcal{L}^{non-rad}}{\mathcal{L}^{rad}}$$

- Λ - $\bar{\Lambda}$ Asymmetry defined as this ratio of cross sections, many factors cancel out

$$A_\Lambda = \frac{\sigma_{vis}(ep \to e'\Lambda X) - \sigma_{vis}(ep \to e'\bar{\Lambda}X)}{\sigma_{vis}(ep \to e'\Lambda X) + \sigma_{vis}(ep \to e'\bar{\Lambda}X)} = \frac{\frac{N_\Lambda}{\epsilon_{rec,\Lambda}} - \frac{N_{\bar{\Lambda}}}{\epsilon_{rec,\bar{\Lambda}}}}{\frac{N_\Lambda}{\epsilon_{rec,\Lambda}} + \frac{N_{\bar{\Lambda}}}{\epsilon_{rec,\bar{\Lambda}}}}$$

Total Asymmetry Results

$$5 < Q^2[\mathrm{GeV}^2] < 100 \qquad 0.1 < y < 0.6$$
$$0.5 < p_T(V^0)[\mathrm{GeV}] < 3.5 \qquad -1.3 < \eta(V^0) < 1.3$$

- The previous measurement considered a slightly different kinematic range, if we integrate those results over the visible range above that we used the result is:

$$A_\Lambda = 0.0025 \pm 0.016(\mathrm{stat.})$$

- Our result over this same kinematic range with the enhanced HERAII statistics is:

$$A_\Lambda = 0.0186 \pm 0.0035(\mathrm{stat.}) \pm 0.0027(\mathrm{syst.})$$

New result is consistent with 0.03±0.02 estimate of Frenklakh & Kharzeev and previous HERA results, but with enhanced HERAII statistics inconsistent with zero.

Asymmetry Distributions

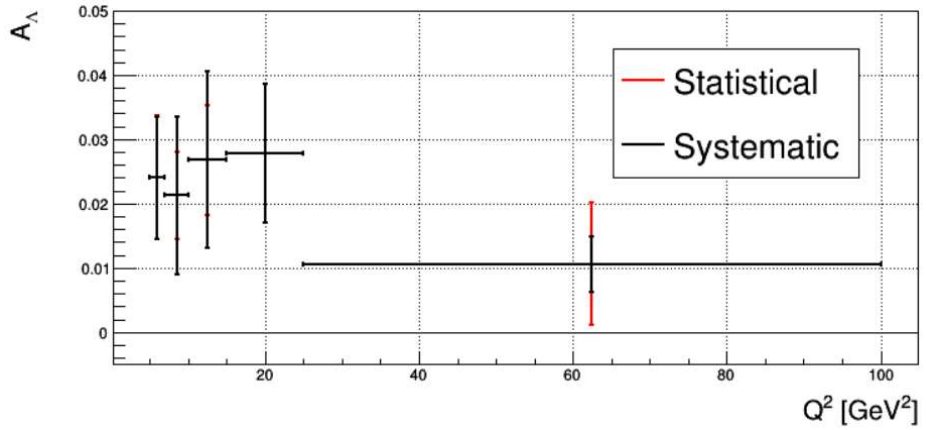

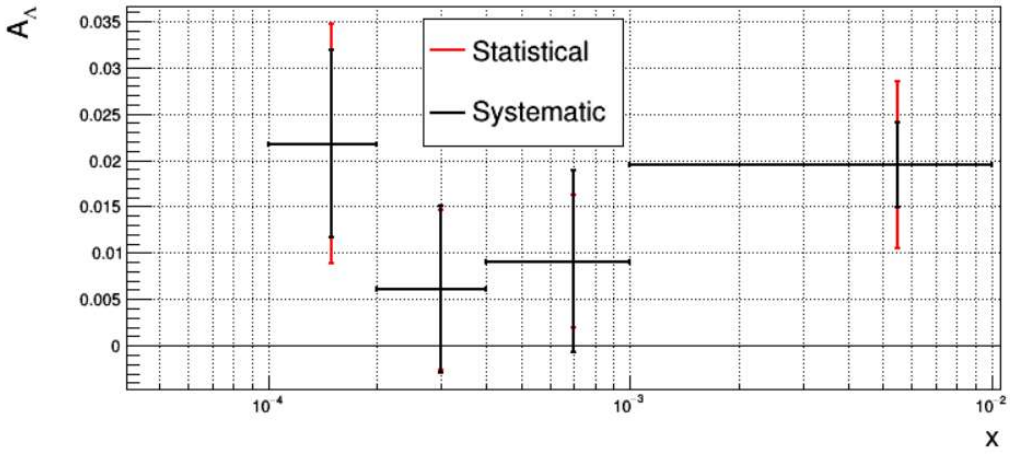

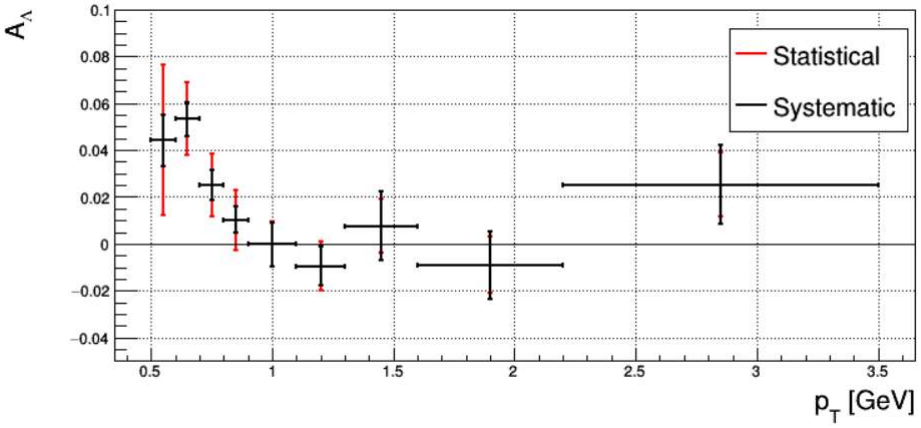

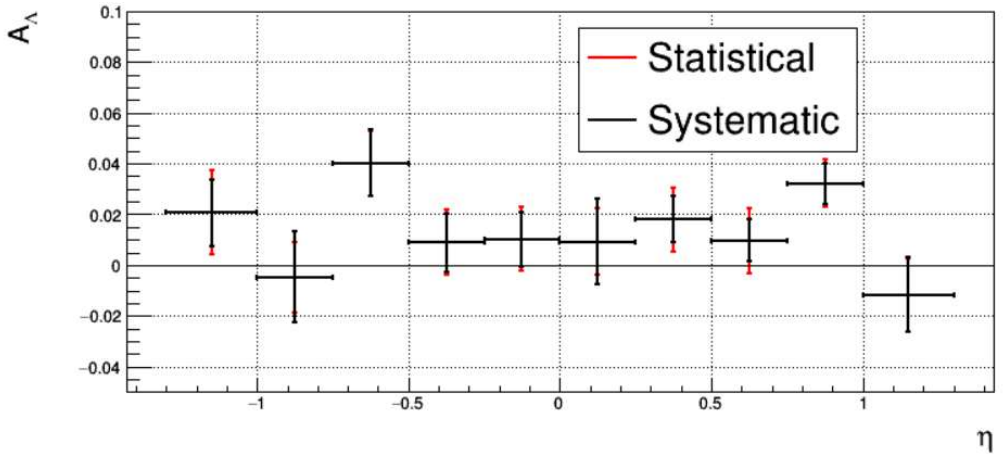

Asymmetry Distributions Comparison

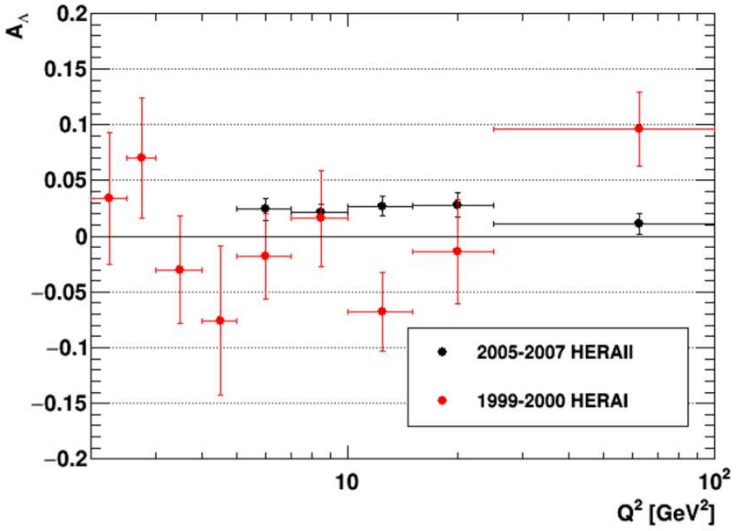

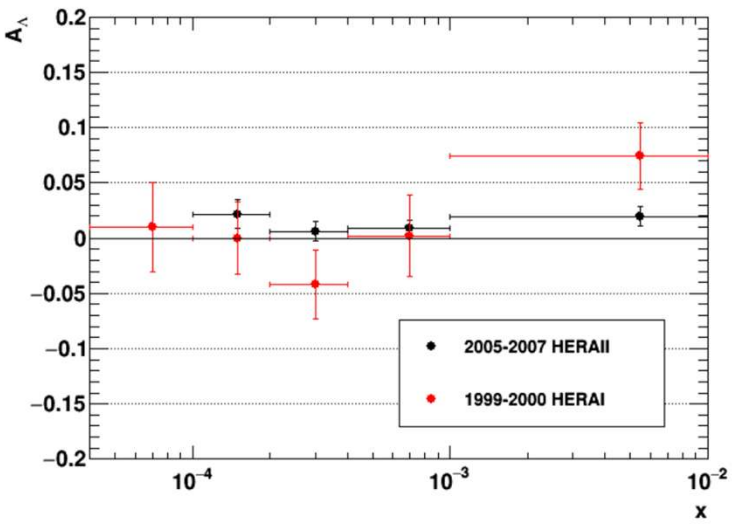

HERAI Visible Range:
2 < Q^2 [GeV^2] < 100
0.1 < y < 0.6
|η(Λ)| < 1.3
0.5 < p_T(Λ)[GeV] < 3.5

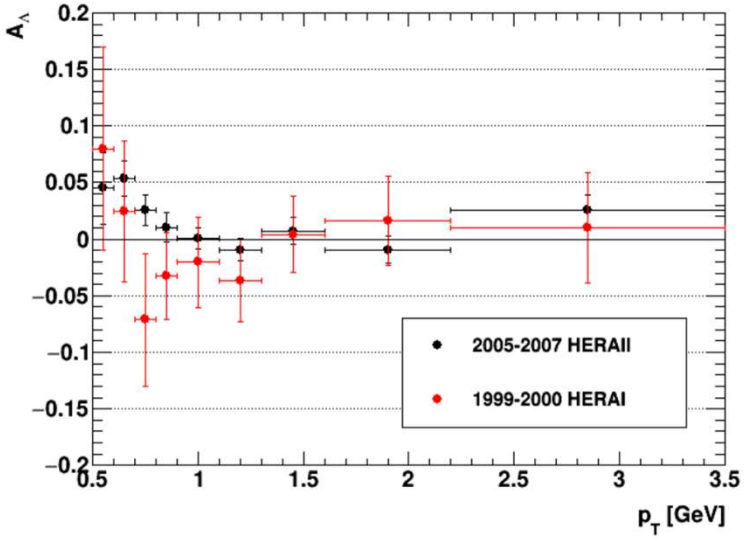

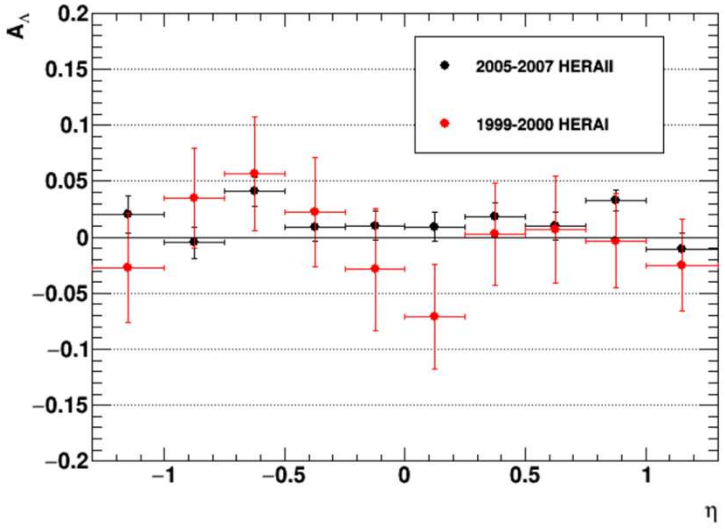

HERAII Visible Range:
5 < Q^2 [GeV^2] < 100
0.1 < y < 0.6
|η(Λ)| < 1.3
0.5 < p_T(Λ)[GeV] < 3.5

Conclusion

- There appears to be a non-zero baryon asymmetry in DIS which suggests transfer of baryon number from the proton target to particles visible in the hadronic final state
- Asymmetry is on the order of a few percent which supports the idea of a baryon junction, more precise theoretical estimates and measurements (possibly at the EIC) needed to conclusively distinguish the valence quark and baryon junction picture
- We are working with the H1 Collaboration to refine results and ensure the small asymmetry on the order of a few percent is well understood with respect to background

Acknowledgements

Thanks to the H1 Collaboration for sharing their wealth of expertise in collaboration meetings and to Stefan Schmitt, Karin Daum, and Daniel Britzger in particular for their continued help in navigating the H1 computing structure and insights that have helped us progress our work

References

[1] A. Bolz. *Measurement of Differential ρ^0 Photoproduction Cross-Sections at HERA*. PhD thesis, U. Heidelberg, Dept. Phys., 2019.

[2] N. Lewis,W. Lv, M.A. Ross, *et al.* Search for baryon junctions in photonuclear processes and isobar collisions at RHIC. *Eur. Phys. J. C* **84**, 590 (2024). https://doi.org/10.1140/epjc/s10052-024-12834-2

[3] N. Magdy, A. Deshpande, R. Lacey, *et al.* Search for baryon junctions in e+A collisions at the electron ion collider. *Eur. Phys. J. C.* **84** (2024). https://doi.org/10.1140/epjc/s10052-024-13702-9

[4] D. Frenklakh, D. Kharzeev, E. Dmitri, W. Li. Signatures of baryon junctions in semi-inclusive deep inelastic scattering. *Phys. Lett. B.* **853** (2024). https://doi.org/10.1016/j.physletb.2024.138680

[5] B. Kopeliovich, B. Povh. Baryon asymmetry of the proton sea at low-x. *Z Phys C - Particles and Fields.* **75** (1997). https://doi.org/10.1007/s002880050515

[6] F. Willeke, J. Beebe-Wang. "Electron Ion Collider Conceptual Design Report 2021." , Feb. 2021. https://doi.org/10.2172/1765663

Backup Slides

Neutral Current Deep-Inelastic Scattering at HERA

Two regimes of events can be defined:

1. Photoproduction ($Q^2 \approx 0$)
   - Soft interaction, events more abundant, includes larger fraction of diffractive events where proton is not broken up in the interaction
   - Worse resolution in event reconstruction, low Q^2 means small scattered electron angle which can sometimes escape nearly colinear with electron beam down the beam pipe
2. Deep inelastic scattering ($Q^2 > 1$ [GeV^2])

- We only consider neutral current DIS where the virtual photon mediates, massive $Z^0, W^{\pm}$ are highly suppressed unless Q^2 is on the order of their respective masses squared, so ~8000 GeV^2
- Lower Q^2 events provide more statistics for baryon production results

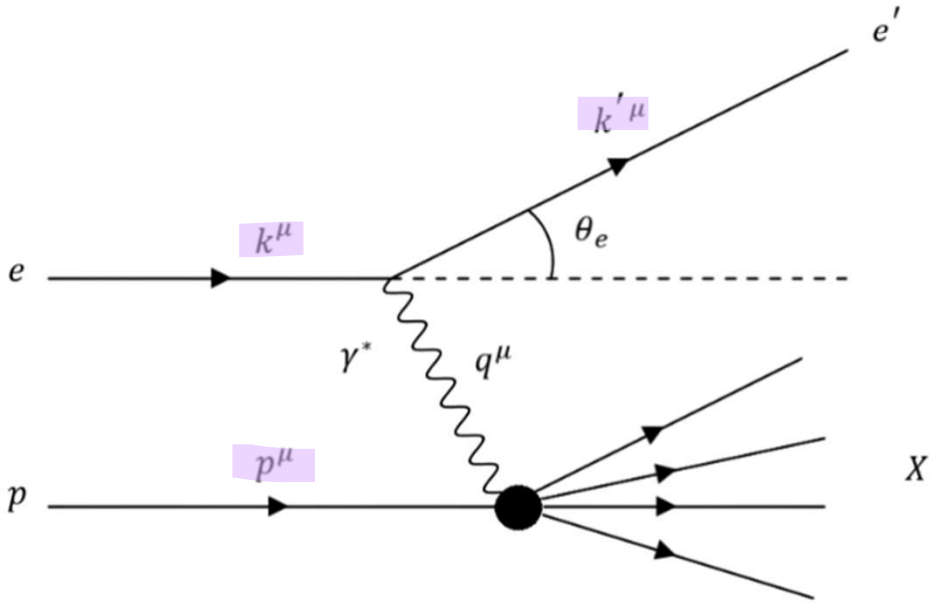

$$Q^2 \equiv -q^\mu q_\mu = -q^2 \qquad Q^2 = 4E_e E_e' \cos^2(\frac{\theta_e}{2})$$

$$y \equiv \frac{p^\mu q_\mu}{p^\nu k_\nu} \qquad y = 1 - \frac{E_e'}{E_e}\sin^2(\frac{\theta_e}{2})$$

$$x \equiv \frac{Q^2}{2p^\mu q_\mu} \qquad x = \frac{Q^2}{ys} = \frac{Q^2}{Q^2 + W^2 - m_p^2}$$

$$Q^2 = xys$$

$$W \equiv \sqrt{(q^\mu + p^\mu)^2} = \sqrt{ys - Q^2 + m_p^2}$$

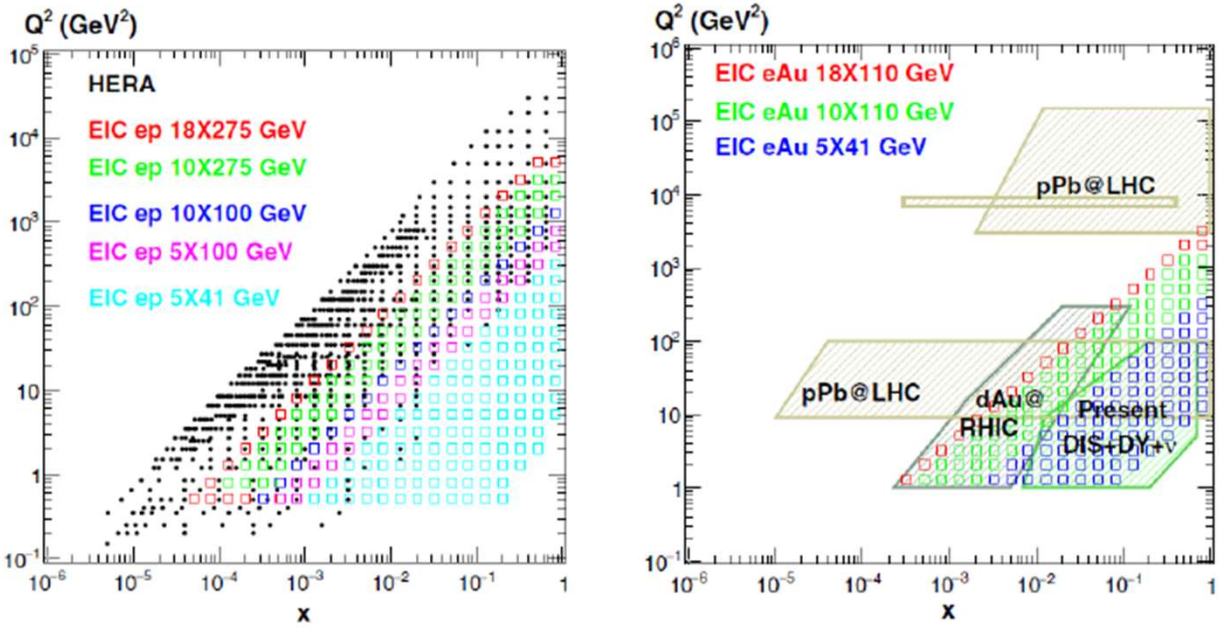

Figure 3.5: Kinematic coverage comparison of previous/current experiments and the proposed EIC (figures from [50]).

https://journals.aps.org/prd/abstract/10.1103/PhysRevD.109.054019

Other Measurements

H1, ZEUS, and HERMES data is preserved and thanks to significant investment from DESY, there are some promising directions for future analyses that can give insight on baryon junction production:

- Proton/antiproton asymmetry measurement
- Strange baryons in diffractive DIS
  - Use as a baseline for non-diffractive DIS measurements
- Proton energy scan data
  - Reach smaller beam rapidities, but limited statistics

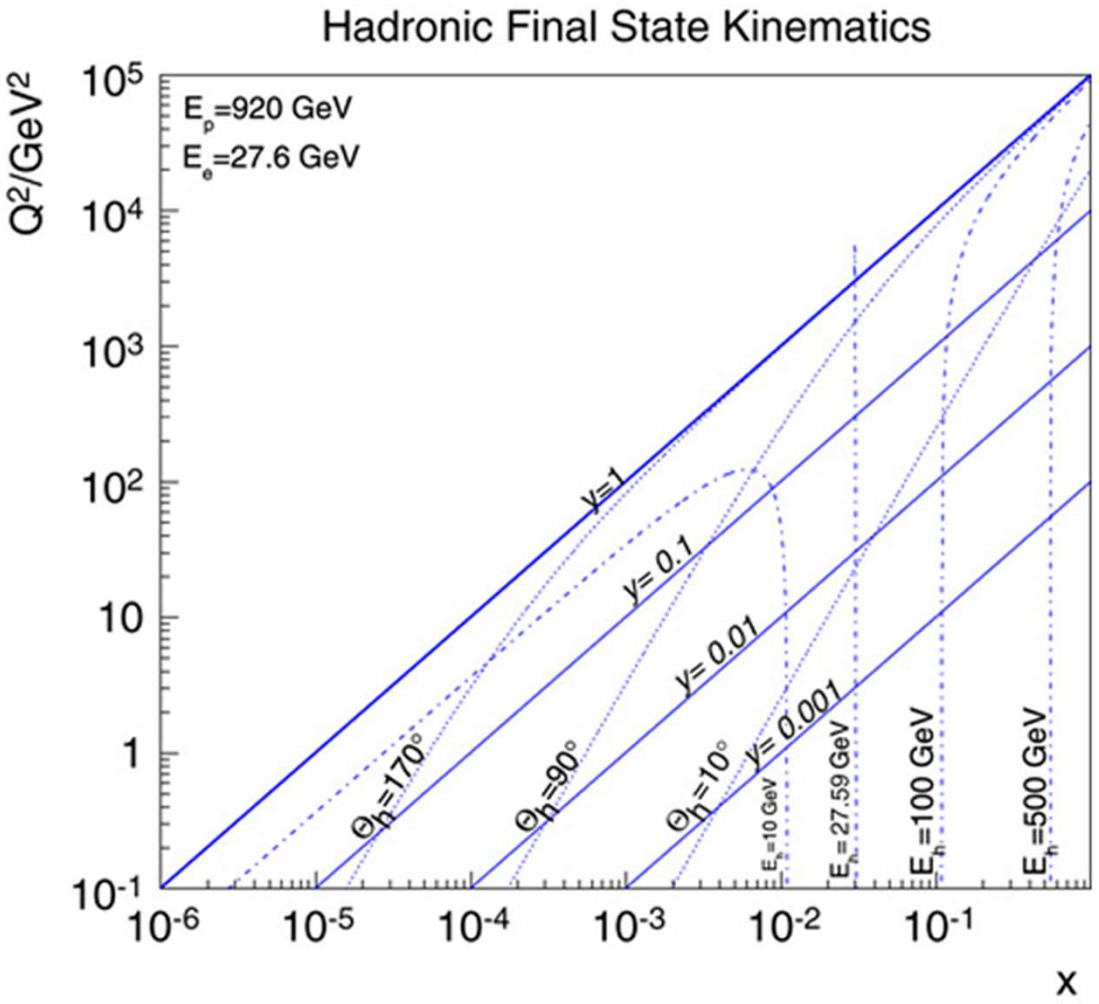
Hadronic Final State Kinematics
E_p=920 GeV
E_e=27.6 GeV
Q^2/GeV^2
10^5
10^4
10^3
10^2
10
1
10^{-1}
10^{-6}
10^{-5}
10^{-4}
10^{-3}
10^{-2}
10^{-1}
x
y=1
y= 0.1
y= 0.01
y= 0.001
Θ_h=170°
Θ_h=90°
Θ_h=10°
E_h=10 GeV
E_h=27.59 GeV
E_h=100 GeV
E_h=500 GeV

H1 Experiment at HERA

- Used electrons and positrons incident on proton (usually referred to as just the “electron” unless distinction required)
  - We are looking at low Q^2 events which are dominated by the virtual photon mediation which couples identically to e^+/e^-

Run Period	e^-p 2005	e^-p 2006	e^+p 2006/2007
Lepton Energy [GeV]		27.6	
Proton Energy [GeV]		920	
Center of Mass Energy [GeV]		319	
Number of lepton bunches	142	180	180
Number of proton bunches	140	180	180
Average (maximum) lepton beam current [mA]	22 (42)	22 (62)	25 (45)
Average (maximum) proton beam current [mA]	78 (102)	79 (108)	89 (112)
Delivered integrated luminosity $[pb^{-1}]$	218	89.7	184
H1 maximum integrated run luminosity $[nb^{-1}]$	260	153	164
Peak luminosity $[\mu b^{-1}/s]$	48.0	46.2	40.8
H1 recorded integrated luminostiy $[pb^{-1}]$	105.4	55.4	131.3
DST7 Data Run Ranges	399629-436893	444307-466997	468531-492541, 492559-500611

$$\mathcal{L} = 292.1 \text{ pb}^{-1}$$

Event Reconstruction

- Scattered electron and HFS each carry enough information to uniquely define DIS kinematics (Q^2, x, y), have a lot of freedom with this for event reconstruction
- Using IΣ reconstruction method, no assumption of electron beam energy (E_0)

Method name	Observables	y	Q^2	$x \cdot E_p$
Electron (e)	$[E_0, E, \theta]$	$1 - \frac{\Sigma_e}{2E_0}$	$\frac{E^2 \sin^2\theta}{1-y}$	$\frac{E(1+\cos\theta)}{2y}$
Double angle (DA) [6,7]	$[E_0, \theta, \gamma]$	$\frac{\tan\frac{\gamma}{2}}{\tan\frac{\gamma}{2}+\tan\frac{\theta}{2}}$	$4E_0^2 \cot^2\frac{\theta}{2}(1-y)$	$\frac{Q^2}{4E_0 y}$
Hadron (h, JB) [4]	$[E_0, \Sigma, \gamma]$	$\frac{\Sigma}{2E_0}$	$\frac{T^2}{1-y}$	$\frac{Q^2}{2\Sigma}$
ISigma (IΣ) [9]	$[E, \theta, \Sigma]$	$\frac{\Sigma}{\Sigma+\Sigma_e}$	$\frac{E^2 \sin^2\theta}{1-y}$	$\frac{E(1+\cos\theta)}{2y}$
IDA [7]	$[E, \theta, \gamma]$	y_{DA}	$\frac{E^2 \sin^2\theta}{1-y}$	$\frac{E(1+\cos\theta)}{2y}$
$E_0 E \Sigma$	$[E_0, E, \Sigma]$	y_h	$4E_0 E - 4E_0^2(1-y)$	$\frac{Q^2}{2\Sigma}$
$E_0 \theta \Sigma$	$[E_0, \theta, \Sigma]$	y_h	$4E_0^2 \cot^2\frac{\theta}{2}(1-y)$	$\frac{Q^2}{2\Sigma}$
$\theta \Sigma \gamma$ [8]	$[\theta, \Sigma, \gamma]$	y_{DA}	$\frac{T^2}{1-y}$	$\frac{Q^2}{2\Sigma}$
Double energy (A4) [7]	$[E_0, E, E_h]$	$\frac{E-E_0}{(xE_p)-E_0}$	$4E_0 y(xE_p)$	$E + E_h - E_0$
$E \Sigma T$	$[E, \Sigma, T]$	$\frac{\Sigma}{\Sigma+E\pm\sqrt{E^2+T^2}}$	$\frac{T^2}{1-y}$	$\frac{Q^2}{2\Sigma}$
$E_0 E T$	$[E_0, E, T]$	$\frac{2E_0-E\mp\sqrt{E^2-T^2}}{2E_0}$	$\frac{T^2}{1-y}$	$\frac{Q^2}{4E_0 y}$
Sigma (Σ) [9]	$[E_0, E, \Sigma, \theta]$	$y_{I\Sigma}$	$Q^2_{I\Sigma}$	$\frac{Q^2}{4E_0 y}$
eSigma ($e\Sigma$) [9]	$[E_0, E, \Sigma, \theta]$	$\frac{2E_0\Sigma}{(\Sigma+\Sigma_e)^2}$	$2E_0 E(1+\cos\theta)$	$\frac{E(1+\cos\theta)(\Sigma+\Sigma_e)}{2\Sigma}$

https://doi.org/10.1016/0168-9002%2895%2900173-5

Thesis Slides Following

Measuring baryon production at HERA, and its potential on baryon junction

Low Q^2 Baryon Asymmetry and Strangeness Production in NC DIS at HERA

MA Thesis Defe ember 11, 2025

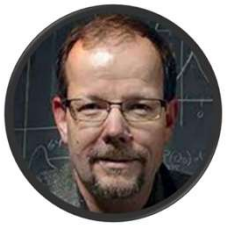

Axel Drees

Co-Advisor

Professor – Stony Brook University

Presenter: Gage Tustin

MA Student – Stony Brook University

Operations Coordinator – Brookhaven

Henry Klest

Co-Advisor

Assistant Physicist – Argonne

Overview

- Motivation for baryon asymmetry measurement in Deep-Inelastic *ep* Scattering (DIS)
  - Will focus on the baryon asymmetry measurement, strange particle production results in the backup slides
- DIS kinematics
- HERA background and data selection
- DIS event selections
- Particle reconstruction
- Measurement description
- Results and conclusions
- Outlook on potential research building off this work

Motivation

- Baryon number is an empirically observed symmetry of nature, but how it is carried and transported is not well understood

Quark Model: Traditionally, baryon number is assigned to valence quarks carrying 1/3 of the baryon number (-1/3 for anti-quarks)

- In this model, the baryon state is viewed as three valence quarks interacting via gluons in a triangular structure

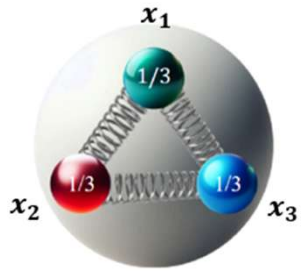

$$B(x_1, x_2, x_3) = \epsilon^{ijk} q(x_1)_i \; q(x_2)_j q(x_3)_k$$

Gluon Junction Model: Y-shaped configuration of gluons connecting valence quarks was proposed in the 1970's as a way of constructing a gauge invariant baryon state [1]

Local
Gauge Invariance

$$P(x_n, x) \equiv \mathcal{P} \exp\left(ig \int_{x_n}^{x} A_\mu dx^\mu\right)$$

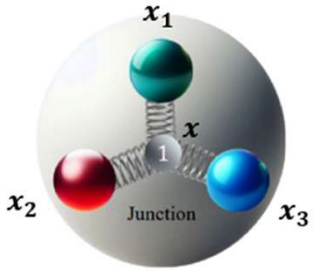

$$B(x_1, x_2, x_3, x) = \epsilon^{ijk} \; [P(x_1, x) \; q(x_1)]_i \; [P(x_2, x) \; q(x_2)]_j \; [P(x_3, x) \; q(x_3)]_k$$

Motivation

- Neither of these models has been conclusively verified as the correct picture, the quark and junction configuration is indistinguishable in most processes
- In relativistic heavy ion-collisions baryon asymmetries have been observed at mid-rapidity (central region perpendicular to the collision axis), which appears to be inconsistent with the valence quark model
  - Valence quarks carry a large momentum fraction of the colliding species, and would need a significant energy transfer to stop them sufficiently to allow transport of baryon number to mid-rapidity
  - At high energies, the valence quarks also have less time to interact due to longitudinal length contraction which suppresses baryon stopping

Nuclear stopping and rapidity loss in Au + Au collisions at $\sqrt{s_{NN}} = 62.4\text{GeV}$

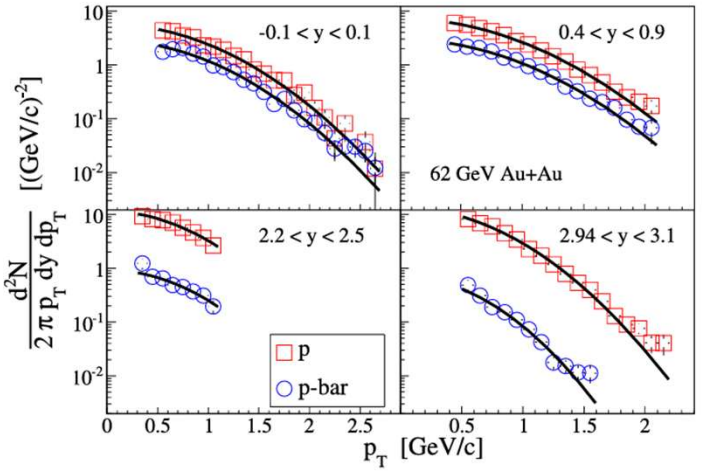

https://doi.org/10.1016/j.physletb.2009.05.049

- STAR has recent publication proposing a method of analyzing charge vs baryon stopping in heavy ion collisions as a way to search for evidence of baryon junctions [2]
- But, looking forward to Electron-Ion Collider (EIC), this should also be able to be distinguished in e-Au [3]
- Deep-inelastic *ep* scattering collisions where only one species provides baryon number should also be able to look for junctions [4,5]

$$y \equiv \frac{1}{2}\ln\left(\frac{E+p_L}{E-p_L}\right)$$

$$\eta \equiv -\ln\left[\tan\left(\frac{\theta}{2}\right)\right]$$

$$\eta = \frac{1}{2}\ln\left(\frac{|\mathbf{p}|+p_L}{|\mathbf{p}|-p_L}\right)$$

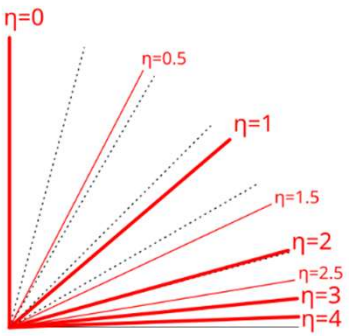

$$m \ll |\mathbf{p}| \Rightarrow E \approx |\mathbf{p}| \Rightarrow \eta \approx y$$

Motivation

- Testing gluonic junctions in *ep* scattering initially seems tricky due to the electron coupling to charged quark constituents rather than directly to the gluons
- Basic idea is that the quark-antiquark component of the virtual photon in the *ep* scattering can interact with the proposed gluon junction and pull it into the hadronic final state to transfer baryon number
- At high energies, the purely gluonic exchange (therefore uncorrelated in proton flavor when valence quarks do not participate) is expected to dominate due to the higher Regge intercept [4]
- David Frenklakh and Dmitri Kharzeev gave us a quick calculation based on their gluon junction framework in this publication and estimate a baryon asymmetry in DIS of 0.03±0.02 within our kinematic range
  - Based on a 3→3 Forward scattering in Regge Theory framework
  - Regge intercept for purely gluonic junction exchange cannot be calculated from first principles, but they estimated it from the Au-Au RHIC Beam Energy Scan data, hence the large errors
- Not a precise estimate but gives us a ballpark expectation

Signatures of baryon junctions in semi-inclusive deep inelastic scattering

David Frenklakh [a b], Dmitri E. Kharzeev [a b c], Wenliang Li [b]

https://doi.org/10.1016/j.physletb.2024.138680

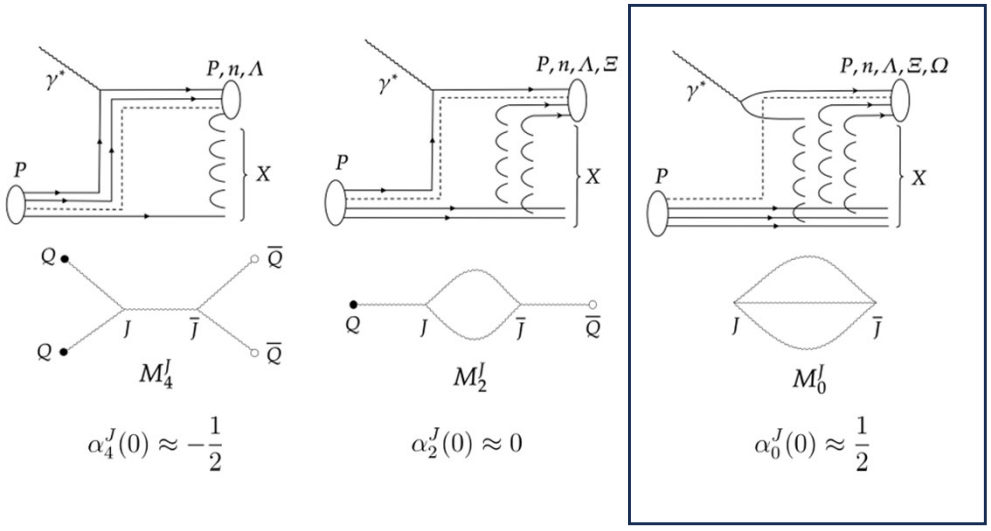

HERA

- At HERA (Hadron-Electron Ring Accelerator) we can study semi-inclusive deep inelastic *ep* scattering and look for baryon asymmetries
- Provided collisions at a primary running mode of E_p=920 GeV and E_e=27.6 GeV → $\sqrt{s}$ =319 GeV
- Accelerator ran from 1992-2007 servicing two fixed target experiments (HERMES and HERA-B) and two general purpose hermetic detectors (H1 and ZEUS)
- H1 collaboration leading efforts in DPHEP (Data Preservation in High Energy Physics) and have updated full analysis software to retain full potential of experimental data
- Baryon production can be analyzed cleanly via strange particle production
  - For Λ, $c\tau = 7.89$ cm, so Λ produced at the primary DIS vertex can be observed at a resolvable secondary decay vertex, background greatly reduced by rejecting track primary vertex fitted tracks
- Can try and look for a Λ - $\overline{\Lambda}$ asymmetry since gluon junction mechanism is flavor blind

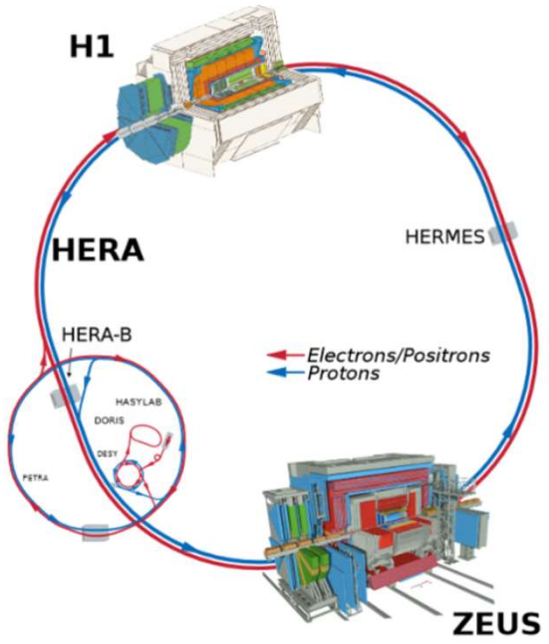

Λ BARYONS
($S = -1$, $I = 0$)
$\Lambda^0 = uds$

Previous Measurement

- Asymmetry measurement at HERA previously done by H1 (shown on right) and ZEUS, but did not have enough statistics to resolve a non-zero asymmetry or to exclude the possibility of an asymmetry on the order of a few percent
- These previous measurements only use 1999-2000 data, ~6x more data available now

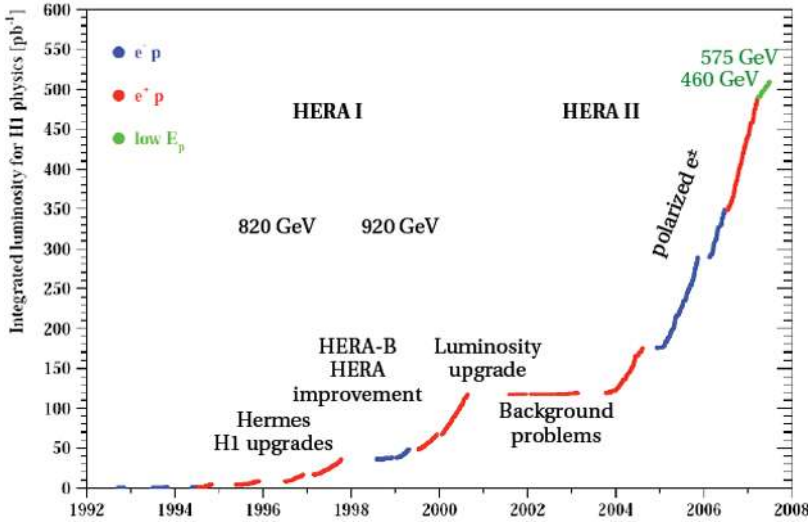

Strangeness Production at low Q^2 in Deep-Inelastic ep Scattering at HERA

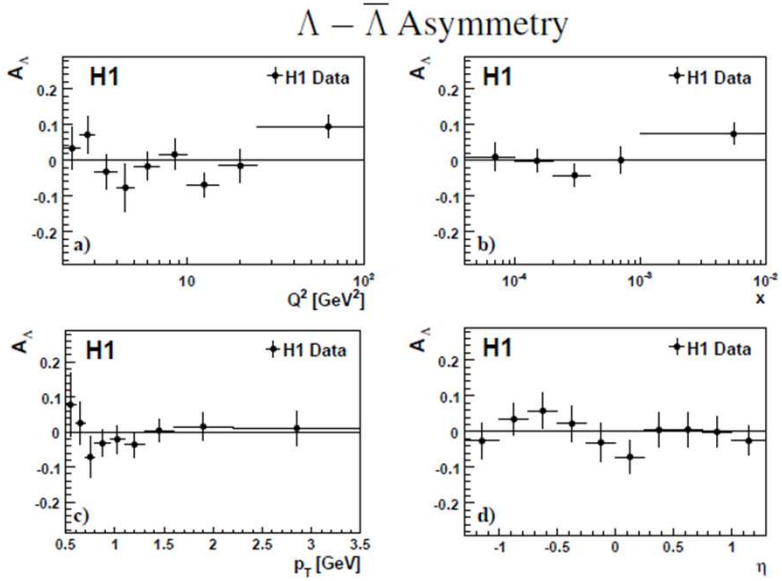

Figure 8: The asymmetry A_Λ of the differential production cross sections of the Λ and $\bar{\Lambda}$ baryons in the laboratory frame as a function of the a) photon virtuality squared Q^2 , b) Bjorken scaling variable x, c) transverse momentum p_T and d) pseudorapidity η. The asymmetry is defined as $A_\Lambda = [\sigma_{vis}(ep \to e\Lambda X) - \sigma_{vis}(ep \to e\bar{\Lambda} X)]/[\sigma_{vis}(ep \to e\Lambda X) + \sigma_{vis}(ep \to e\bar{\Lambda} X)]$. The error bars show the statistical uncertainty.

https://doi.org/10.1140/epjc/s10052-009-0995-1

Neutral Current Deep-Inelastic *ep* Scattering at HERA

- Kinematics of DIS events can be completely described by four Lorentz scalars: Q^2, x, y, s
  - All can be written in terms of highlighted four momentums on the right
- Q^2 is the negative four momentum of the virtual photon squared (negative sign convention to keep quantity positive)
- x (also known as Bjorken- x) is the fractional momentum of the struck quark with respect to the proton's momentum
- y is the inelasticity (not to be confused with y as rapidity which is standard in heavy ion physics), can be interpreted as the fractional energy lost by the electron in the scattering
- s is the center-of-mass energy of the colliding system squared
- Sometimes useful but not used in our analysis, W is the invariant mass of the hadronic final state (HFS) denoted X

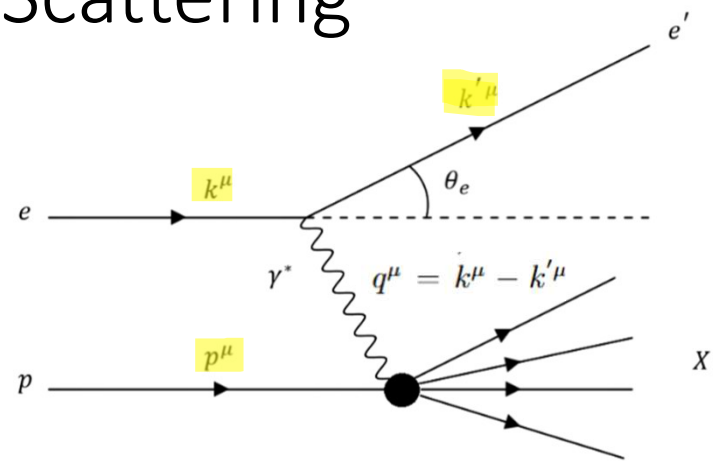

$$Q^2 \equiv -q^\mu q_\mu = -q^2 \qquad Q^2 = 4E_e E_e' \cos^2(\frac{\theta_e}{2})$$

$$y \equiv \frac{p^\mu q_\mu}{p^\nu k_\nu} \qquad y = 1 - \frac{E_e'}{E_e}\sin^2(\frac{\theta_e}{2})$$

$$x \equiv \frac{Q^2}{2p^\mu q_\mu} \qquad x = \frac{Q^2}{ys} = \frac{Q^2}{Q^2 + W^2 - m_p^2}$$

$$Q^2 = xys$$

$$W \equiv \sqrt{(q^\mu + p^\mu)^2} = \sqrt{ys - Q^2 + m_p^2}$$

Neutral Current Deep-Inelastic *ep* Scattering at HERA

Two regimes of events can be defined:

1. Photoproduction ($Q^2 \approx 0$)
   - Soft interaction, events more abundant, includes diffractive events where proton is not broken up in the interaction
   - Worse resolution in event reconstruction, low Q^2 means small scattered electron angle which can sometimes escape nearly colinear with electron beam down the beam pipe
2. Deep inelastic scattering ($Q^2 > 1$ [GeV^2])
   - Proton completely broken up into a HFS

We only consider neutral current DIS where the virtual photon mediates, massive $Z^0, W^{\pm}$ are highly suppressed unless Q^2 is on the order of their respective masses squared, so ~8000 GeV^2

- We only consider 5 < Q^2 [GeV^2] < 100 so these contributions are negligible

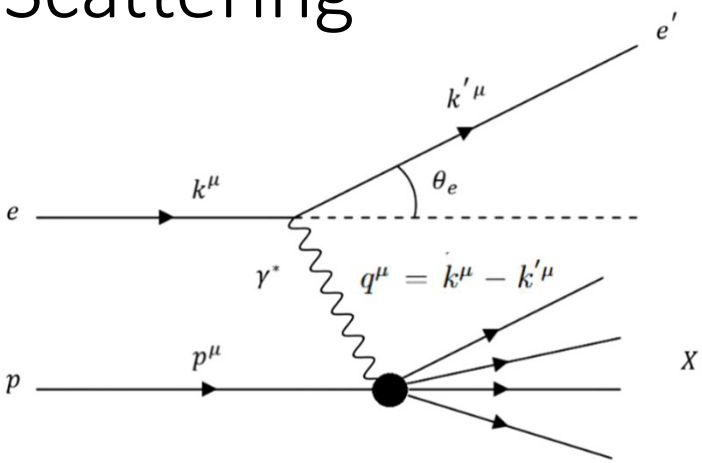

$$Q^2 \equiv -q^\mu q_\mu = -q^2 \qquad Q^2 = 4E_e E_e' \cos^2(\frac{\theta_e}{2})$$

$$y \equiv \frac{p^\mu q_\mu}{p^\nu k_\nu} \qquad y = 1 - \frac{E_e'}{E_e}\sin^2(\frac{\theta_e}{2})$$

$$x \equiv \frac{Q^2}{2p^\mu q_\mu} \qquad x = \frac{Q^2}{ys} = \frac{Q^2}{Q^2 + W^2 - m_p^2}$$

$$Q^2 = xys$$

$$W \equiv \sqrt{(q^\mu + p^\mu)^2} = \sqrt{ys - Q^2 + m_p^2}$$

H1 Detector

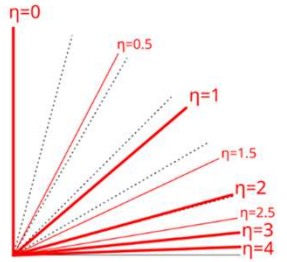

$$\eta \equiv -\ln\left[\tan\left(\frac{\theta}{2}\right)\right]$$

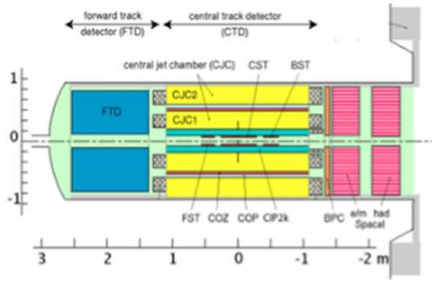

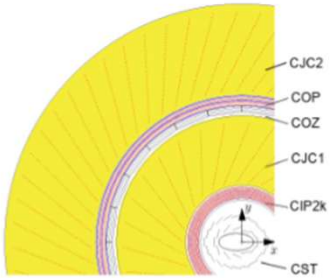

- Tracking System:
  - Two central drift chambers (CJC1 and CJC2) for charged particle trajectories
  - Central Silicon Tracker (CST) – silicon tracking for resolving interaction vertices just outside beam pipe
  - Tracking well understood in the $|\eta| < 1.3$ range
  - Good resolution for charged particle tracks with $p_T > 0.12$ GeV
- SpaCal – calorimeter in backward direction for precise detection of scattered electron in lower Q^2 events ($5 < Q^2\ [\mathrm{GeV}^2] < 120$), consisting of long, thin scintillating fibers for precise position and energy measurement
  - Most statistics for baryon production exist in low Q^2 event range, limiting factor in how how we go based on SpaCal, elliptical beampipe installed post HERAII luminosity upgrade causes issues for $Q^2 < 5\ \mathrm{GeV}^2$

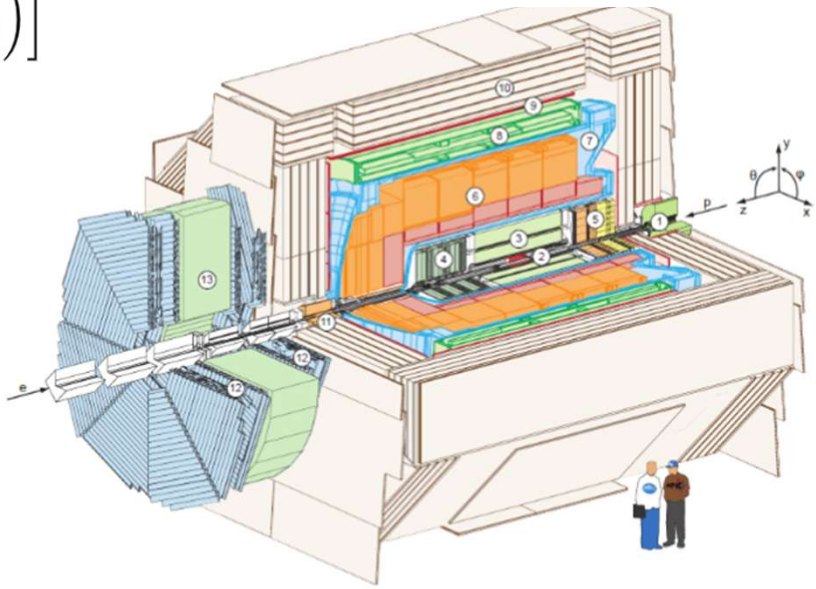

1. Beam pipe and beam magnets
2. Silicon tracking detector
3. Central tracking detector
4. Forward tracking detector
5. Spacal calorimeter (em and had)
6. Liquid Argon calorimeter (em and had)
7. Liquid Argon cryostat
8. Superconductiong coil
9. Muon chambers
10. Instrumented iron (streamer tube detectors)
11. Plug calorimeter
12. Forward muon detector
13. Muon toroid magnet

HERAII Running Years Used

- Some background issues were leftover from the HERAII luminosity upgrade in 2004 (proton-gas interactions), so 2005-2007 years safely used after this was sorted out
- Used electrons and positrons incident on proton (usually referred to as just the "electron" unless distinction required)
  - We are looking at low Q^2 events which are dominated by the virtual photon mediation which couples identically to e^+/e^-

Run Period	e^-p 2005	e^-p 2006	e^+p 2006/2007
Lepton Energy [GeV]	27.6		
Proton Energy [GeV]	920		
Center of Mass Energy [GeV]	319		
Number of lepton bunches	142	180	180
Number of proton bunches	140	180	180
Average (maximum) lepton beam current [mA]	22 (42)	22 (62)	25 (45)
Average (maximum) proton beam current [mA]	78 (102)	79 (108)	89 (112)
Delivered integrated luminosity $[pb^{-1}]$	218	89.7	184
H1 maximum integrated run luminosity $[nb^{-1}]$	260	153	164
Peak luminosity $[\mu b^{-1}/s]$	48.0	46.2	40.8
H1 recorded integrated luminostiy $[pb^{-1}]$	105.4	55.4	131.3
DST7 Data Run Ranges	399629-436893	444307-466997	468531-492541, 492559-500611

$$\mathcal{L} = 292.1 \text{ pb}^{-1}$$

Event Reconstruction

- Scattered electron and HFS each carry enough information to uniquely define DIS kinematics (Q^2, x, y), have a lot of freedom with this for event reconstruction
- Using IΣ reconstruction method
  - No assumption of electron beam energy (E_0), so minimal reconstruction issues to to Initial State Radiation (ISR)

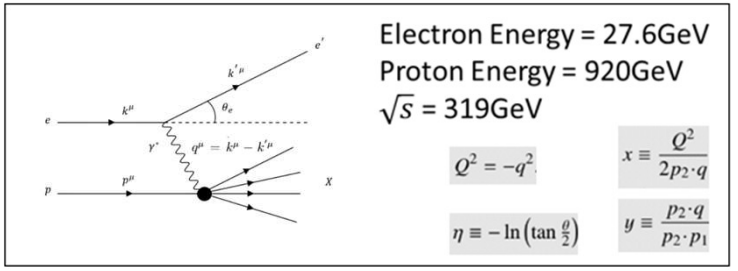

$$\Sigma = \sum_h (E_h - p_{z,h}), \quad T = \sqrt{(\sum_h p_{x,h})^2 + (\sum_h p_{y,h})^2}$$

Method name	Observables	y	Q^2	$x \cdot E_p$
Electron (e)	$[E_0, E, \theta]$	$1 - \frac{\Sigma_e}{2E_0}$	$\frac{E^2 \sin^2\theta}{1-y}$	$\frac{E(1+\cos\theta)}{2y}$
Double angle (DA) [6,7]	$[E_0, \theta, \gamma]$	$\frac{\tan\frac{\gamma}{2}}{\tan\frac{\gamma}{2}+\tan\frac{\theta}{2}}$	$4E_0^2 \cot^2\frac{\theta}{2}(1-y)$	$\frac{Q^2}{4E_0 y}$
Hadron (h, JB) [4]	$[E_0, \Sigma, \gamma]$	$\frac{\Sigma}{2E_0}$	$\frac{T^2}{1-y}$	$\frac{Q^2}{2\Sigma}$
ISigma (IΣ) [9]	$[E, \theta, \Sigma]$	$\frac{\Sigma}{\Sigma+\Sigma_e}$	$\frac{E^2 \sin^2\theta}{1-y}$	$\frac{E(1+\cos\theta)}{2y}$
IDA [7]	$[E, \theta, \gamma]$	y_{DA}	$\frac{E^2 \sin^2\theta}{1-y}$	$\frac{E(1+\cos\theta)}{2y}$
$E_0 E\Sigma$	$[E_0, E, \Sigma]$	y_h	$4E_0 E - 4E_0^2(1-y)$	$\frac{Q^2}{2\Sigma}$
$E_0\theta\Sigma$	$[E_0, \theta, \Sigma]$	y_h	$4E_0^2 \cot^2\frac{\theta}{2}(1-y)$	$\frac{Q^2}{2\Sigma}$
$\theta\Sigma\gamma$ [8]	$[\theta, \Sigma, \gamma]$	y_{DA}	$\frac{T^2}{1-y}$	$\frac{Q^2}{2\Sigma}$
Double energy (A4) [7]	$[E_0, E, E_h]$	$\frac{E-E_0}{(xE_p)-E_0}$	$4E_0 y(xE_p)$	$E + E_h - E_0$
$E\Sigma T$	$[E, \Sigma, T]$	$\frac{\Sigma}{\Sigma+E\pm\sqrt{E^2+T^2}}$	$\frac{T^2}{1-y}$	$\frac{Q^2}{2\Sigma}$
$E_0 ET$	$[E_0, E, T]$	$\frac{2E_0-E\mp\sqrt{E^2-T^2}}{2E_0}$	$\frac{T^2}{1-y}$	$\frac{Q^2}{4E_0 y}$
Sigma (Σ) [9]	$[E_0, E, \Sigma, \theta]$	$y_{I\Sigma}$	$Q^2_{I\Sigma}$	$\frac{Q^2}{4E_0 y}$
eSigma ($e\Sigma$) [9]	$[E_0, E, \Sigma, \theta]$	$\frac{2E_0\Sigma}{(\Sigma+\Sigma_e)^2}$	$2E_0 E(1+\cos\theta)$	$\frac{E(1+\cos\theta)(\Sigma+\Sigma_e)}{2\Sigma}$

https://doi.org/10.1016/0168-9002%2895%2900173-5

2005-2007 HERA II e^+p/ e^-p Data/MC Reconstructed Event Selections (using lΣ reconstruction)

$5 < Q^2\ [\mathrm{GeV}^2] < 100$
$0.1 < y < 0.6$
$-30 < z_{VTX}\ [\mathrm{cm}] < 30$
$35 < (E - p_z)\ [\mathrm{GeV}] < 70$

Final State Initial State

$$E - p_z = (E'_e - p'_{z,e}) + \sum_{hfs}(E_i - p_{z,i}) = (E_e - p_{z,e}) + (E_p - p_{z,p}) = 55\,\mathrm{GeV}$$

*For a perfect detector

- Reject events with missing FS particles, missing electron, detector issues

s61 > 0 *Trigger requirements change between run, but requires transverse momentum above some threshold, z vertex measurement within detector region, and a SpaCal energy deposit above some threshold

- p_T > 900 MeV
- SpaCal energy deposit > 9 GeV

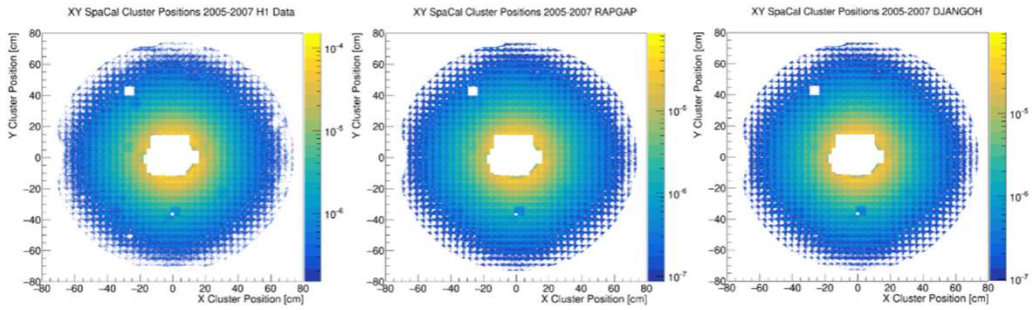

- SpaCal energy deposit > 11 GeV
- Scattered Electron Cluster Radius in SpaCal (Ecra) < 3.5cm
- SpaCal Cuts to eliminate dead trigger cells

HERA II 2005-2007 e^+p/ e^-p Looping over µODS particle candidates

Strange Channels:

$K_s^0 \to \pi^+\pi^- \quad (69.20 \pm 0.05)\%$

$\Lambda \to p\pi^- \quad (63.90 \pm 0.5)\%$

H1 Analysis Framework provides initial rough selections, loops over identified secondary decay vertices and combines tracks whose trajectories can be reasonably fitted to the decay vertex position

- Displaced decay vertex with two oppositely charged daughters
- p_T (p) >= 0.2 GeV
- p_T (π) >= 0.1 GeV (We strengthen this cut later)
- Track Length (π) >= 10 cm
- M(p+ π) <=1.5 GeV (M(Λ) ~ 1.1511)
- $p_{T,rel}$ (daughters w.r.t. Λ) < 0.15 GeV
- χ^2 (fit of daughter tracks to secondary vertex) < 5
- Radial Distance of Secondary vertex from primary >= 1.5 cm

HERA II 2005-2007 e^+p/ e^-p $\Lambda + \bar{\Lambda}$ Cut Evolution

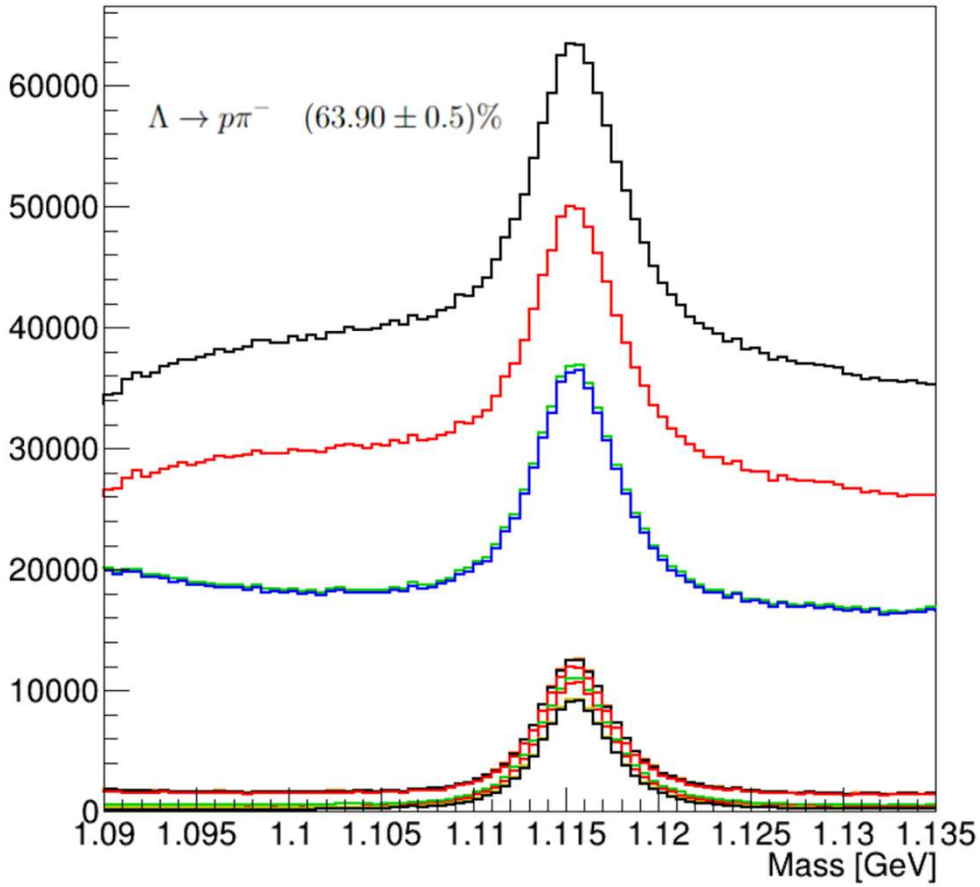

Cut 0 – Black: Starting Point
(Raw Candidates After Event Selection + H1FindLambda.C)

Cut 1- Red: $|\eta(\Lambda)| < 1.3$

Cut 2- Green: $0.5 < p_T(\Lambda)[\mathrm{GeV}] < 3.5$

Cut 3- Blue: Track Start Radius < 35cm

Cut 4- Orange: Reject Primary Vertex Fitted Tracks

Cut 5- Black: Rejecting Tracks with Multiple Secondary Vertex Hypotheses (Keep Candidate with best Chi2 vertex fit)

Cut 6- Red: p_T (π) > 0.12 GeV (same as in 2009 Analysis)

Cut 7- Green: $L_{\frac{dE}{dx}}(\mathrm{p}) > 0.001$

Cut 8- Blue: $L_{\frac{dE}{dx}}(\pi) > 0.001$

Cut 9- Magenta: $|S_{dca}$ (p)| > 0.2

Cut 10- Red: $|S_{dca}$ (π)| > 0.2 } $S_{dca} = \frac{d_{ca}}{\delta d_{ca}}$

Cut 11- Yellow: M(π+π) < 0.465 GeV ||
M(π+π) > 0.530 GeV

Cut 12- Black: M($e^+ + e^-$) > 0.05 GeV

Candidate Control Plots are in Backup Slides

HERA II 2005-2007 e^+p/ e^-p $\Lambda + \bar{\Lambda}$ Cut Evolution

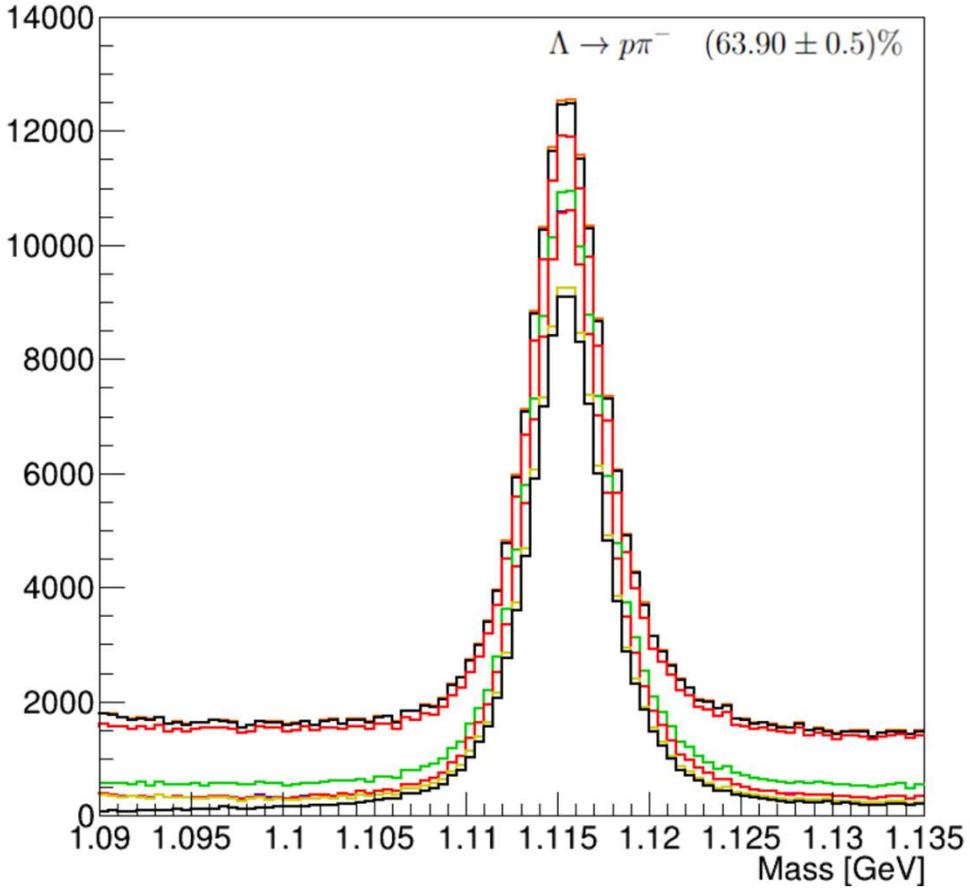

Cut 4- Orange: Reject Primary Vertex Fitted Tracks

Cut 5- Black: Rejecting Tracks with Multiple Secondary Vertex Hypotheses (Keep Candidate with best Chi2 vertex fit)

Cut 6- Red: p_T (π) > 0.12 GeV (same as in 2009 Analysis)

Cut 7- Green: $L_{\frac{dE}{dx}}(\mathrm{p}) > 0.001$

Cut 8- Blue: $L_{\frac{dE}{dx}}(\pi) > 0.001$

Cut 9- Magenta: $|S_{dca}$ (p)| > 0.2

Cut 10- Red: $|S_{dca}$ (π)| > 0.2

} $S_{dca} = \frac{d_{ca}}{\delta d_{ca}}$

Cut 11- Yellow: M(π+π) < 0.465 GeV ||

M(π+π) > 0.530 GeV

Cut 12- Black: M($e^+ + e^-$) > 0.05 GeV

Monte Carlo Generators

H1 Detector Configuration	Rad DJANGOH14 $Q^2 > 2$	Rad Non-Rad DJANGOH14 $Q^2 > 2$	Rad RAPGAP31 $Q^2 > 2$	Non-Rad RAPGAP31 $Q^2 > 2$	Rad PYTHIA62 $0 < Q^2 < 4$
2004/2005 e^-p	8872-8891, 8732-8743	5866-5873	8701-8708, 8930-8932	5887-5892	7274-7283, 7909-7981, 7250-7261, 7940-7951
2006 e^-p	8892-8922, 8723-8731	5874-5877	8696-8700, 8933-8935	5893-5894	7284-7292, 7973-7982, 7331, 7262-7273, 8004-8015
2006/2007 e^+p	8923-8926, 8715-8722, 8927-8929, 8709-8714	5855-5862, 5863-5865	8690-8695, 8936-8939, 8686-8689, 8940-8941	5878-5883, 5884-5886	7307-7319, 7800-7812, 7237-7249, 7766-7778
Lumi $[nb^{-1}]$	4108957	3560233	5293265	3397124	14580680

- RAPGAP31 Event Generator
  - Higher order QCD effects simulated with the Color Dipole Model (CDM)
  - Used for primary detector efficiency calculation due to better described HFS distributions comparing Data and MC
- DJANGOH14 Event Generator
  - Higher order QCD effects simulated with Parton Shower (MEPS)
  - Alternate calculation of detector efficiencies used for systematic uncertainty associated with measurement's Monter Carlo model dependence
- PYTHIA62 Event Generator
  - Also uses Parton Shower methods, but this MC set is used for estimations of photoproduction background since this set was generated with $Q^2 < 2\ \mathrm{GeV}^2$
- Events simulate the DIS process, then products fed into GEANT3 simulation (expect for non-radiative sets) of the H1 detector to calculate detector efficiencies
- Can use the same exact code for data reconstruction with simulated Monte Carlo Data

Peak Extractions in RooFit

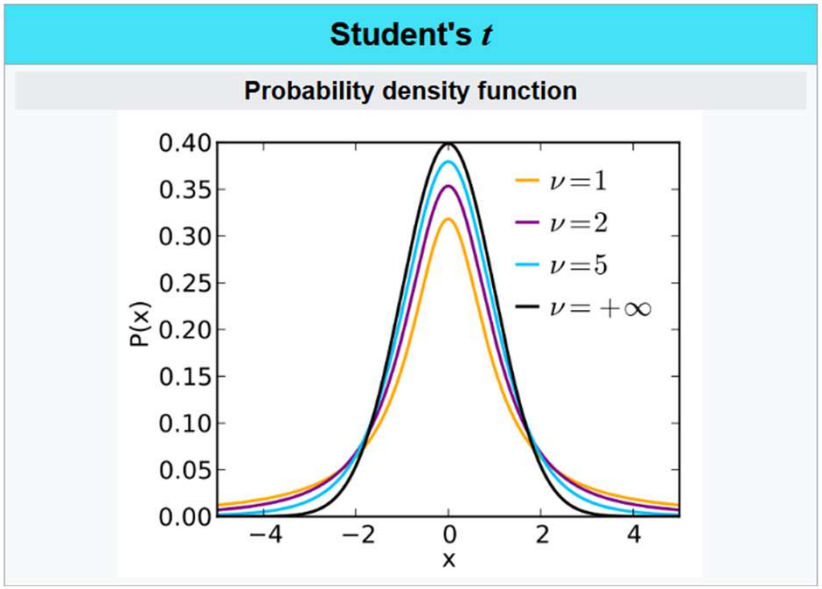

- Log Likelihood fits in RooFit – very high signal to background ratio, minimal background data benefits from fit using Poisson statistics in this method as opposed to Guassian with standard binned χ^2 in terms of fit convergence
- Composite fits using Student's T-Distribution for the signal shape and two different choices of BG function:

Composite PDF 1: Two body phase space shape

$$\underbrace{\frac{\Gamma(\frac{\nu+1}{2})}{\sqrt{\pi\nu}\Gamma\frac{\nu}{2}}(1+\frac{(\frac{m_\Lambda-\mu}{\sigma})^2}{\nu})^{-\frac{\nu+1}{2}}}_{\text{T-Distribution}} + \underbrace{(m_\Lambda - m_\pi - m_p)^{a_0} e^{(a_1(m_\Lambda-m_\pi-m_p))}}_{\text{BG PDF 1}}$$

Composite PDF 2: 4th order Polynomial, used for systematic uncertainty in the BG shape

$$\underbrace{\frac{\Gamma(\frac{\nu+1}{2})}{\sqrt{\pi\nu}\Gamma\frac{\nu}{2}}(1+\frac{(\frac{m_\Lambda-\mu}{\sigma})^2}{\nu})^{-\frac{\nu+1}{2}}}_{\text{T-Distribution}} + \underbrace{[b_0 + b_1 m_\Lambda + b_2 m_\Lambda^2 + b_3 m_\Lambda^3 + b_4 m_\Lambda^4]}_{\text{BG PDF 2}}$$

- Use the same process for extracting counts in data and reconstructed MC for calculating detector efficiencies

Λ Peak Extraction in Data

Primary: $\frac{\Gamma(\frac{\nu+1}{2})}{\sqrt{\pi\nu}\Gamma\frac{\nu}{2}}(1+\frac{(\frac{m_\Lambda-\mu}{\sigma})^2}{\nu})^{-\frac{\nu+1}{2}}+(m_\Lambda-m_\pi-m_p)^{a_0}e^{(a_1(m_\Lambda-m_\pi-m_p))}$

Alt: $\frac{\Gamma(\frac{\nu+1}{2})}{\sqrt{\pi\nu}\Gamma\frac{\nu}{2}}(1+\frac{(\frac{m_\Lambda-\mu}{\sigma})^2}{\nu})^{-\frac{\nu+1}{2}}+[b_0+b_1m_\Lambda+b_2m_\Lambda^2+b_3m_\Lambda^3+b_4m_\Lambda^4]$

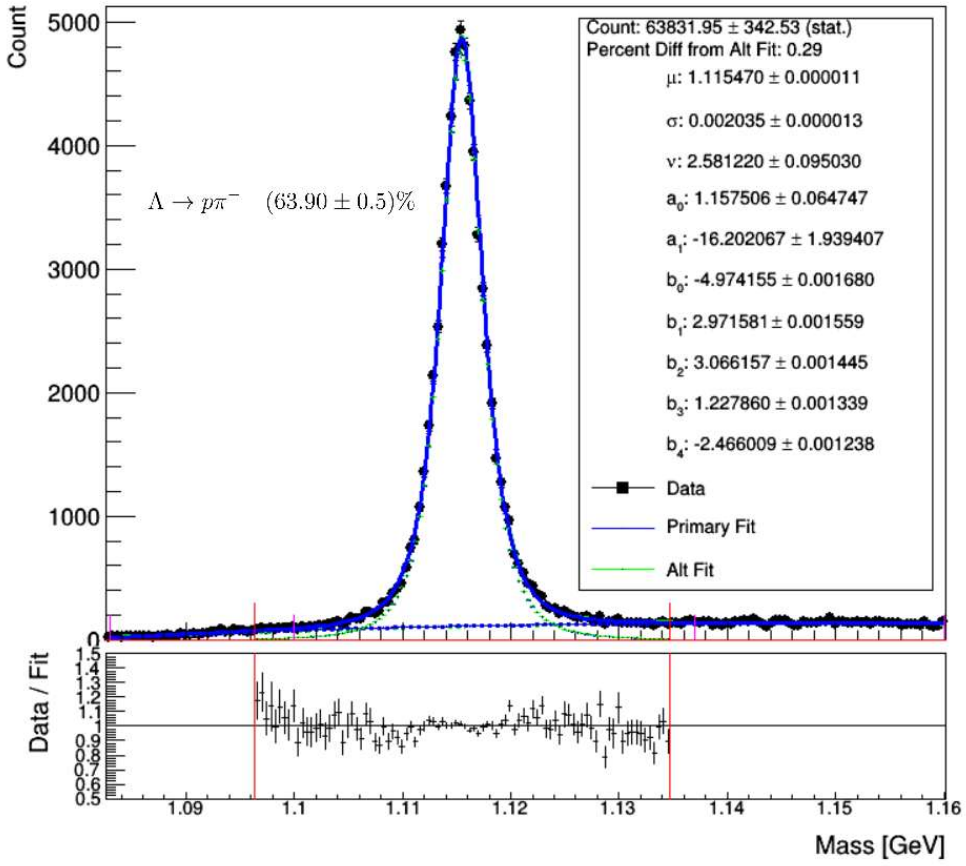

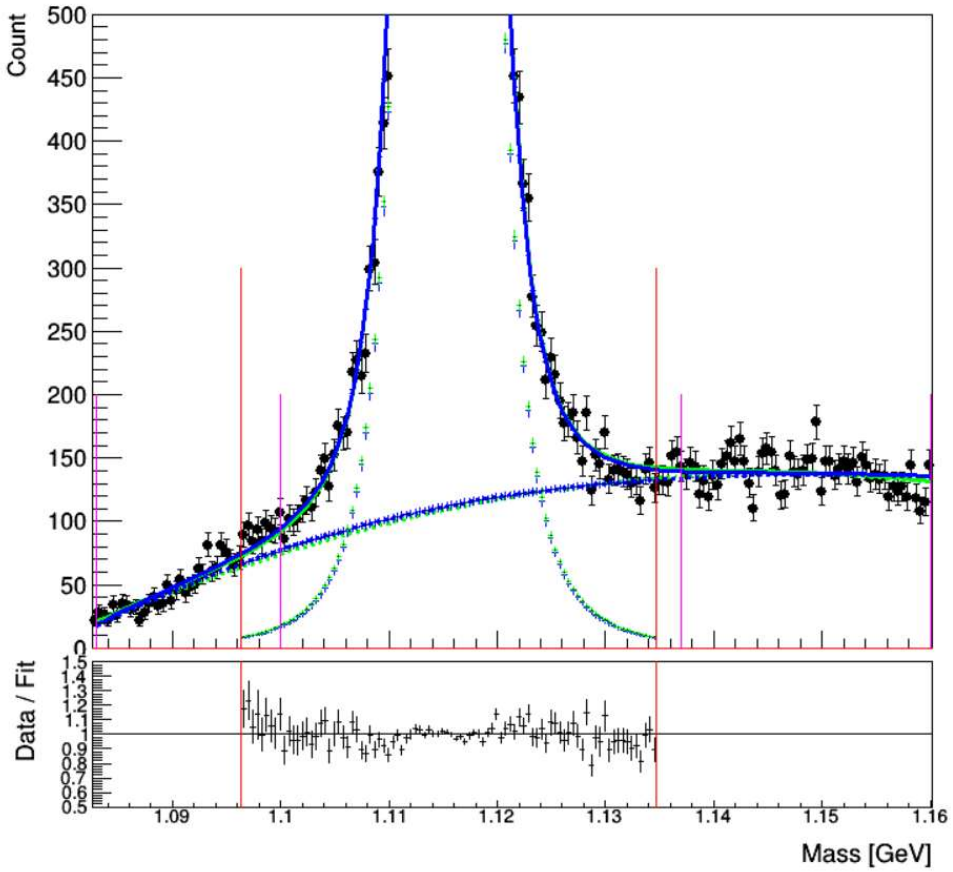

$\bar{\Lambda}$ Peak Extraction in Data

Primary: $\frac{\Gamma(\frac{\nu+1}{2})}{\sqrt{\pi\nu}\Gamma\frac{\nu}{2}}(1+\frac{(\frac{m_\Lambda-\mu}{\sigma})^2}{\nu})^{-\frac{\nu+1}{2}}+(m_\Lambda-m_\pi-m_p)^{a_0}e^{(a_1(m_\Lambda-m_\pi-m_p))}$

Alt: $\frac{\Gamma(\frac{\nu+1}{2})}{\sqrt{\pi\nu}\Gamma\frac{\nu}{2}}(1+\frac{(\frac{m_\Lambda-\mu}{\sigma})^2}{\nu})^{-\frac{\nu+1}{2}}+[b_0+b_1m_\Lambda+b_2m_\Lambda^2+b_3m_\Lambda^3+b_4m_\Lambda^4]$

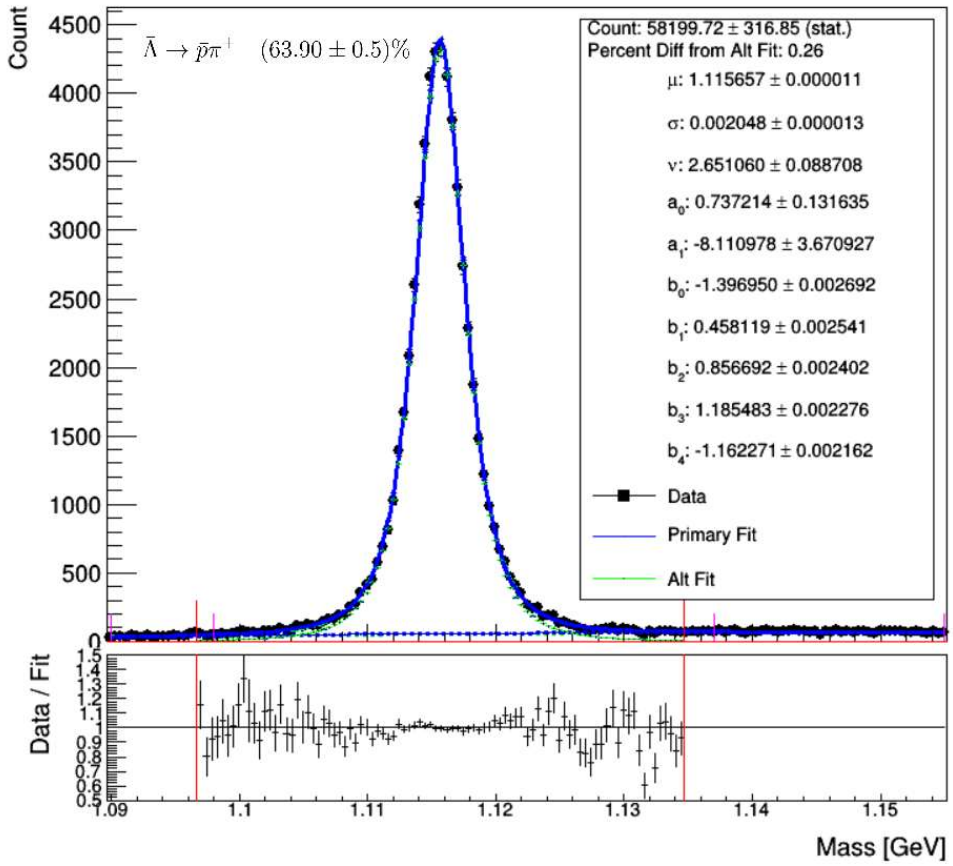

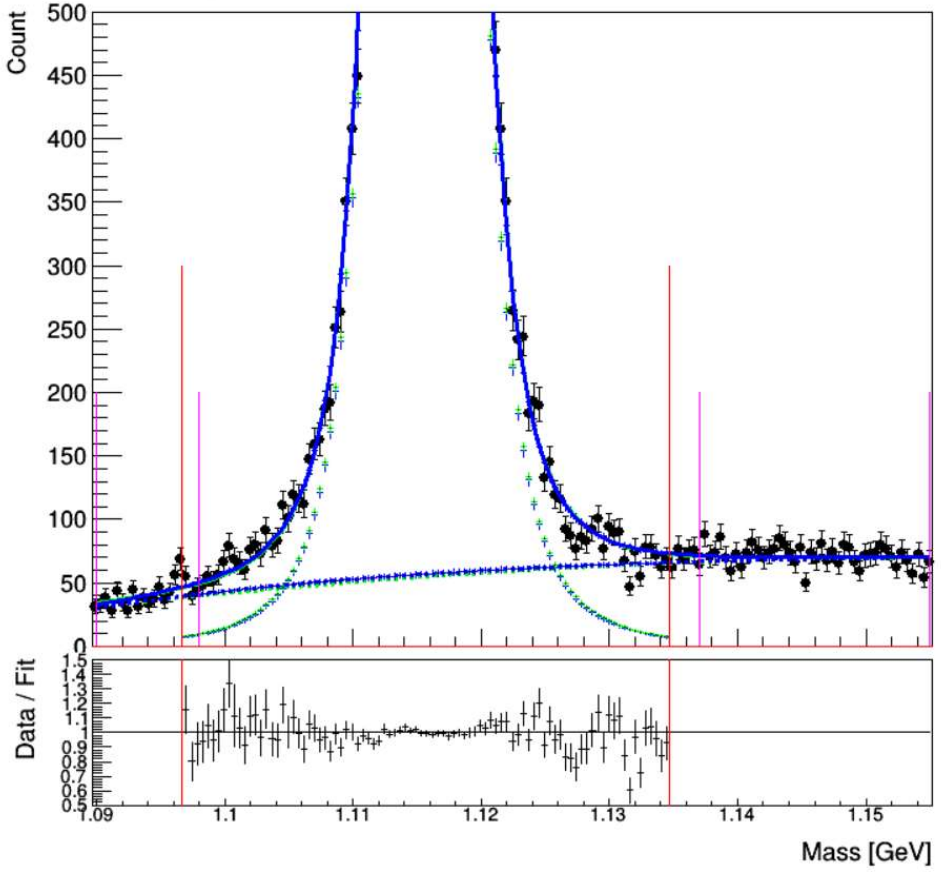

Cross Section Definitions

- Full normalized count of V^0 (particles identified in secondary decay vertex) defined in terms of this cross section within the detector's visible range:

$$5 < Q^2[\mathrm{GeV}^2] < 100 \qquad 0.1 < y < 0.6$$
$$0.5 < p_T(V^0)[\mathrm{GeV}] < 3.5 \qquad -1.3 < \eta(V^0) < 1.3$$

$$\sigma_{vis}(ep \to e' V^0 X) = \frac{N}{\mathcal{L} \cdot \epsilon \cdot BR \cdot (1 + \delta_{QED})}$$

$$\epsilon = \epsilon_{rec} \cdot \epsilon_{trig} \qquad \epsilon_{rec} = \frac{N_{rec}^{MC}}{N_{gen}^{MC}} \qquad 1 + \delta_{QED} = \frac{N_{gen}(V^0)^{rad}}{N_{gen}(V^0)^{non-rad}} \cdot \frac{\mathcal{L}^{non-rad}}{\mathcal{L}^{rad}}$$

- Λ - $\bar{\Lambda}$ Asymmetry defined as this ratio of cross sections, many factors cancel out

$$A_\Lambda = \frac{\sigma_{vis}(ep \to e'\Lambda X) - \sigma_{vis}(ep \to e'\bar{\Lambda} X)}{\sigma_{vis}(ep \to e'\Lambda X) + \sigma_{vis}(ep \to e'\bar{\Lambda} X)} = \frac{\frac{N_\Lambda}{\epsilon_{rec,\Lambda}} - \frac{N_{\bar{\Lambda}}}{\epsilon_{rec,\bar{\Lambda}}}}{\frac{N_\Lambda}{\epsilon_{rec,\Lambda}} + \frac{N_{\bar{\Lambda}}}{\epsilon_{rec,\bar{\Lambda}}}}$$

Detector Efficiencies

- Correction for bin migration effects and detector inefficiencies for particle counts is done with this:

$$\epsilon_{rec} = \frac{N_{rec}^{MC}}{N_{gen}^{MC}}$$

- Trigger efficiencies calculated via detector simulation (simulation found to be accurate within 1% comparing with trigger efficiencies calculated with independent monitor triggers in data in previous analyses – more important for full normalized cross section measurements)
- We extract the total number of particles we observe from MC in the invariant mass peaks and compare to the true number of Λ or $\overline{\Lambda}$ provided by the generator within our visible range that we could potentially reconstruct, corrects data to truth level
  - Important that GEANT3 has reasonable description of reconstructed quantities, especially with respect to variables we impose selections on (Control Plots)

Detector Efficiencies

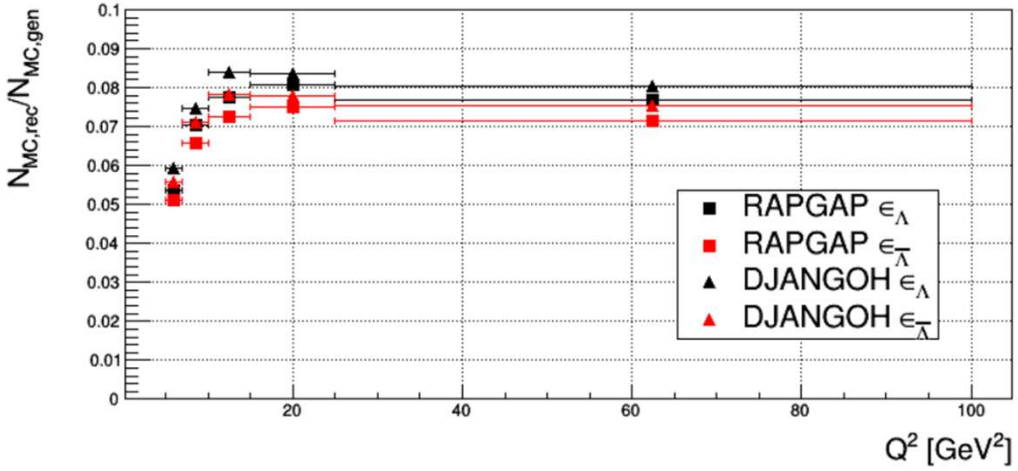

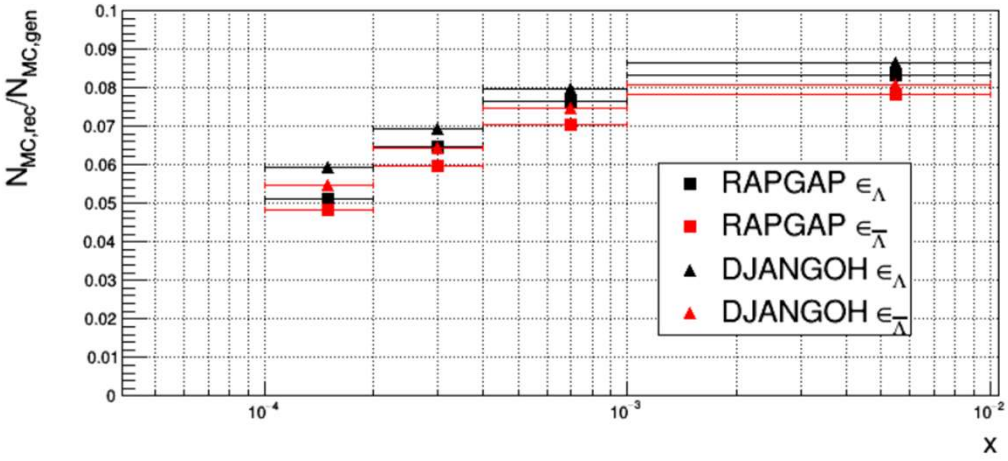

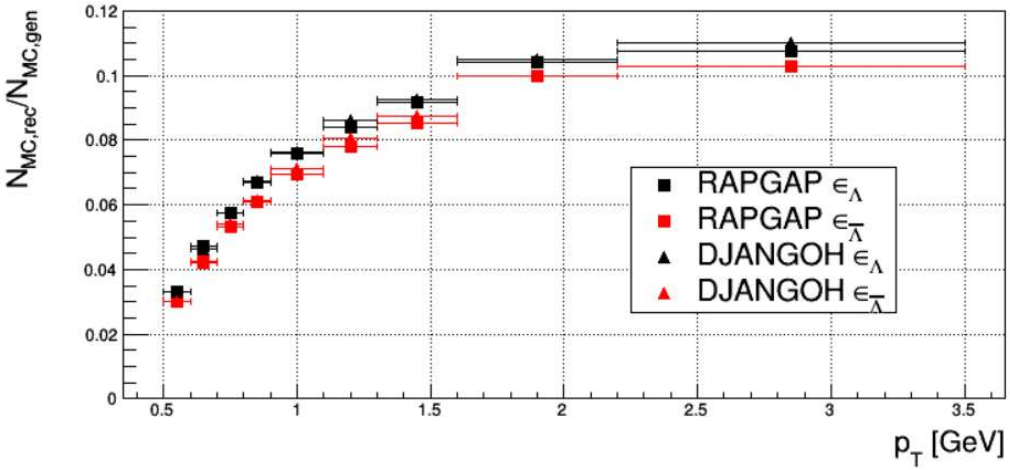

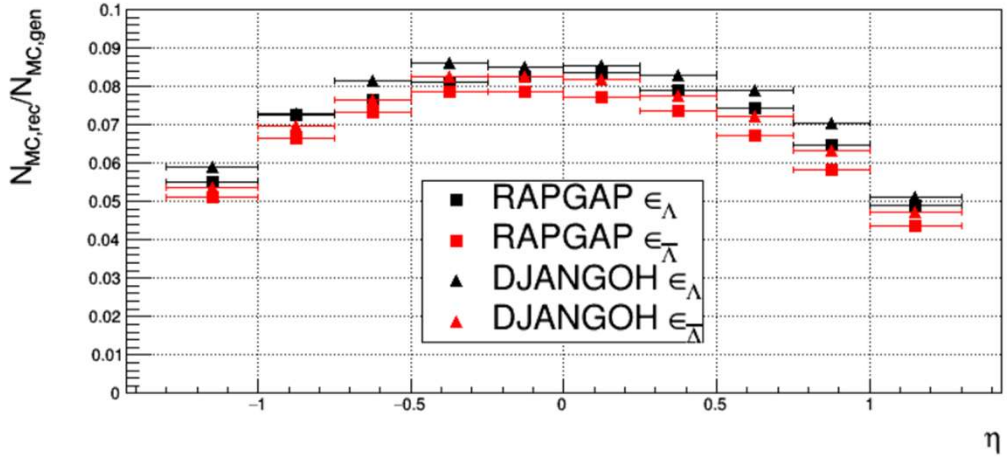

Uncertainties

$$\sigma_{vis}(ep \to e' V^0 X) = \frac{N}{\mathcal{L} \cdot \epsilon \cdot BR \cdot (1 + \delta_{QED})}$$

$$A_\Lambda = \frac{\sigma_{vis}(ep \to e'\Lambda X) - \sigma_{vis}(ep \to e'\overline{\Lambda} X)}{\sigma_{vis}(ep \to e'\Lambda X) + \sigma_{vis}(ep \to e'\overline{\Lambda} X)}$$

For Asymmetry we have three primary sources of systematic uncertainty:

- Signal Extraction
- Model (RAPGAP vs DJANGOH)
- MC Nuclear Interaction

Other systematics from cross sections cancel in the ratio

Source
~~E'_e~~
~~θ_e~~
signal extraction
model
~~trigger efficiency~~
~~track reco~~
~~luminosity~~
~~branching ratio~~

Uncertainties

Statistical-

- The statistical uncertainty used is the yield uncertainties calculated in RooFit which takes into account the propagated uncertainties of the RooFit parameters combined with the $\sqrt{N}$ statistical uncertainty (N total number of observed counts in final invariant mass range)

Systematic- $\delta A_\Lambda = |A_\Lambda - A_{\Lambda,variation}|$

- Systematic uncertainties are taken as the full difference between the nominal asymmetry value (using RAPGAP for detector efficiency) and the asymmetry recalculated for the variation
  - Ex: For the model uncertainty, the asymmetry is calculated once with RAPGAP and once with DJANGOH and the uncertainty associated with this variation is the absolute value of their difference, this way correlated effects are properly accounted for

Systematic Uncertainty Variations

$$\delta A_\Lambda = |A_\Lambda - A_{\Lambda,variation}|$$

- Variation 1: 4th order Polynomial as BG Function
- Variation 2: Different Signal extraction range (6 FWHM → 8 FWHM)
- Variation 3: Only Fit BG and subtract raw signal
- Variation 4: Assume MC description of Nuclear Interactions is 100% incorrect
- Variation 5: Calculate detector efficiencies with DJANGOH instead of RAPGAP

MC Nuclear Interaction Estimations

- For the expected asymmetry on the order of a few percent, we must make sure interactions with detector material is well described in Monte Carlo
- Monte Carlo has access to truth level information, so we can use those datasets to count how many Λ or $\overline{\Lambda}$ that pass all of our selections come from interactions with the detector material in the GEANT simulation
- If the Monte Carlo perfectly described the real detector, these would be all accounted for in the detector efficiency calculation
- For this uncertainty we assume MC underestimates this background by a conservative 100% and recalculate the asymmetry with this estimated excess of Λ ($\overline{\Lambda}$ is found to not contribute in the MC study as expected)

- H1 detector simulation in previous studies is known to have ~7% less material between the beam line and CJC1 in MC compared to data and ~12% More material in MC between CJC1 and CJC2 by investigating energy loss of pion tracks
  - Should be well accounted for by our estimation of 100% inaccuracy

Total Asymmetry Results for 2005-2006 HERAII DST7

$5 < Q^2[\mathrm{GeV}^2] < 100$ $\quad 0.1 < y < 0.6$

$0.5 < p_T(V^0)[\mathrm{GeV}] < 3.5$ $\quad -1.3 < \eta(V^0) < 1.3$

$$A_\Lambda = 0.0186 \pm 0.0035(\mathrm{stat.}) \pm 0.0027(\mathrm{syst.})$$

Individual Systematic Error Contributions:

Variation Method	δA_Λ
RAPGAP vs DJANGOH	0.0016
Nuclear Interactions	0.0018
Alternate BG Fit	0.000013
Raw Signal Extraction	0.000061
Signal Extraction Range	0.000062

- Then can follow same procedures and calculated efficiencies within different bins to see Asymmetry distributions

Asymmetry Distributions

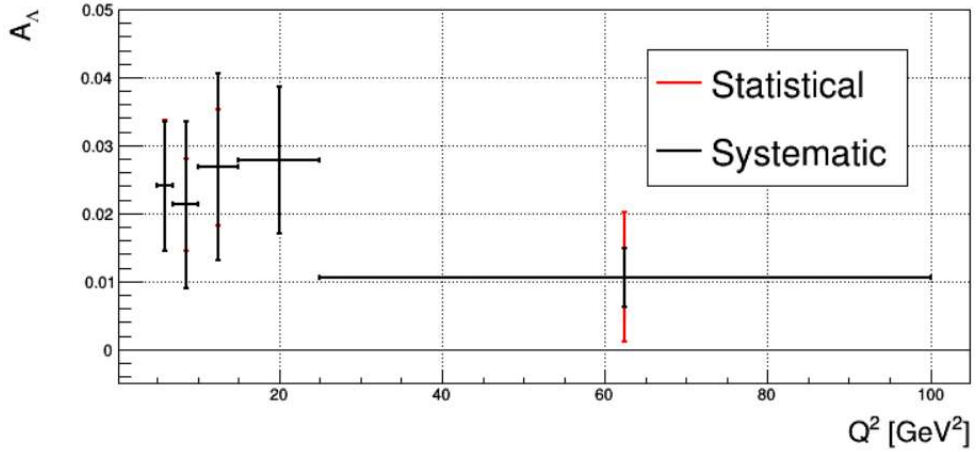

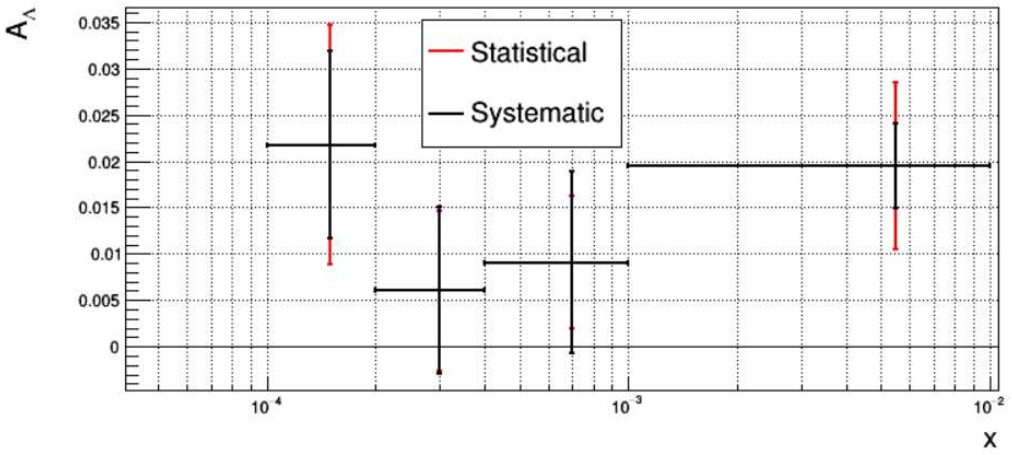

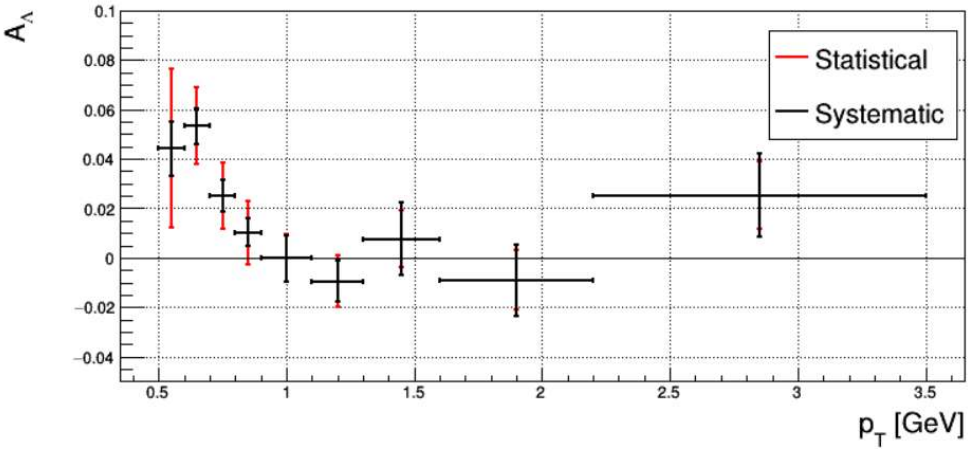

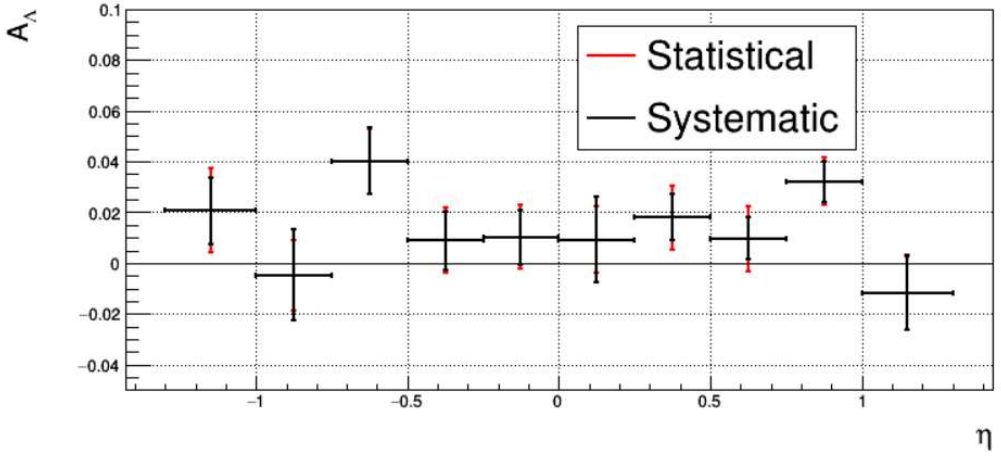

Uncertainty Contributions in Distributions

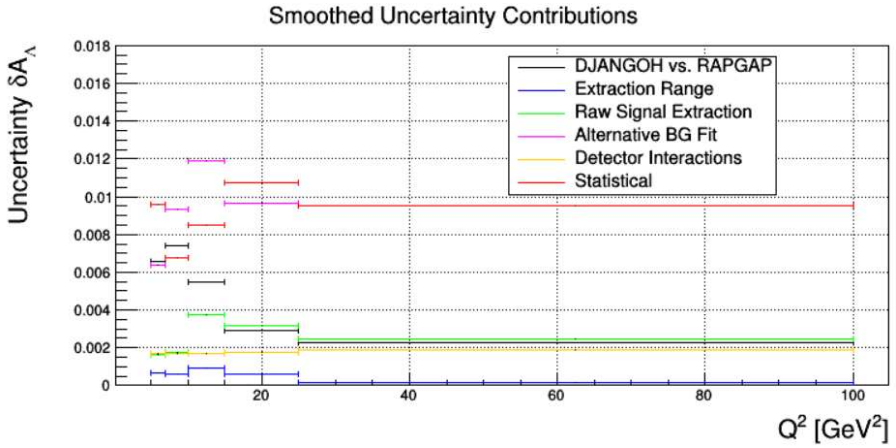

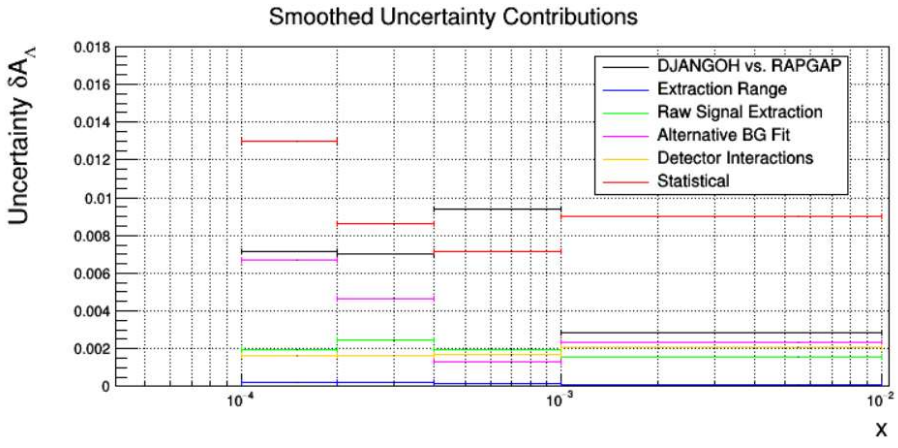

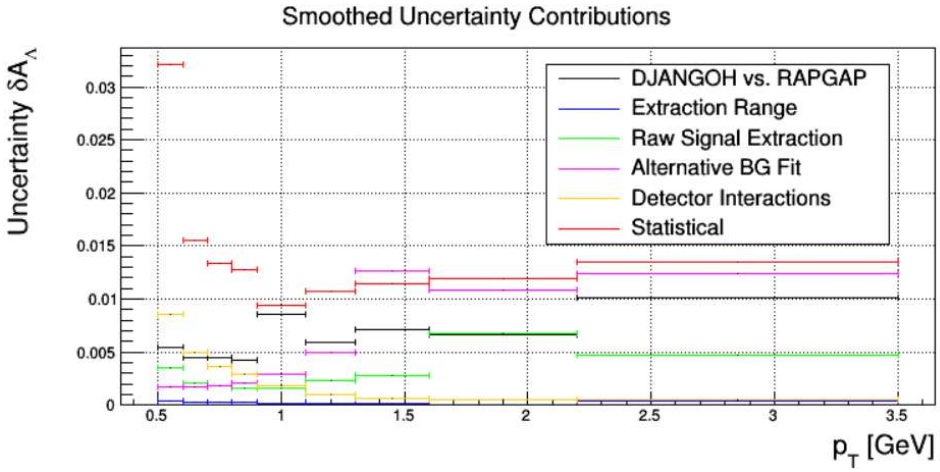

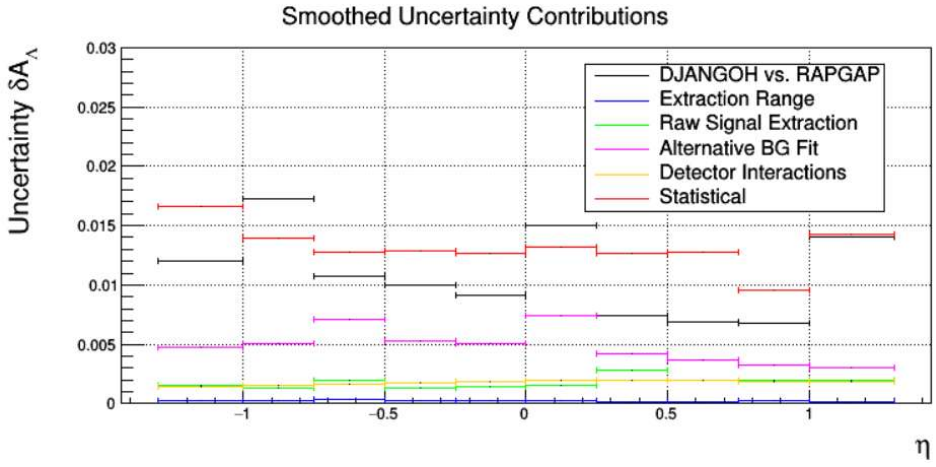

Guassian Smoothing of Systematic Uncertainty Distributions

- Always some unphysical statistical fluctuations of uncertainties bin to bin
  - So as not to overestimate or underestimate uncertainties a standard smoothing procedure is implemented
- Taking a normalized Gaussian at each point in the systematic uncertainty distribution with (sigma = twice the Bin Width of given point)
- Then re-calculate the systematic errors as a weighted average at the given point where each bin may contribute some (mostly from neighboring points) weighted by each values gaussian distribution bleeding into other bins
- If an uncertainty is re-calculated to be less than 85% of its originally value, we just take the 85% value to not accidentally underestimate anything
- Done for all systematic error contributions
- Smoothed vs Unsmoothed Error Contributions in Backup Slides

Conclusion

$$A_\Lambda = 0.0186 \pm 0.0035(\text{stat.}) \pm 0.0027(\text{syst.})$$

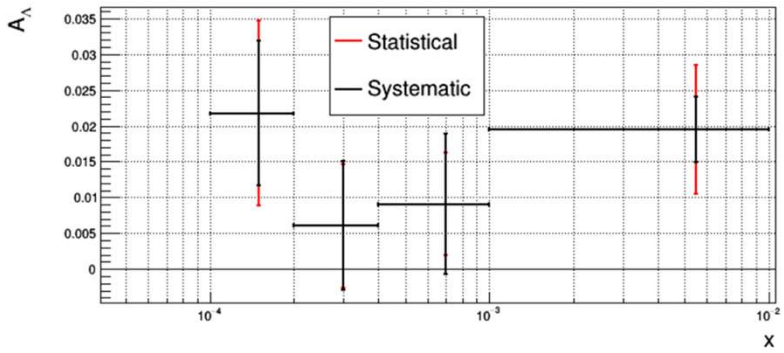

- There does appear to be a non-zero baryon asymmetry in DIS which suggests transfer of baryon number from the proton target to particles visible in the hadronic final state
- Asymmetry is on the order of a few percent and at low-x which supports the idea of a baryon junction, more precise theoretical estimates and measurements (possibly at the EIC) needed to conclusively distinguish the valence quark and baryon junction picture but this result provides good indication of baryon junction and justifies further research in the area
- Working with H1 Collaboration to finalize a preliminary result to share at DIS 2026 and open results to broader audience

EIC Outlook

- EIC is expected to provide collisions up to $\sqrt{s} = 141$ GeV
  - Therefore cannot reach as low in x as HERA at $\sqrt{s} = 319$ GeV, another reason why DPHEP efforts from H1 are so important
- BUT still low enough in x to see baryon junction signatures and the EIC is expected to provide up to 100x more integrated luminosity thanks to advances in accelerator science and will have the advantage of advancements in detector design as well for precise particle identification [6]
- Allows high precision tests of many processes, and can also more accurately map out baryon asymmetries in DIS

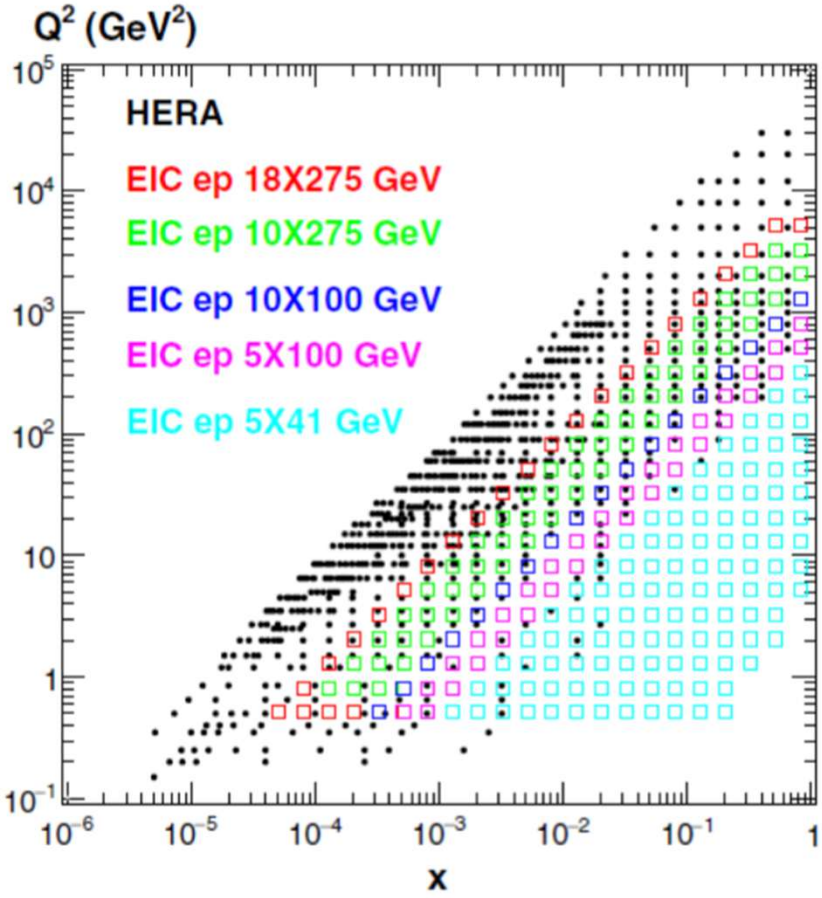

https://doi.org/10.1103/PhysRevD.109.054019

Further Research

- Strange Particle production – enhanced HERAII statistics and update on previous 2009 publication which had a DST5 bug present in the analysis
  - Plots on the right from H1 Collaboration Meeting December 9, 2012 from researchers working on K_S^0 production in DIS at HERA II
  - Bad description of FRUNZ – Fraction of unized z-hits on pion tracks in the CJC, skewed results by ~12% in the publication, has not been corrected

Strangeness Production at low Q^2 in Deep-Inelastic ep Scattering at HERA

https://doi.org/10.1016/j.physletb.2024.138680

FRUNZ for pions from K^0 on DST5

- Fraction of unused z hits on the pion tracks:

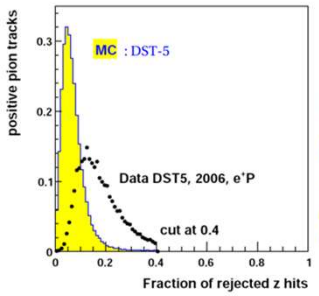

K^0 finder cuts at 0.4

Data distribution is cut off

DST5 data is not well described by MC

MC has much lower tail than data

The K0 efficiency was definitely overstimated by MC ⇒ cross sectoin was low

Fig -6 **Lumi nor.**

FRUNZ for pions from K^0 on DST7

Fraction of unused z hits on pion tracks:

DST7 data is better described by MC

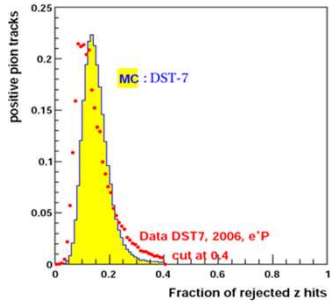

Lumi nor.

Fig -7

Further Research

- Semi-Inclusive Deep Inelastic Scattering (SIDIS)
  - Where some HFS particles are measured in DIS, can use strange particles
- Used to extract transverse momentum dependent parton distribution functions (TMD PDFs)
- Current measurements only use fixed target data, these usually require multi-dimensional binning with respect to kinematic variables, so need a lot of statistics → K_s^0 SIDIS
- H1 data can extend phase space of previous measurements and K_s^0 data can provide new constraints on strange sea quark TMDs

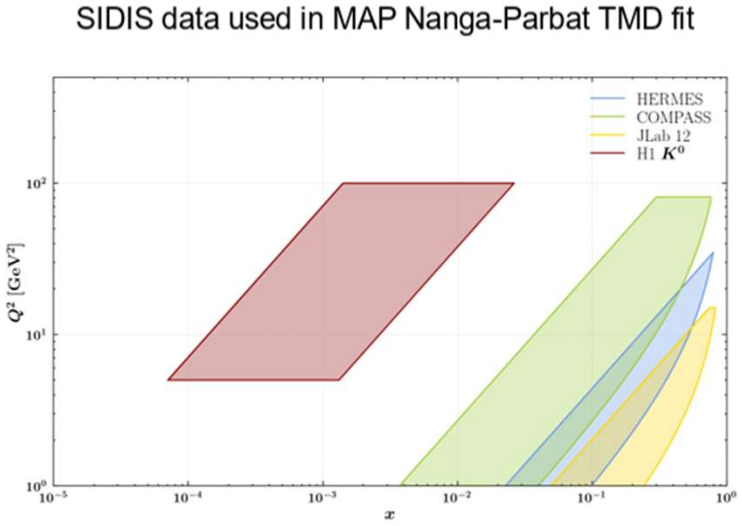

Further Research

- ALICE Λ_c^+ / D^0 measurements with p-p and p-pB colliding systems show significant enhancement with respect to perturbative QCD and Monte Carlo models using fragmentation functions derived from e+/e- collisions
- Interesting to see if enhancement also exists in DIS, questions universality of fragmentation functions
- Only photoproduction of charmed particles has been investigated previously →

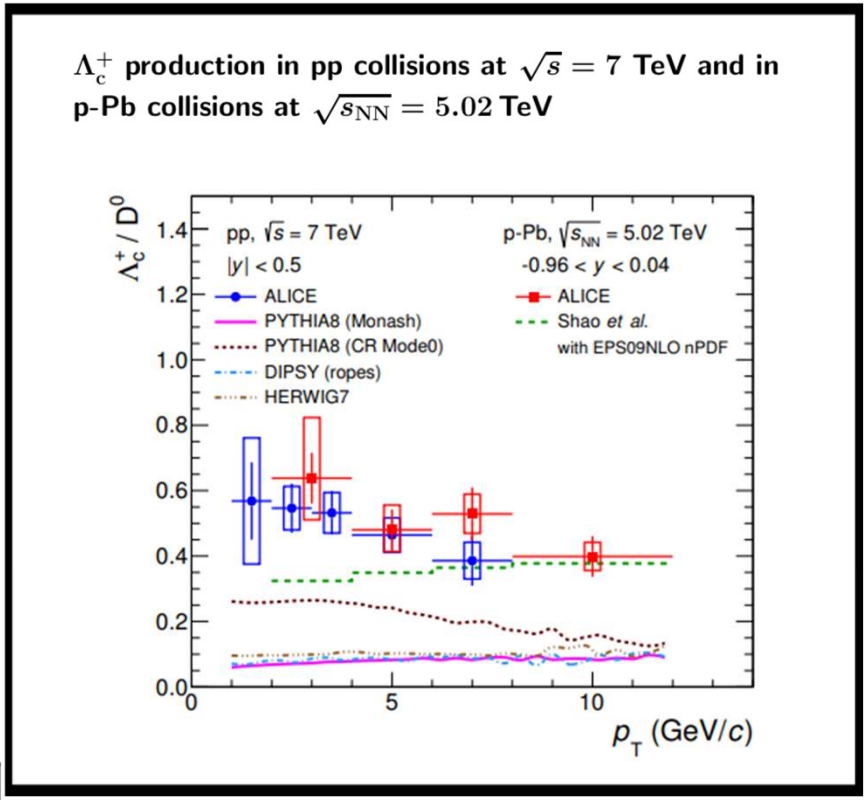

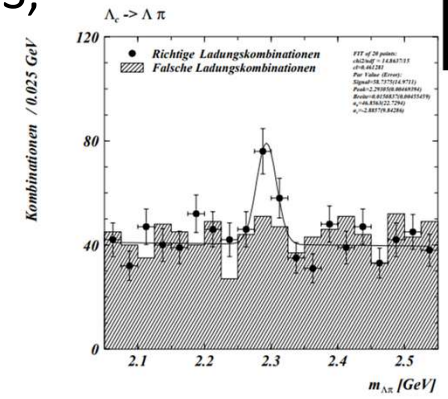

Λ_c^+ Channels:

pK_s^0 $(1.59 \pm 0.08)\%$

$\Lambda\pi^+$ $(1.30 \pm 0.07)\%$

$pK^-\pi^+$ $(6.28 \pm 0.32)\%$

D^0 Channels:

$K^-\pi^+$ $(3.93 \pm 0.04)\%$

Rough Initial Charm Peaks

Λ_c^+ Channels:

pK_s^0 $(1.59 \pm 0.08)\%$
$\Lambda\pi^+$ $(1.30 \pm 0.07)\%$
$pK^-\pi^+$ $(6.28 \pm 0.32)\%$

D^0 Channels:

$K^-\pi^+$ $(3.93 \pm 0.04)\%$

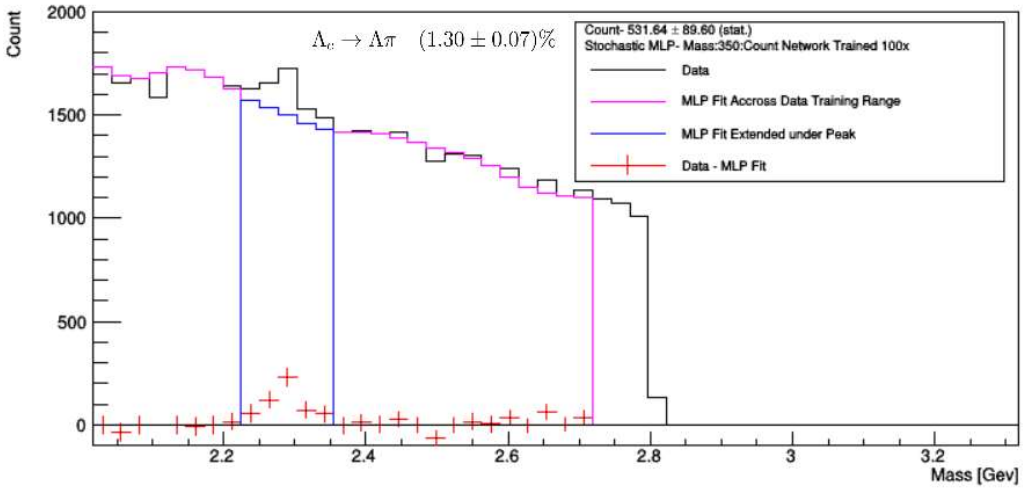

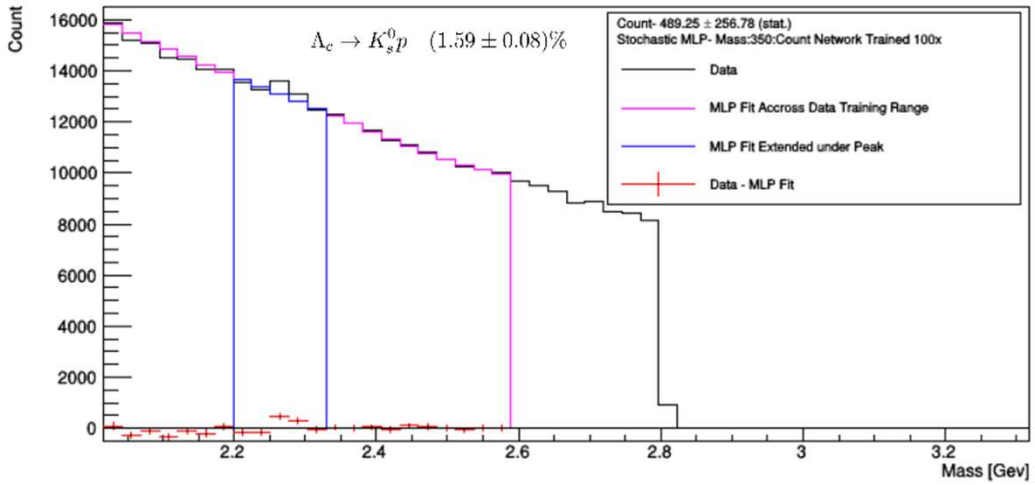

- Using our sample of Λ and K_S^0 combining with tracks of appropriate charge coming from DIS vertex (using analogous cuts as done for strange particle tracks)
- Using MLP class (Multi Layer Perceptron) in Root to model background, no assumptions of functional form for quick count estimate
- Rough statistics as expected, but there is hope for a calculation!

References not directly linked in the presentation

[1] X. Artru. String model with baryons: Topology; classical motion. *Nuclear Physics B.* **85** (1975). https://doi.org/10.1016/0550-3213(75)90019-X

[2] N. Lewis,W. Lv, M.A. Ross, *et al.* Search for baryon junctions in photonuclear processes and isobar collisions at RHIC. *Eur. Phys. J. C* **84**, 590 (2024). https://doi.org/10.1140/epjc/s10052-024-12834-2

[3] N. Magdy, A. Deshpande, R. Lacey, *et al.* Search for baryon junctions in e+A collisions at the electron ion collider. *Eur. Phys. J. C.* **84** (2024). https://doi.org/10.1140/epjc/s10052-024-13702-9

[4] D. Frenklakh, D. Kharzeev, E. Dmitri, W. Li. Signatures of baryon junctions in semi-inclusive deep inelastic scattering. *Phys. Lett. B.* **853** (2024). https://doi.org/10.1016/j.physletb.2024.138680

[5] B. Kopeliovich, B. Povh. Baryon asymmetry of the proton sea at low-x. *Z Phys C - Particles and Fields.* **75** (1997). https://doi.org/10.1007/s002880050515

[6] F. Willeke, J. Beebe-Wang. "Electron Ion Collider Conceptual Design Report 2021." , Feb. 2021. https://doi.org/10.2172/1765663

Armenteros Podolanski Plot

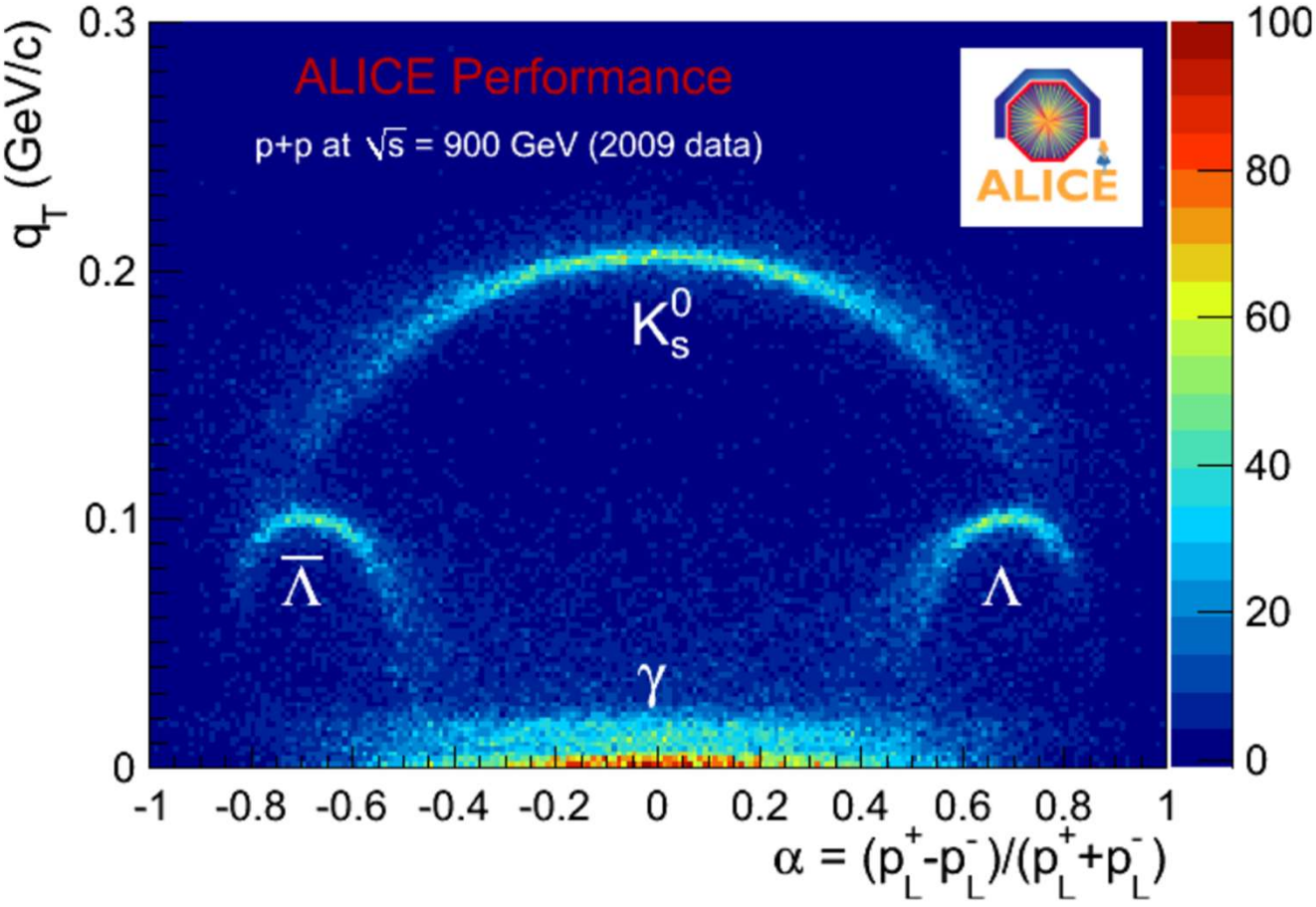

https://cds.cern.ch/record/1323010/plots

Backup

Diff Pt Bound

Requiring pT>1.0 GeV

$$A_\Lambda = 0.0146 \pm 0.0044(\text{stat.}) \pm 0.011$$

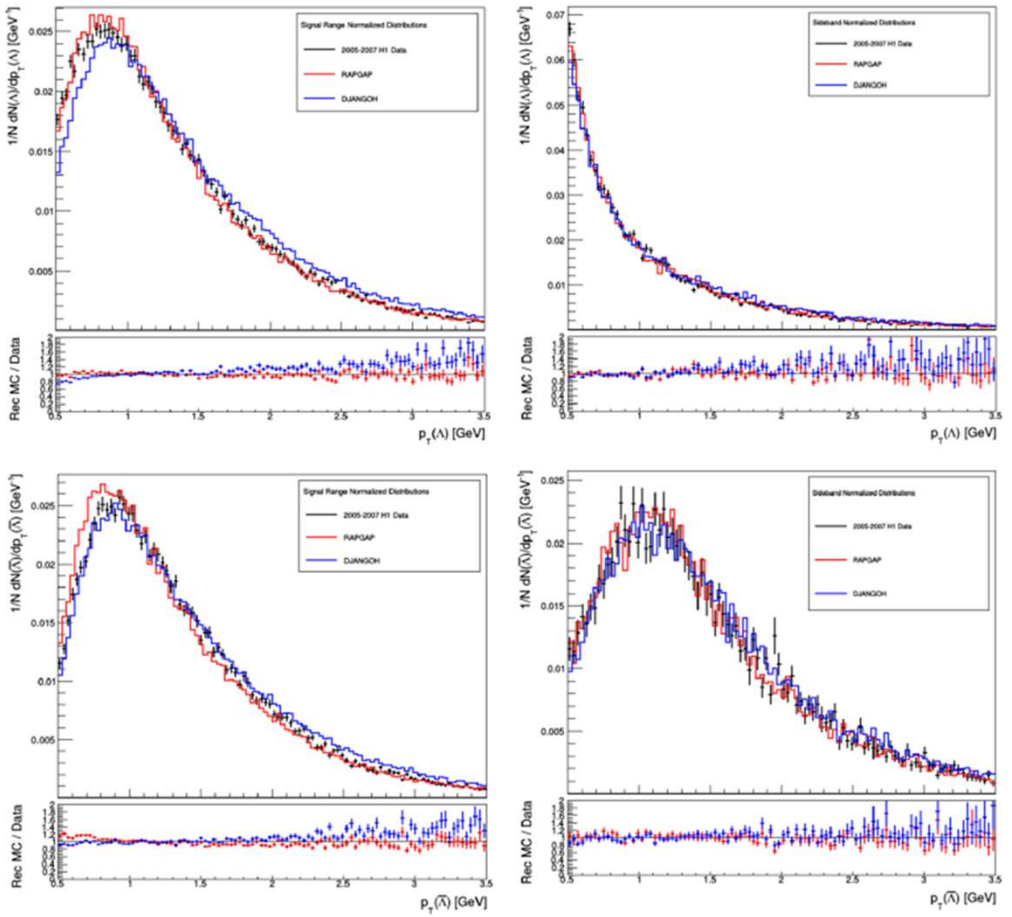

Figure 5.14: Normalized p_T distributions of Λ (top) and $\bar{\Lambda}$ (bottom) candidates in the signal (left) and sideband (right) ranges for Data and MC. These are the distributions following the DIS event selections and all selective cuts.

DIS Control Plots

- Figures in the following slides taken from the draft of my thesis

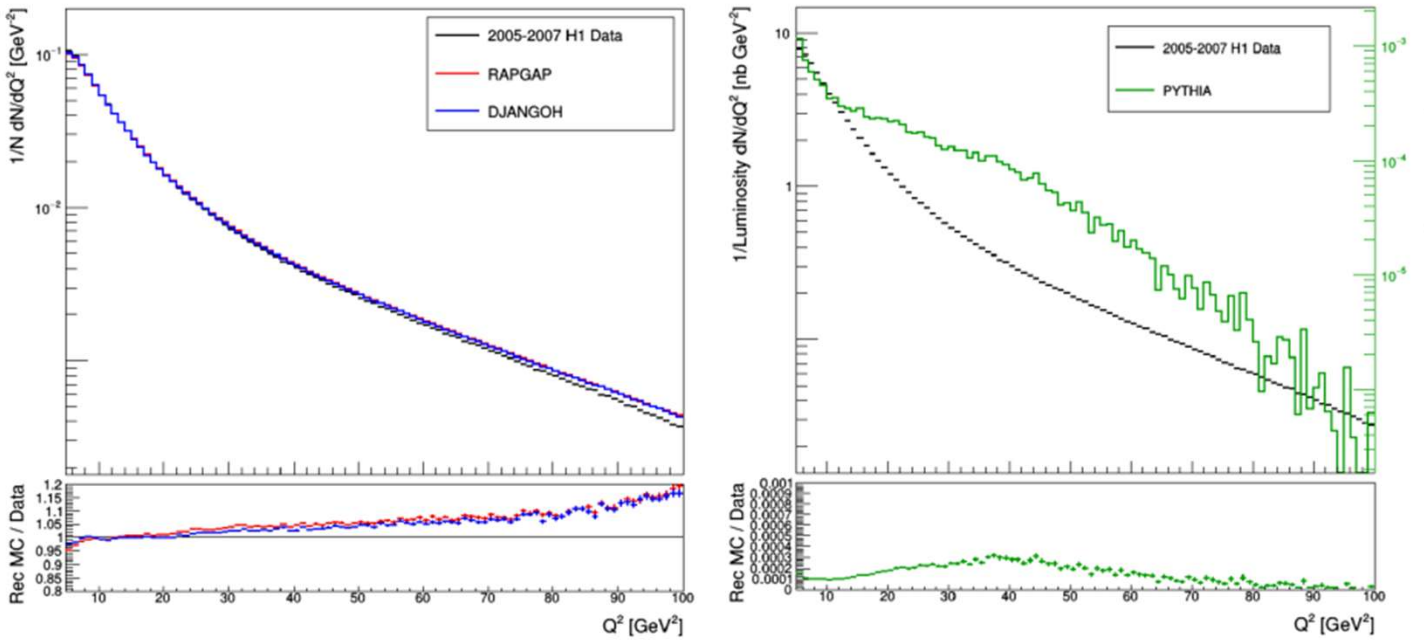

Figure 4.3: Normalized distributions of Q^2 in data and generated $Q^2 > 2$ MC simulation (left) and NC DIS cross sections in data and generated $Q^2 <$ 4+photoproduction (right). Distributions are results of events in respective data sets run through all of our event selections.

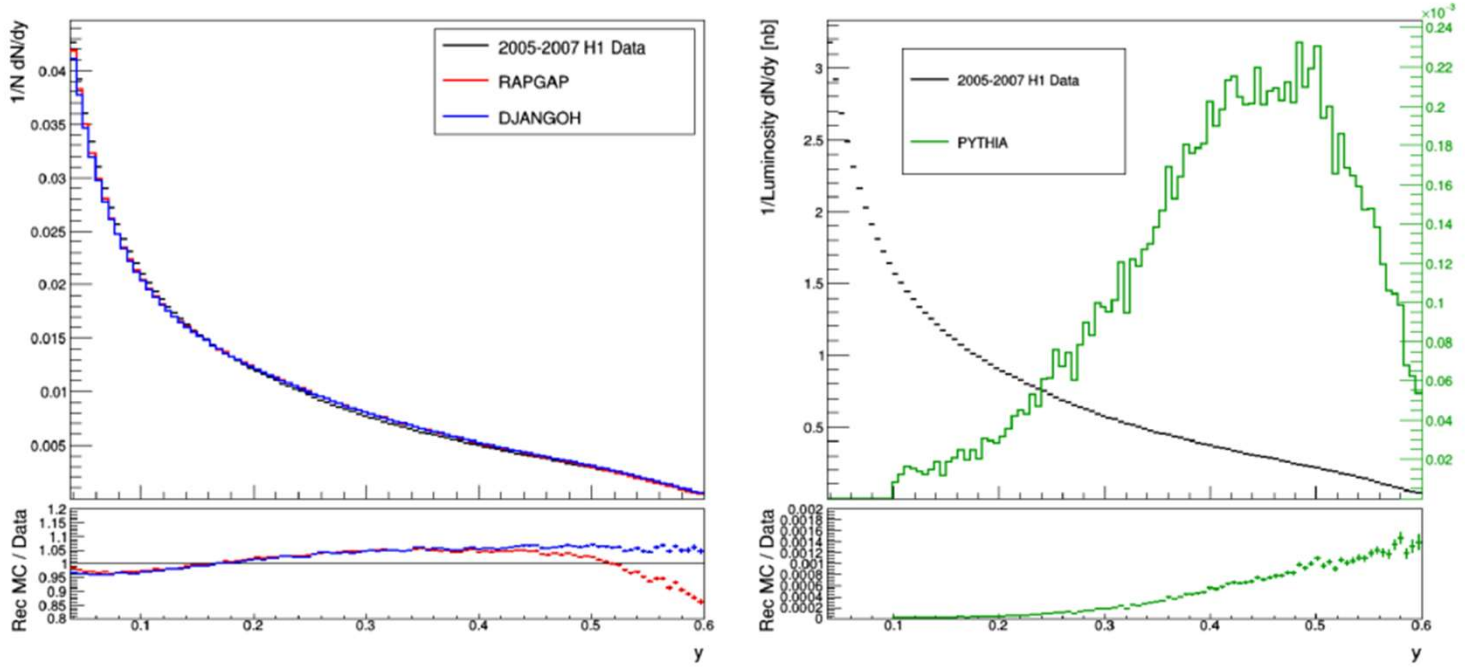

Figure 4.4: Normalized distributions of y in data and generated $Q^2 > 2$ MC simulation (left) and NC DIS cross sections in data and generated $Q^2 < 4$+photoproduction (right). Distributions are results of events in respective data sets run through all of our event selections.

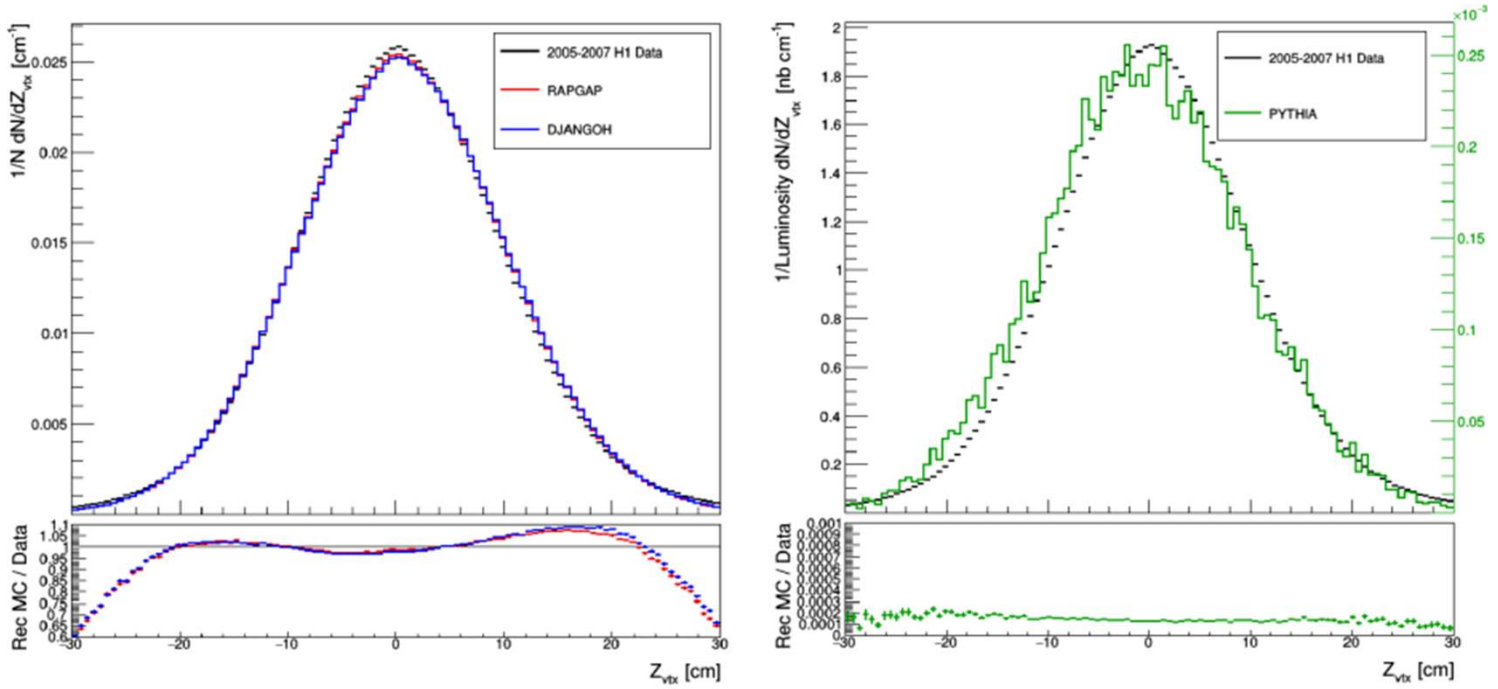

Figure 4.5: Normalized distributions of event z_{vtx} in data and generated $Q^2 > 2$ MC simulation (left) and NC DIS cross sections in data and generated $Q^2 < 4$+photoproduction (right). Distributions are results of events in respective data sets run through all of our event selections.

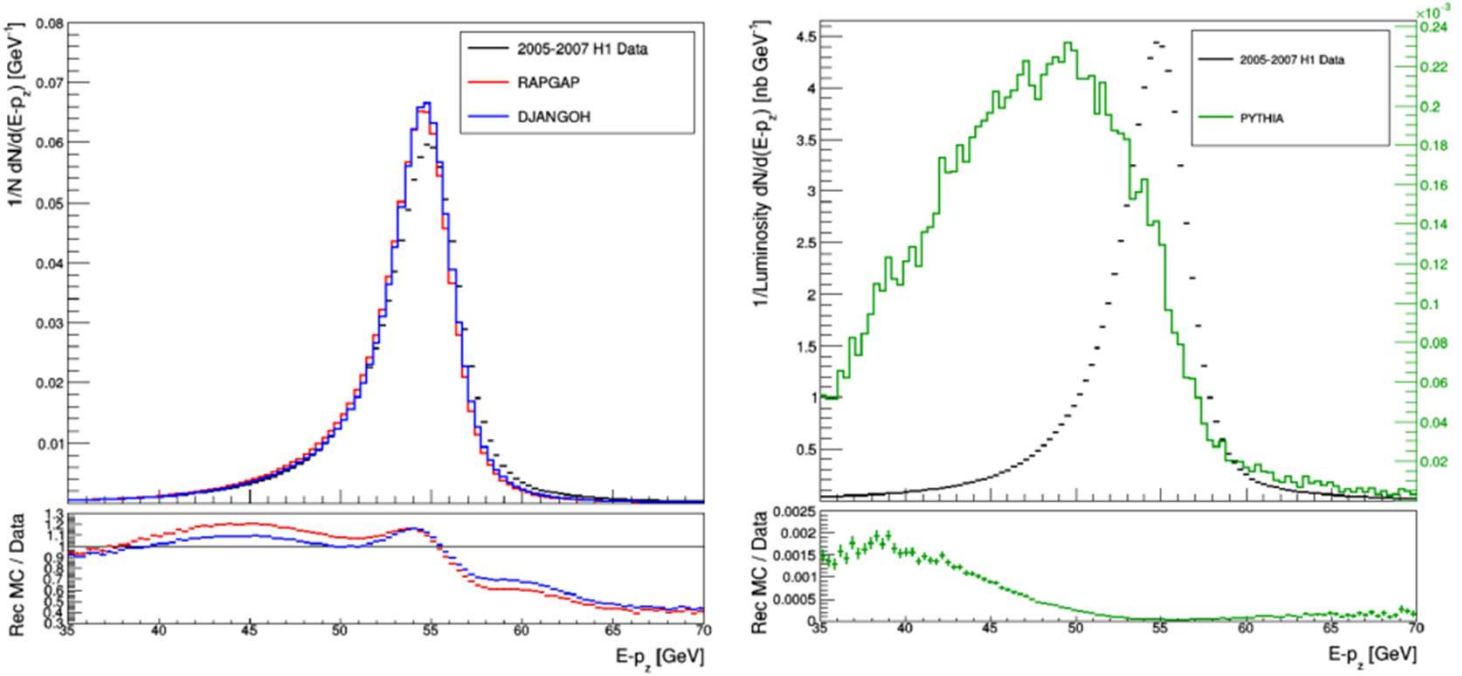

Figure 4.6: Normalized distributions of $E - p_z$ in data and generated $Q^2 > 2$ MC simulation (left) and NC DIS cross sections in data and generated $Q^2 <$ 4+photoproduction (right). Distributions are results of events in respective data sets run through all of our event selections.

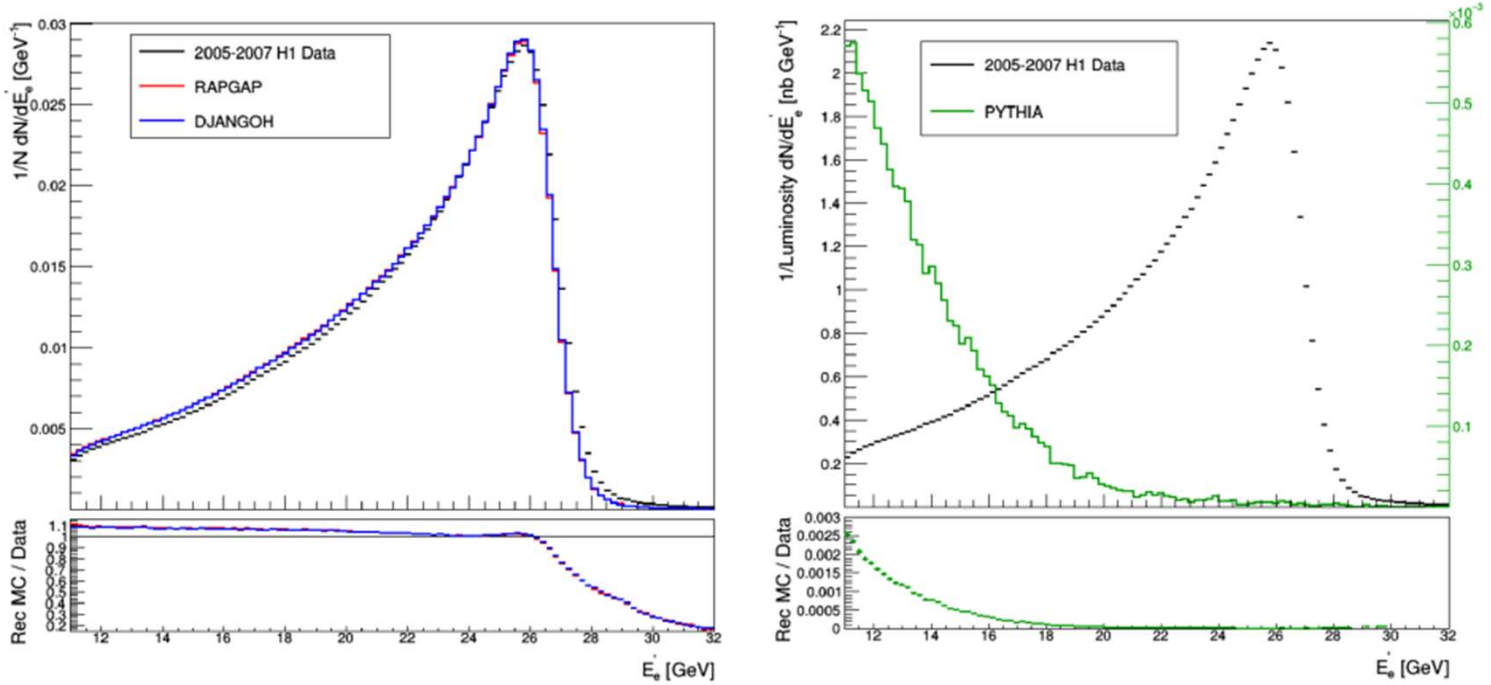

Figure 4.7: Normalized distributions of scattered electron energy E'_e in data and generated $Q^2 > 2$ MC simulation (left) and NC DIS cross sections in data and generated $Q^2 < 4$+photoproduction (right). Distributions are results of events in respective data sets run through all of our event selections.

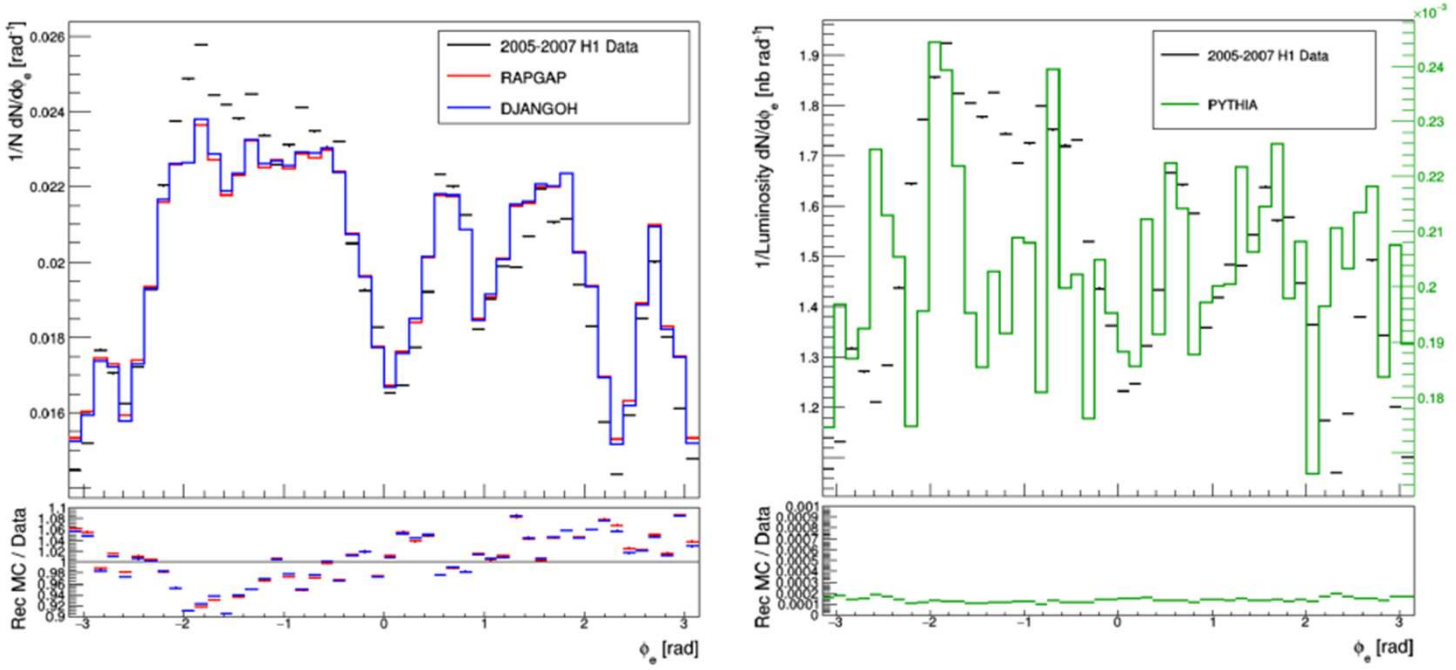

Figure 4.8: Normalized distributions of ϕ_e in data and generated $Q^2 > 2$ MC simulation (left) and NC DIS cross sections in data and generated $Q^2 < 4$+photoproduction (right). Distributions are results of events in respective data sets run through all of our event selections.

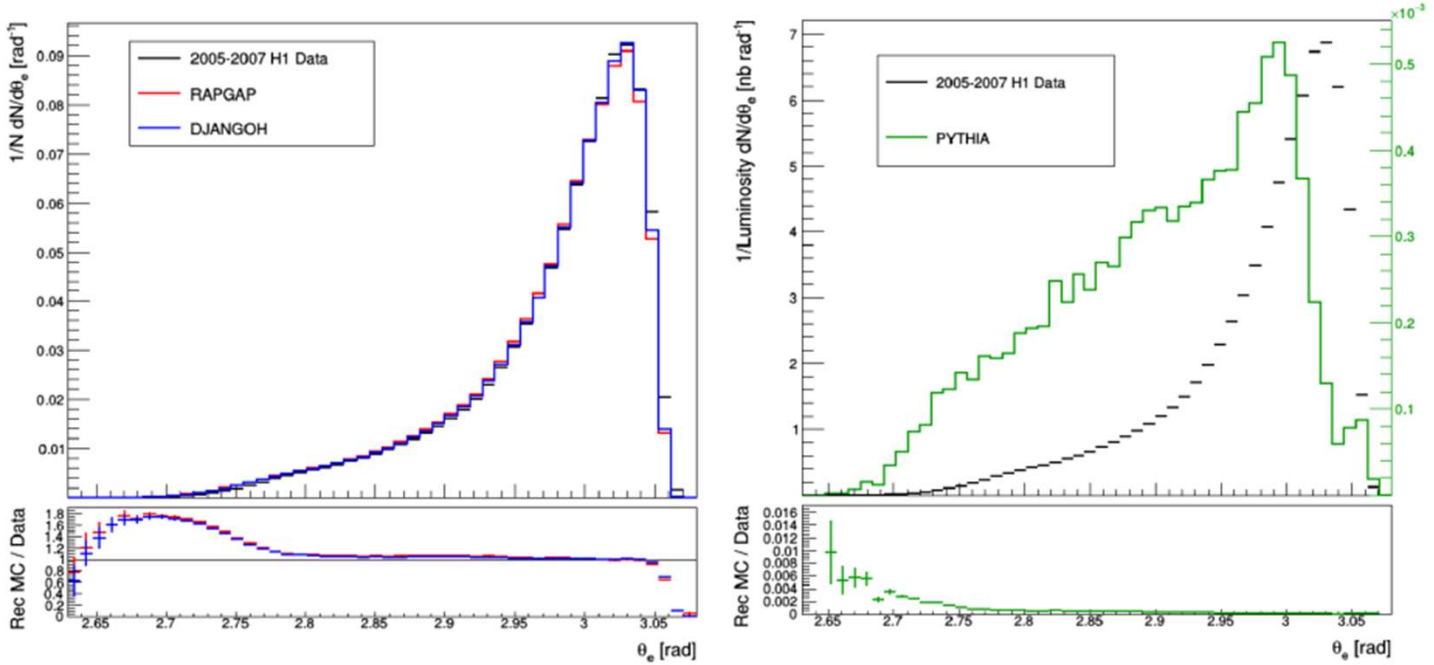

Figure 4.9: Normalized distributions of θ_e in data and generated $Q^2 > 2$ MC simulation (left) and NC DIS cross sections in data and generated $Q^2 < 4$+photoproduction (right). Distributions are results of events in respective data sets run through all of our event selections.

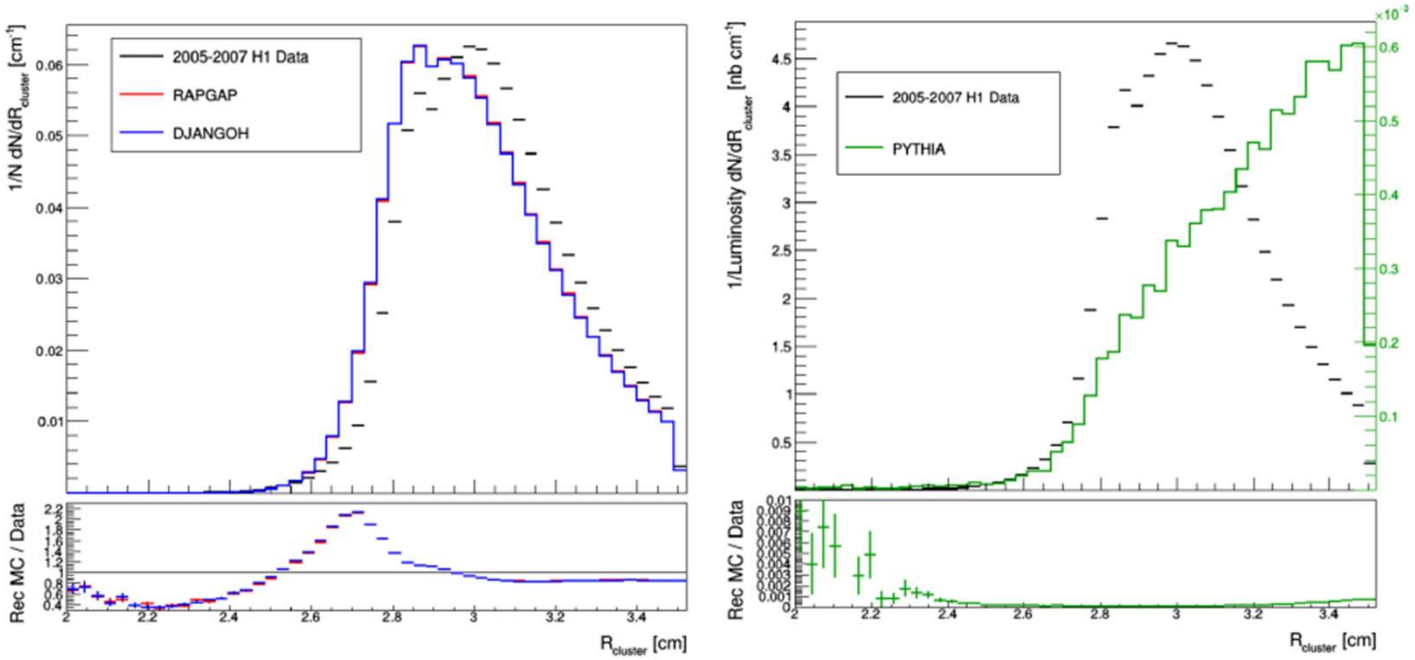

Figure 4.10: Normalized distributions of $R_{cluster}$ in data and generated $Q^2 > 2$ MC simulation (left) and NC DIS cross sections in data and generated $Q^2 <$ 4+photoproduction (right). Distributions are results of events in respective data sets run through all of our event selections.

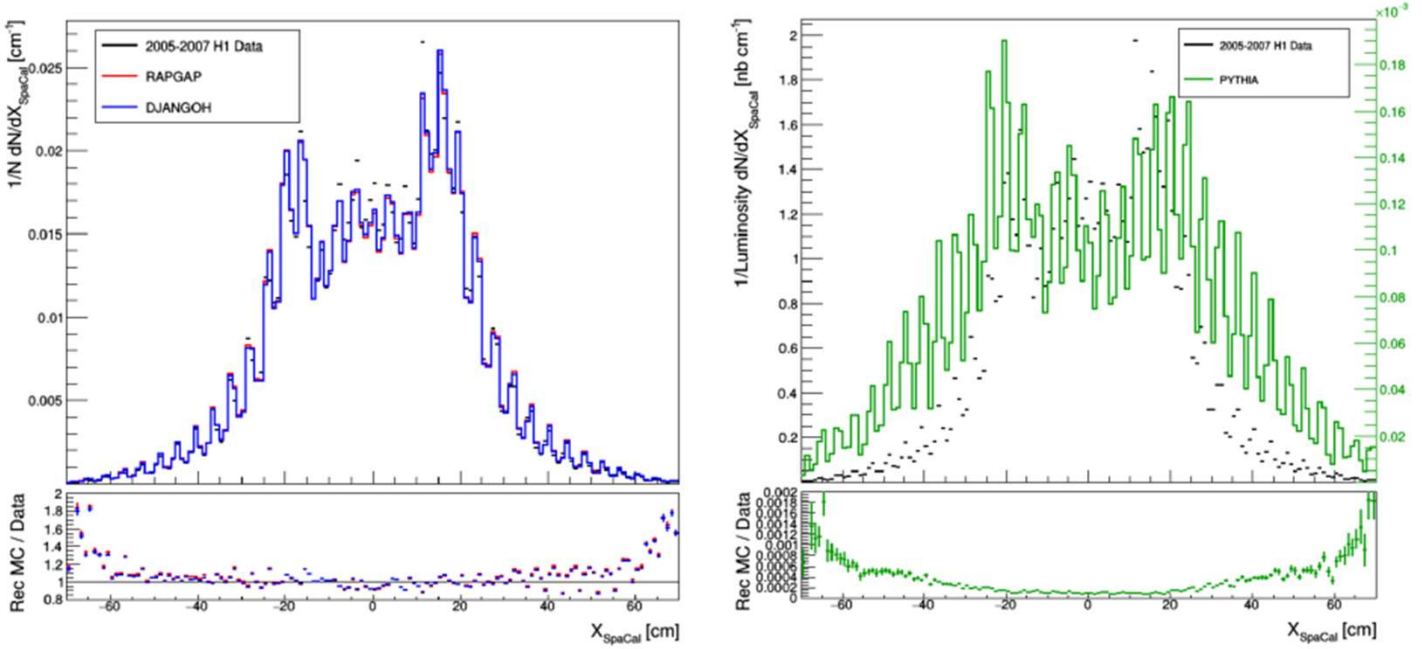

Figure 4.11: Normalized distributions of x_{SpaCal} in data and generated $Q^2 > 2$ MC simulation (left) and NC DIS cross sections in data and generated $Q^2 <$ 4+photoproduction (right). Distributions are results of events in respective data sets run through all of our event selections.

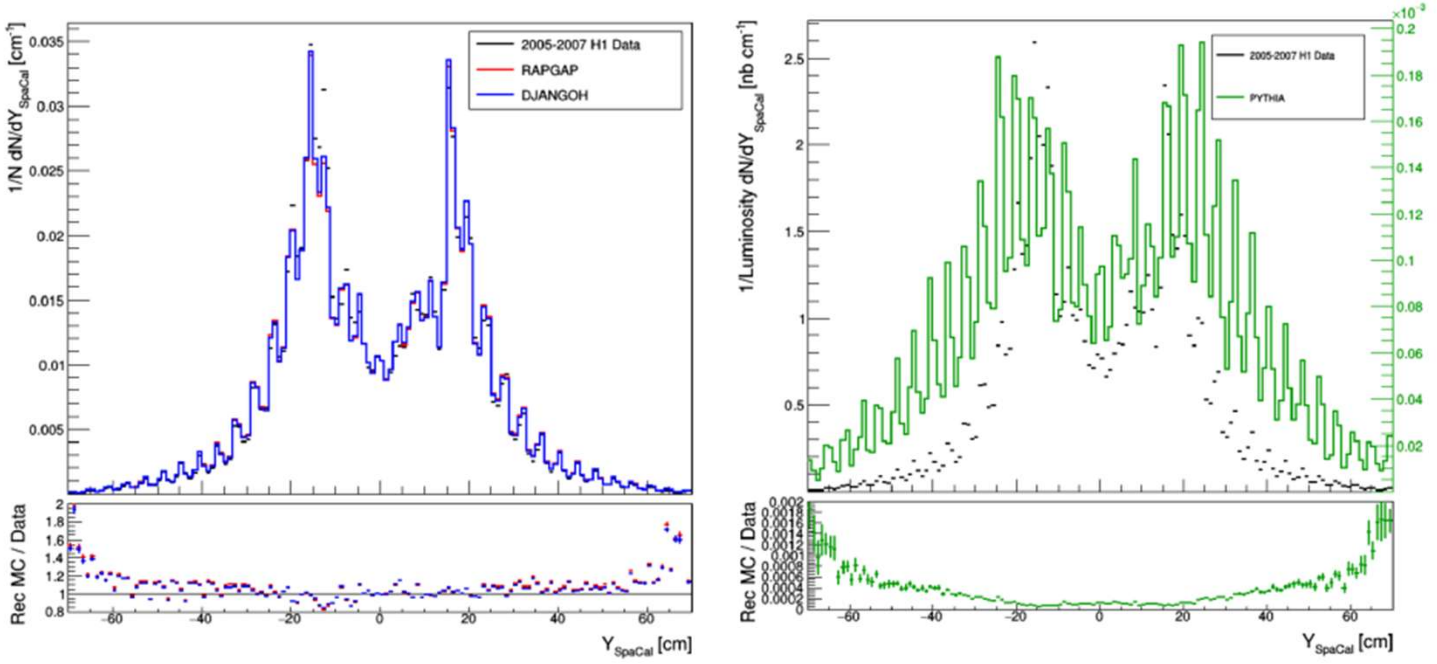

Figure 4.12: Normalized distributions of y_{SpaCal} in data and generated $Q^2 > 2$ MC simulation (left) and NC DIS cross sections in data and generated $Q^2 <$ 4+photoproduction (right). Distributions are results of events in respective data sets run through all of our event selections.

Asym Control Plots

- Figures in the following slides taken from the draft of my thesis

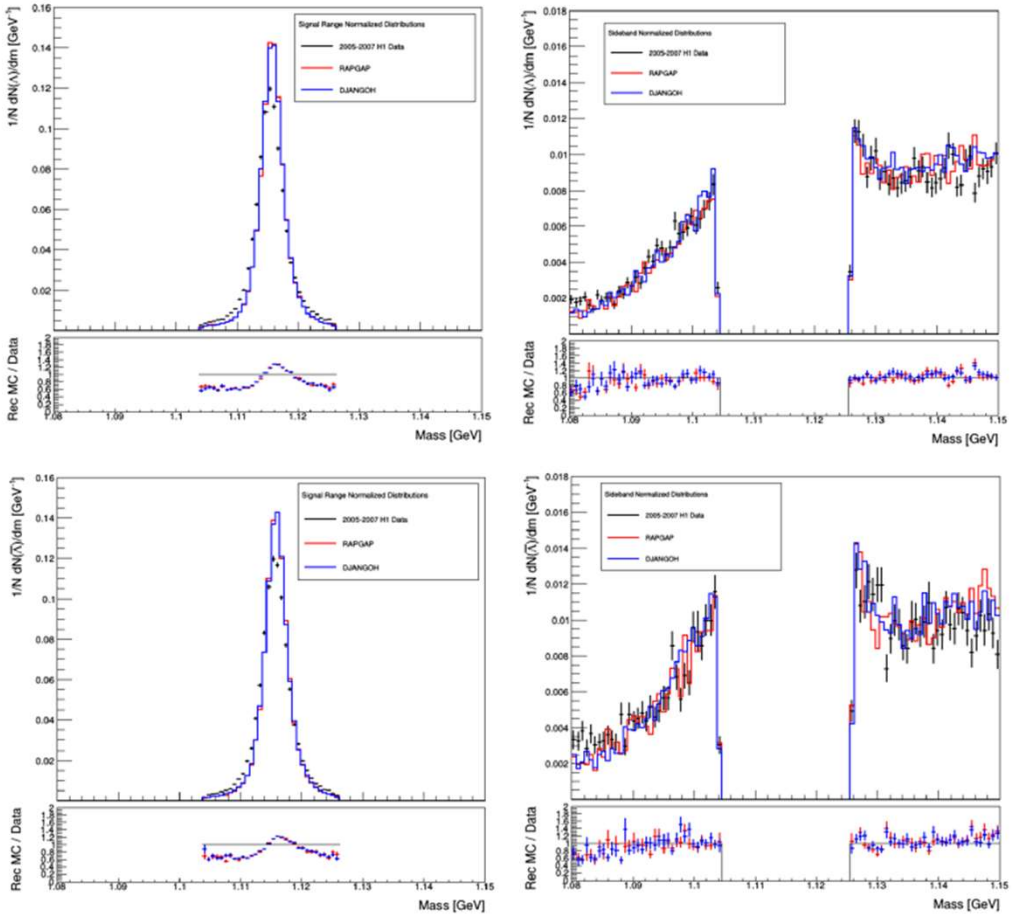

Figure 5.6: Normalized invariant mass distributions of Λ (top) and $\bar{\Lambda}$ (bottom) in the signal (left) and sideband (right) ranges for Data and MC. These are the distributions following the DIS event selections and all selective cuts.

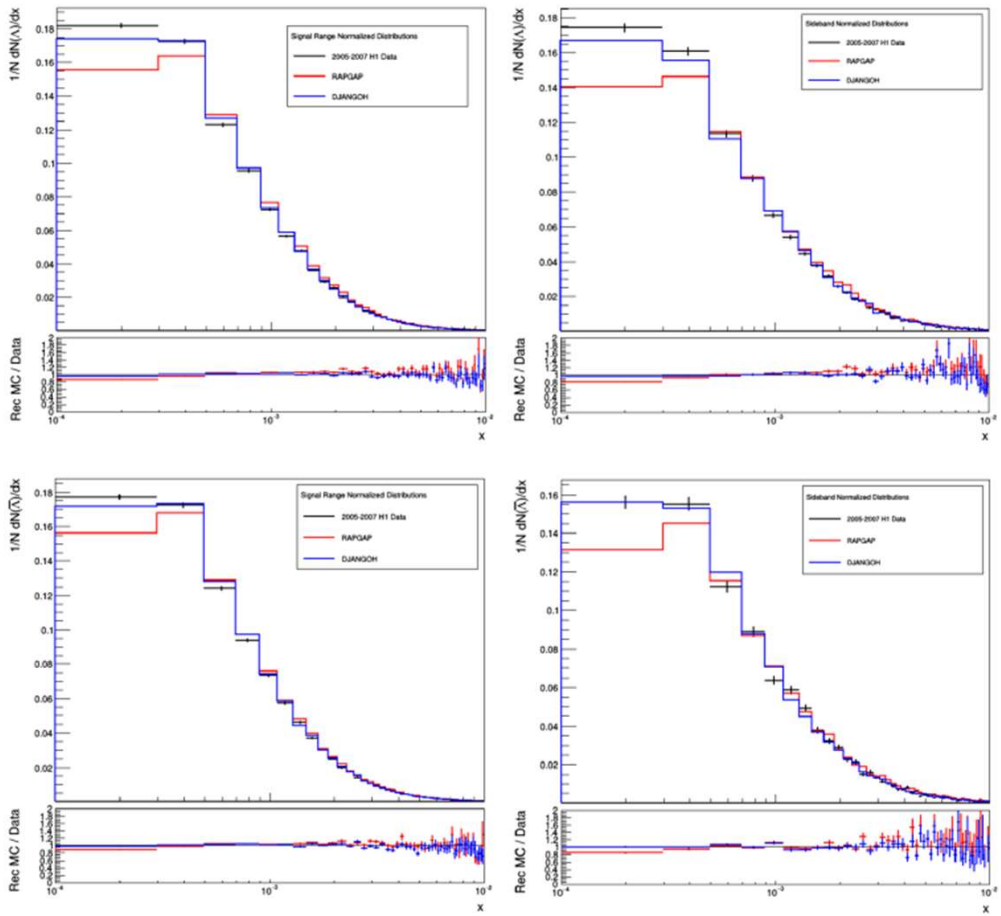

Figure 5.11: Normalized Bjorken-x distributions of Λ (top) and $\bar{\Lambda}$ (bottom) candidates in the signal (left) and sideband (right) ranges for Data and MC. These are the distributions following the DIS event selections and all selective cuts.

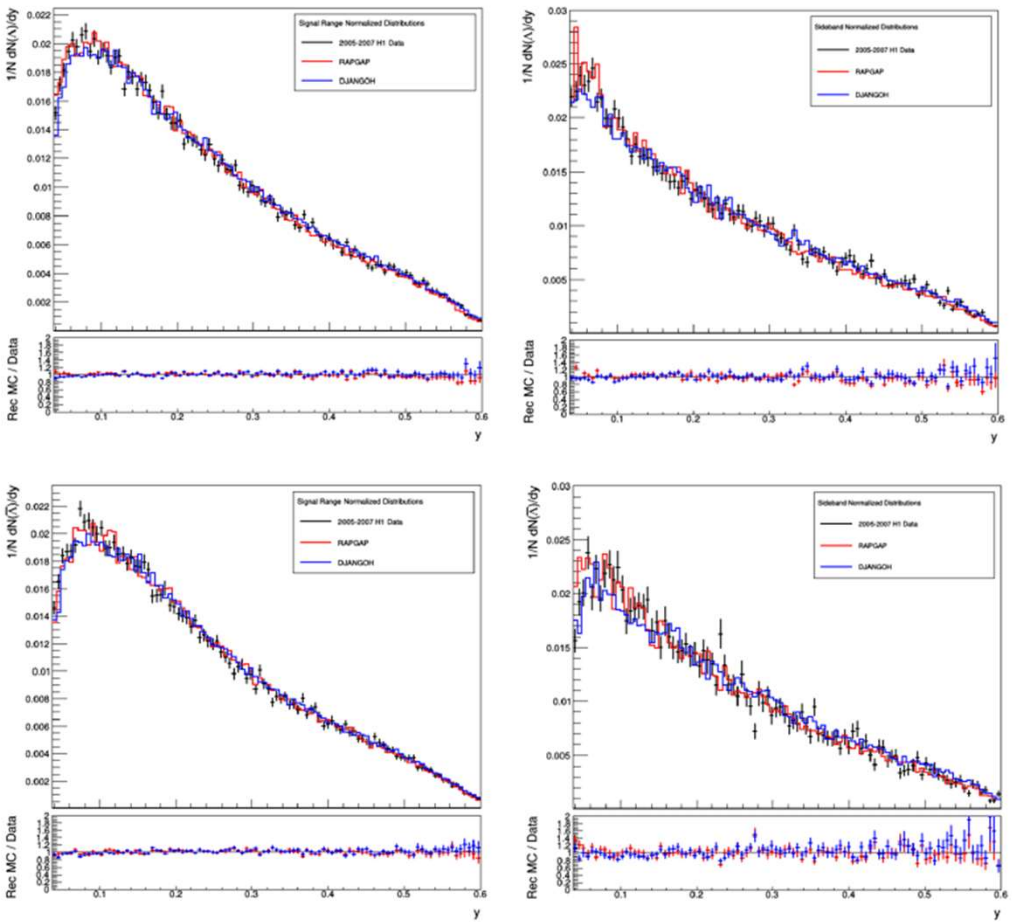

Figure 5.12: Normalized inelasticity (y) distributions of Λ (top) and $\bar{\Lambda}$ (bottom) candidates in the signal (left) and sideband (right) ranges for Data and MC. These are the distributions following the DIS event selections and all selective cuts.

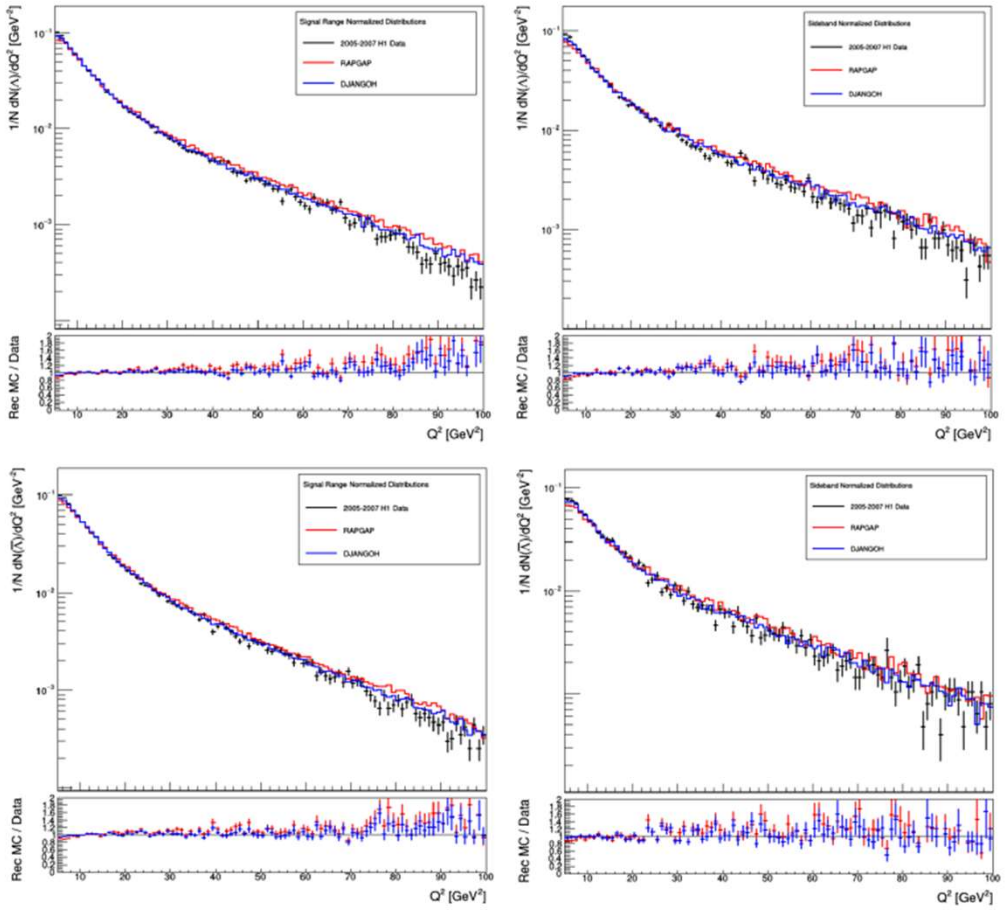

Figure 5.13: Normalized Q^2 distributions of Λ (top) and $\bar{\Lambda}$ (bottom) candidates in the signal (left) and sideband (right) ranges for Data and MC. These are the distributions following the DIS event selections and all selective cuts.

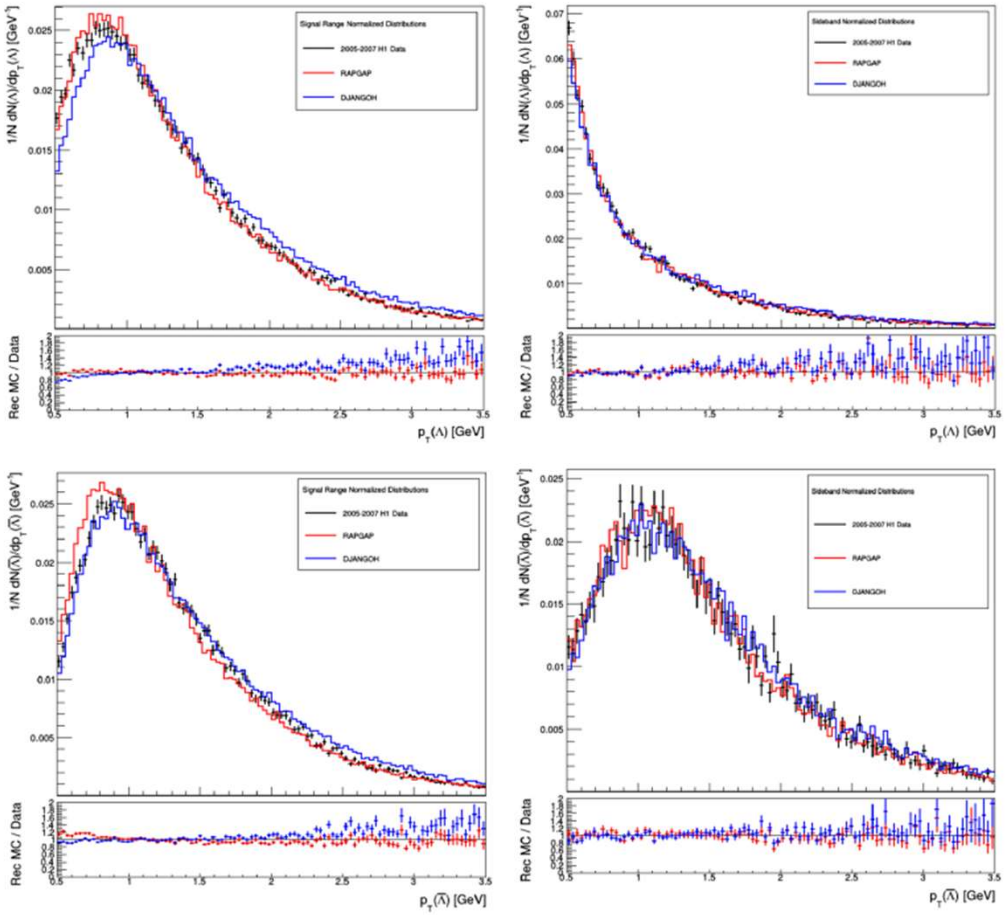

Figure 5.14: Normalized p_T distributions of Λ (top) and $\bar{\Lambda}$ (bottom) candidates in the signal (left) and sideband (right) ranges for Data and MC. These are the distributions following the DIS event selections and all selective cuts.

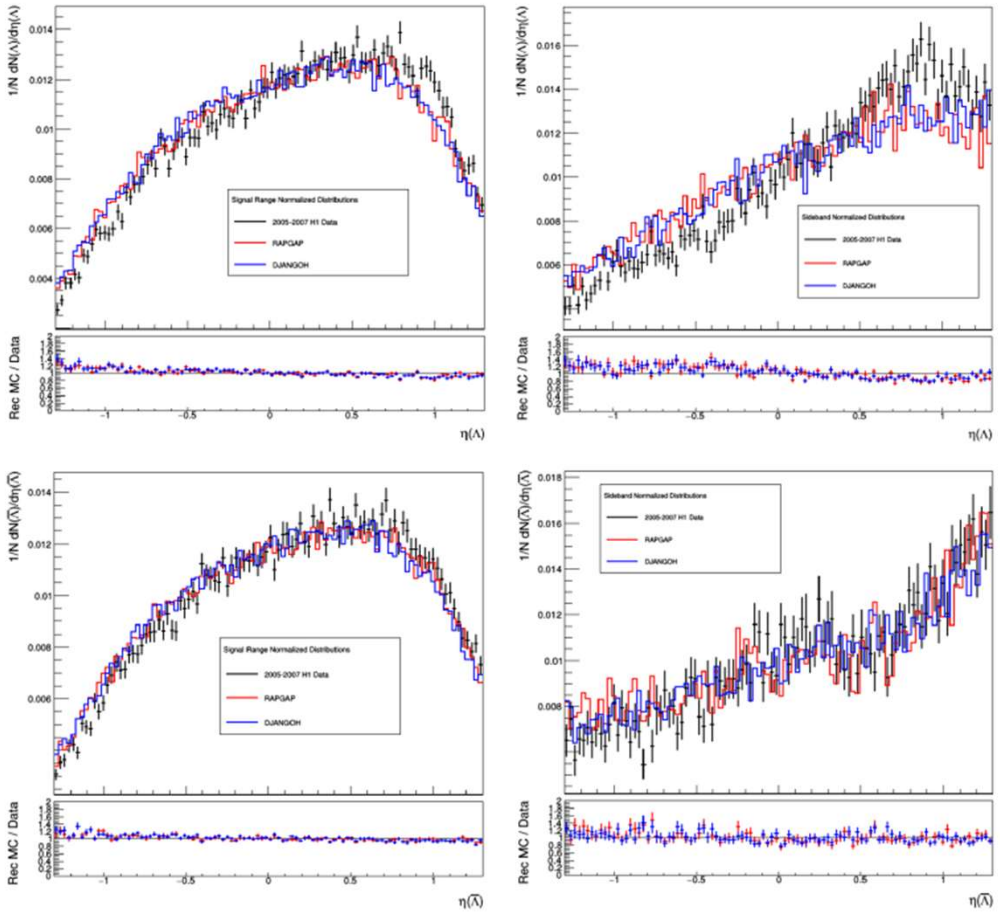

Figure 5.15: Normalized psuedorapidity (η) distributions of Λ (top) and $\bar{\Lambda}$ (bottom) candidates in the signal (left) and sideband (right) ranges for Data and MC. These are the distributions following the DIS event selections and all selective cuts.

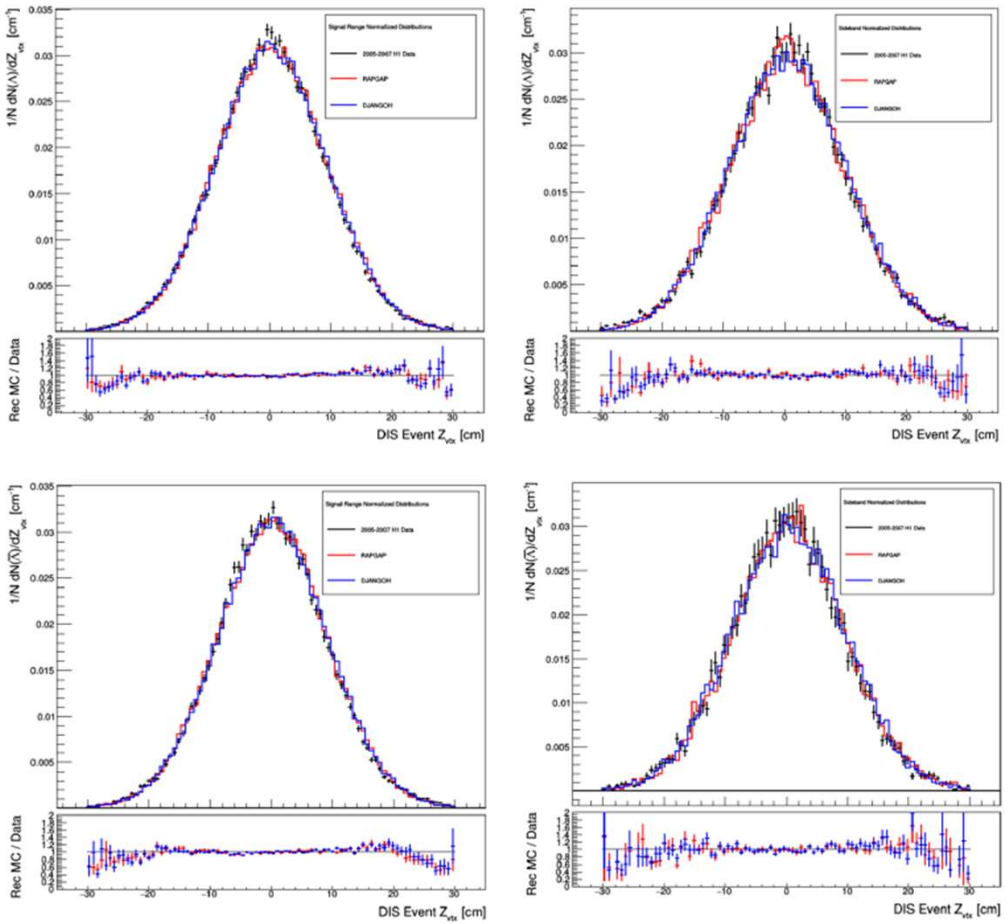

Figure 5.16: Normalized DIS event z vertex distributions of Λ (top) and $\bar{\Lambda}$ (bottom) candidates in the signal (left) and sideband (right) ranges for Data and MC. These are the distributions following the DIS event selections and all selective cuts.

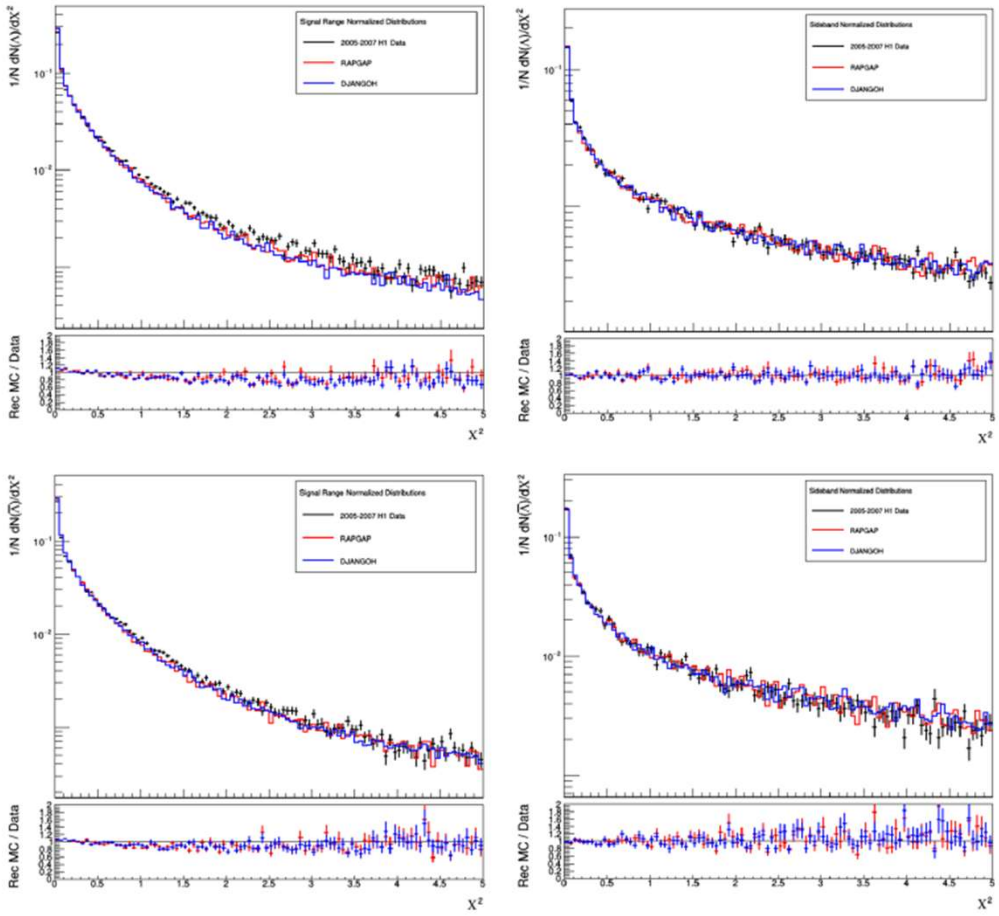

Figure 5.17: Normalized secondary vertex fit χ^2 distributions of Λ (top) and $\bar{\Lambda}$ (bottom) candidates in the signal (left) and sideband (right) ranges for Data and MC. These are the distributions following the DIS event selections and all selective cuts.

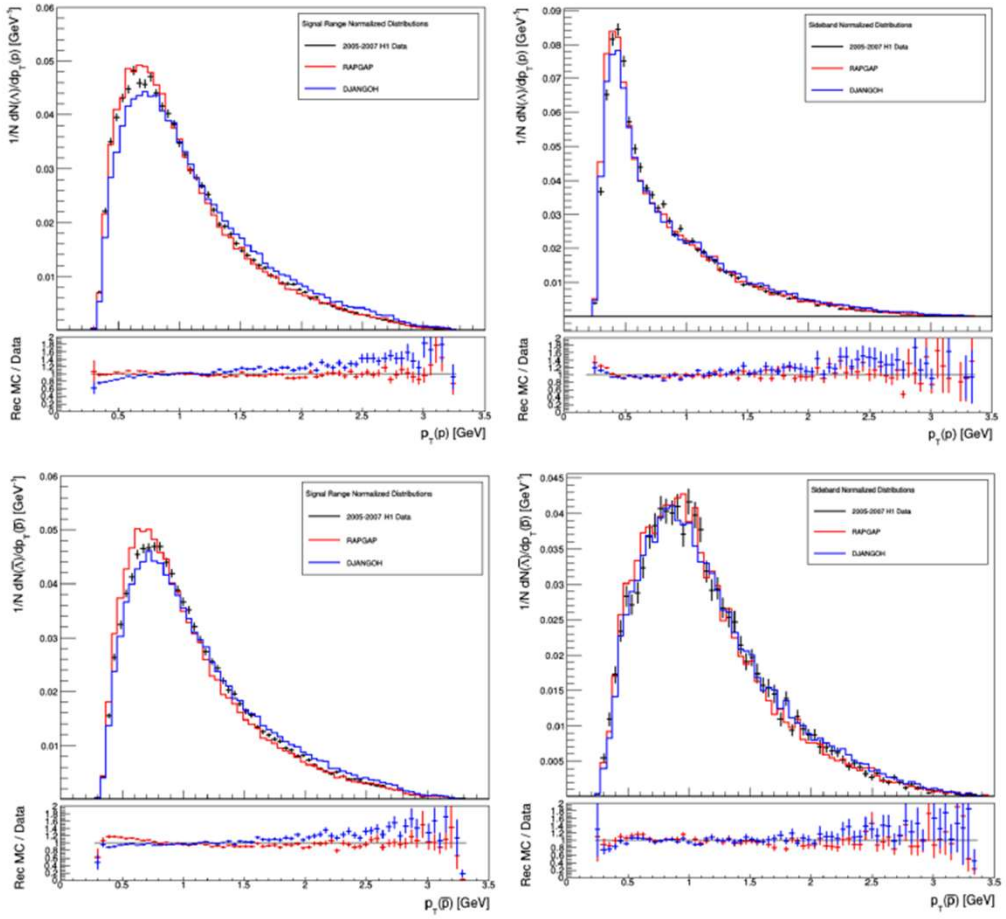

Figure 5.18: Normalized proton track p_T distributions of Λ (top) and $\bar{\Lambda}$ (bottom) candidates in the signal (left) and sideband (right) ranges for Data and MC. These are the distributions following the DIS event selections and all selective cuts.

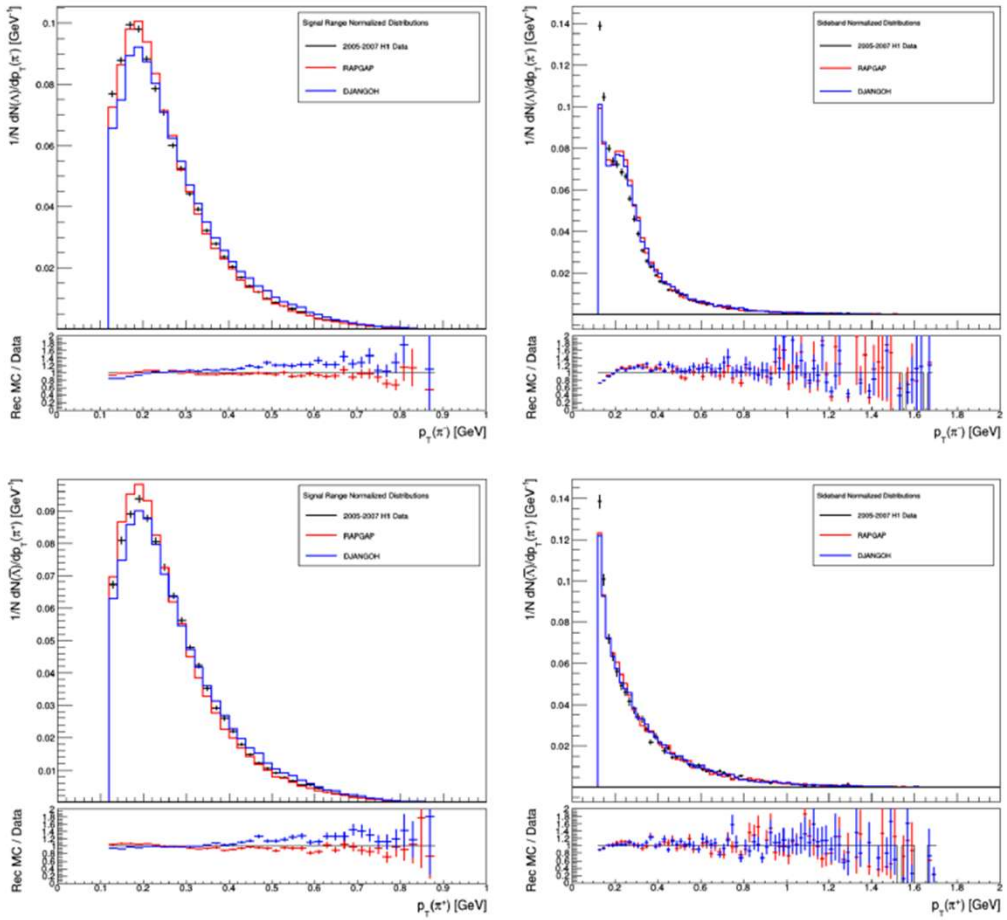

Figure 5.19: Normalized pion track p_T distributions of Λ (top) and $\bar{\Lambda}$ (bottom) candidates in the signal (left) and sideband (right) ranges for Data and MC. These are the distributions following the DIS event selections and all selective cuts.

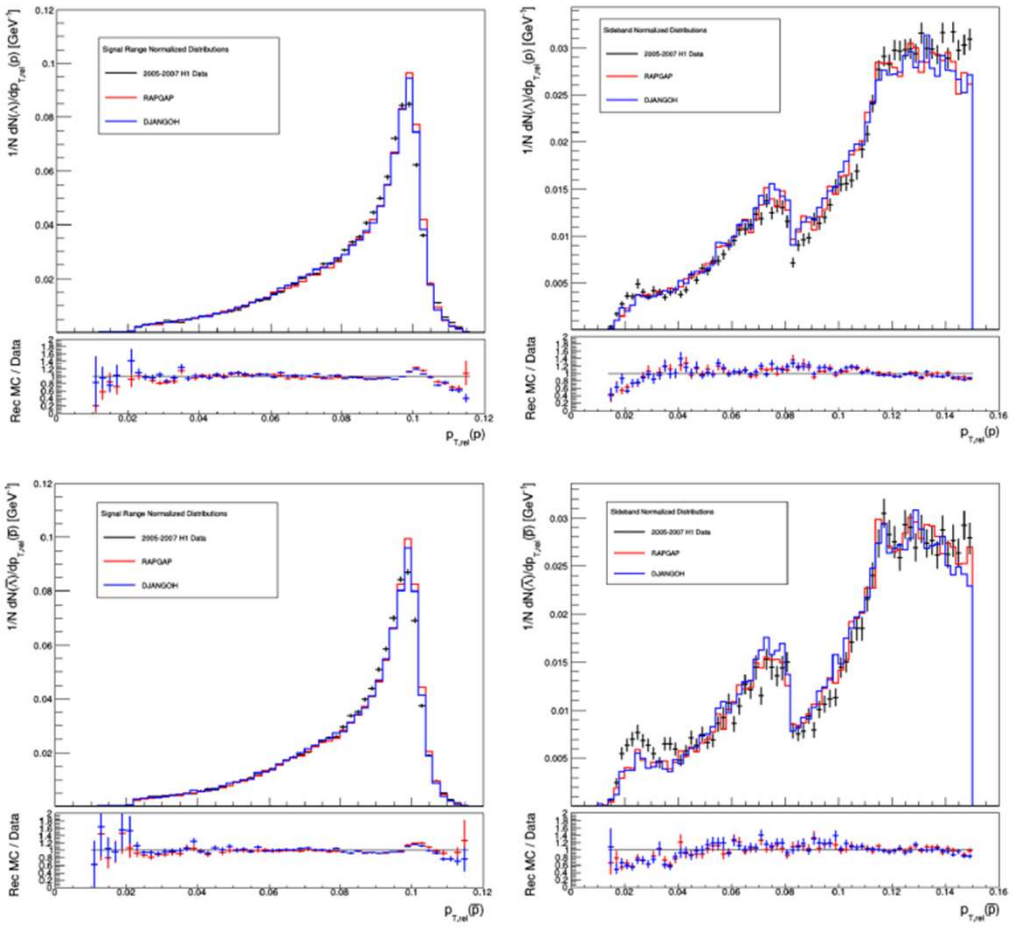

Figure 5.20: Normalized proton track $p_{T,rel}$ distributions of Λ (top) and $\bar{\Lambda}$ (bottom) candidates in the signal (left) and sideband (right) ranges for Data and MC. These are the distributions following the DIS event selections and all selective cuts.

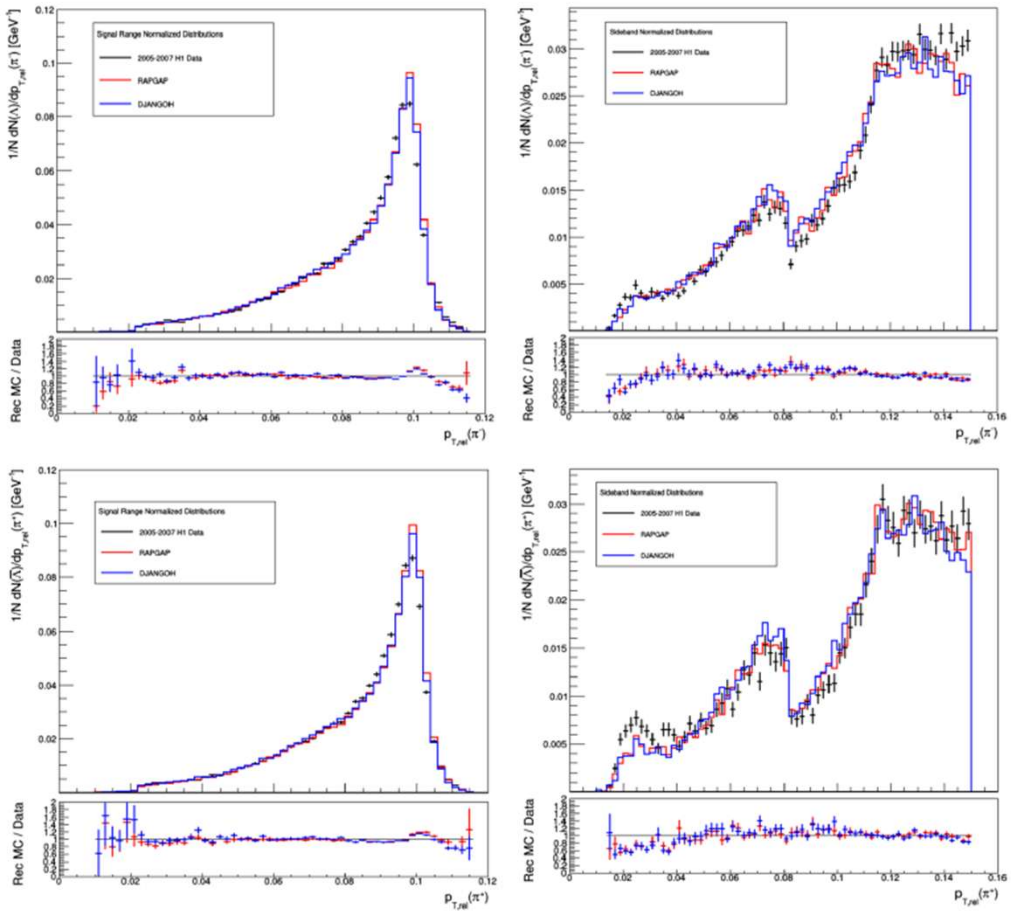

Figure 5.21: Normalized pion track $p_{T,rel}$ distributions of Λ (top) and $\bar{\Lambda}$ (bottom) candidates in the signal (left) and sideband (right) ranges for Data and MC. These are the distributions following the DIS event selections and all selective cuts.

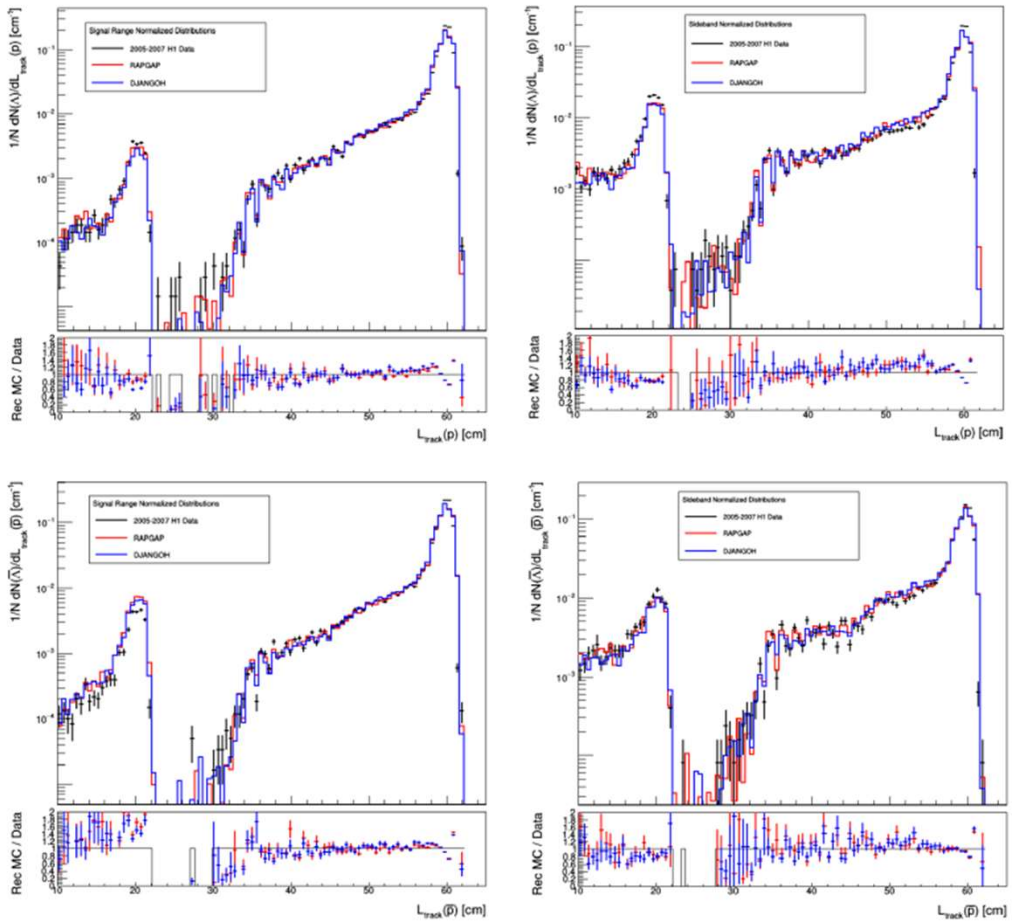

Figure 5.22: Normalized proton track length distributions of Λ (top) and $\bar{\Lambda}$ (bottom) candidates in the signal (left) and sideband (right) ranges for Data and MC. These are the distributions following the DIS event selections and all selective cuts.

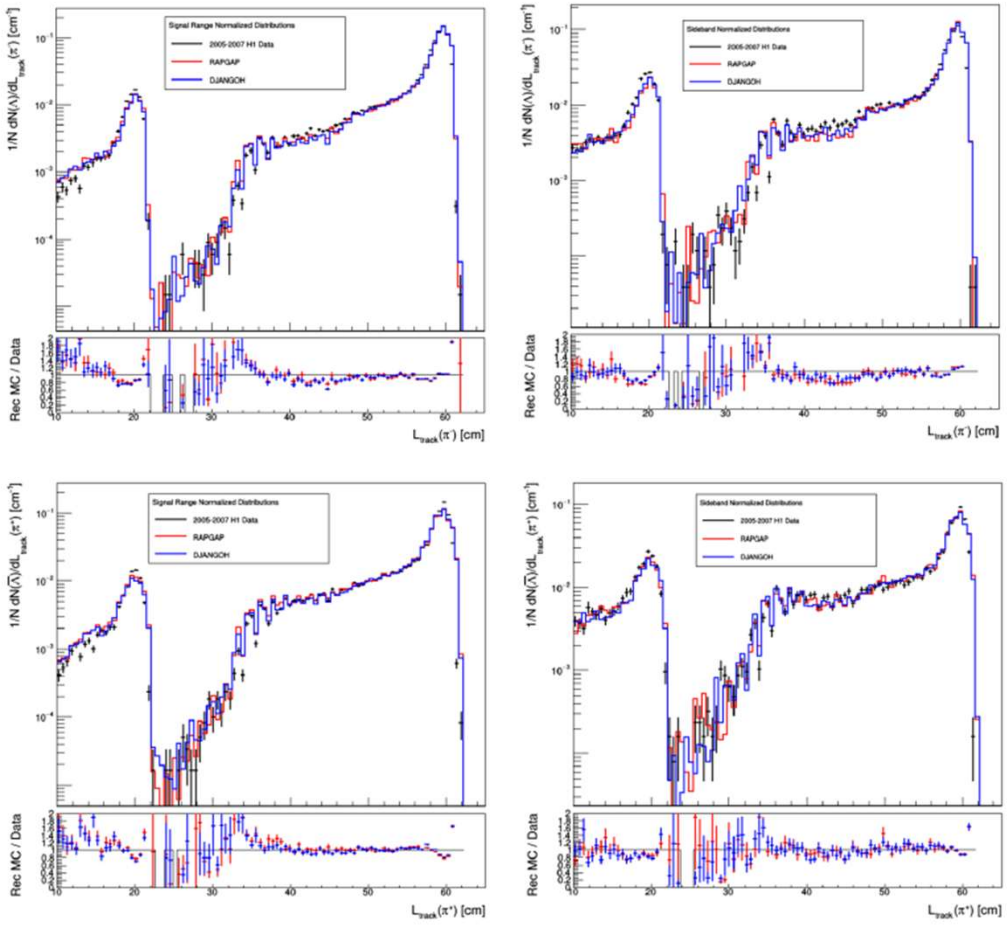

Figure 5.23: Normalized pion track length distributions of Λ (top) and $\bar{\Lambda}$ (bottom) candidates in the signal (left) and sideband (right) ranges for Data and MC. These are the distributions following the DIS event selections and all selective cuts.

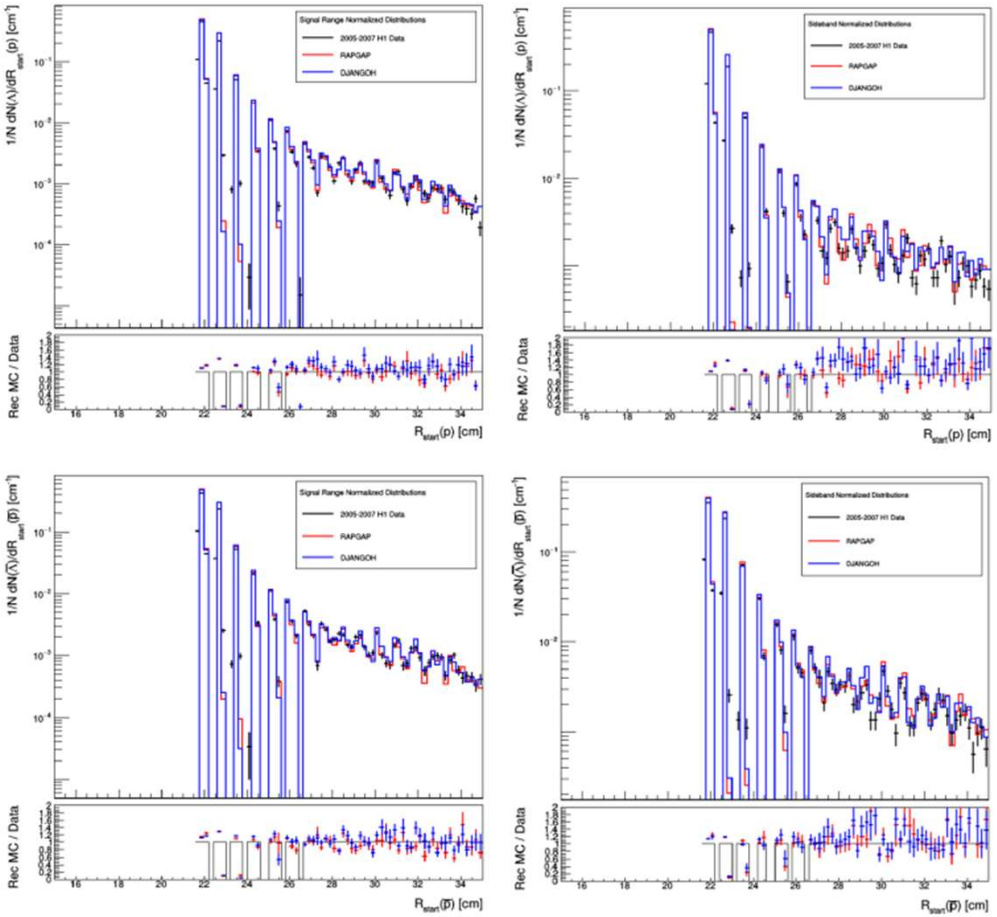

Figure 5.24: Normalized proton track radius start distributions of Λ (top) and $\bar{\Lambda}$ (bottom) candidates in the signal (left) and sideband (right) ranges for Data and MC. These are the distributions following the DIS event selections and all selective cuts.

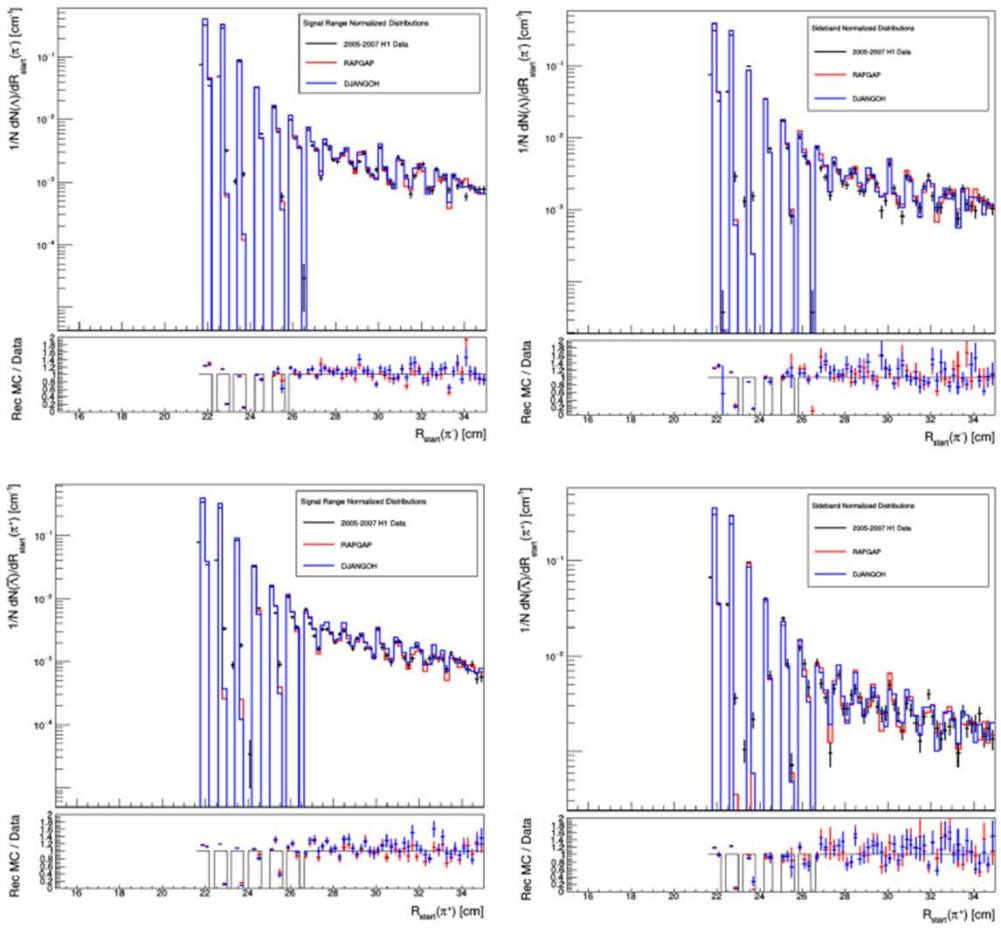

Figure 5.25: Normalized pion track radius start distributions of Λ (top) and $\bar{\Lambda}$ (bottom) candidates in the signal (left) and sideband (right) ranges for Data and MC. These are the distributions following the DIS event selections and all selective cuts.

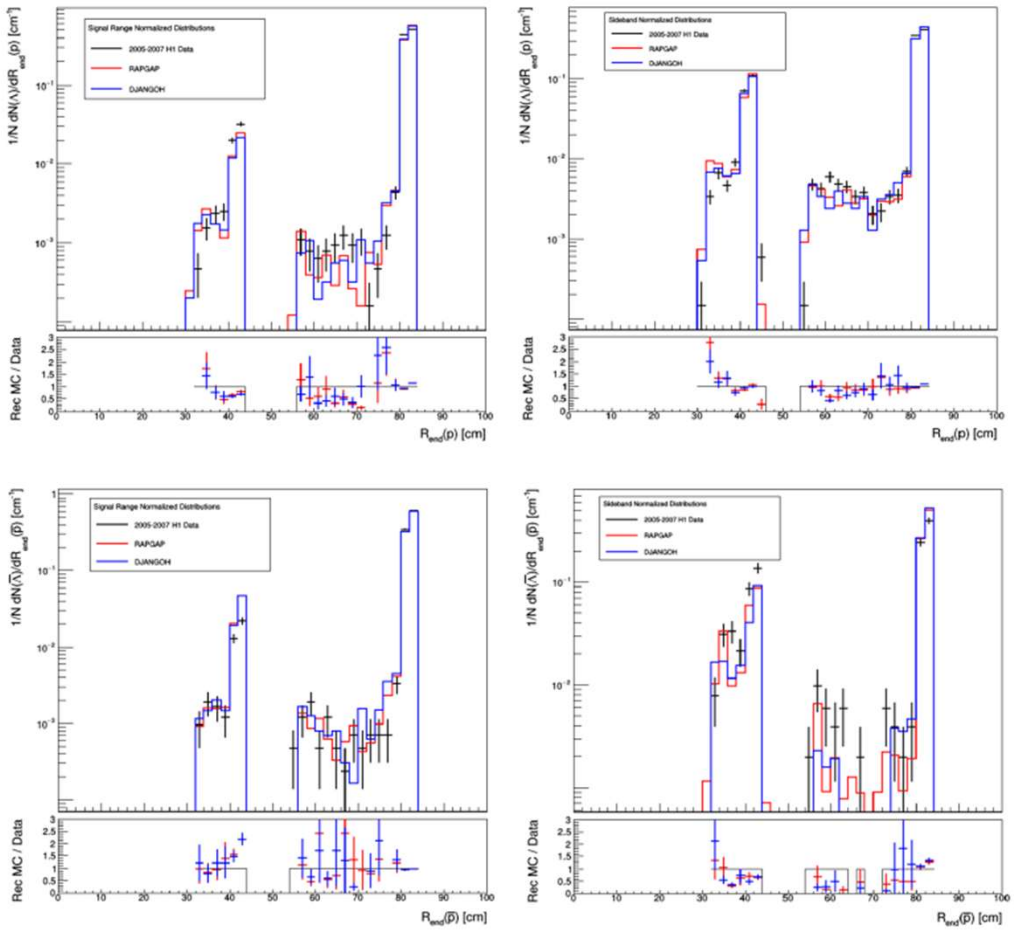

Figure 5.26: Normalized proton track radius end distributions of Λ (top) and $\bar{\Lambda}$ (bottom) candidates in the signal (left) and sideband (right) ranges for Data and MC. These are the distributions following the DIS event selections and all selective cuts.

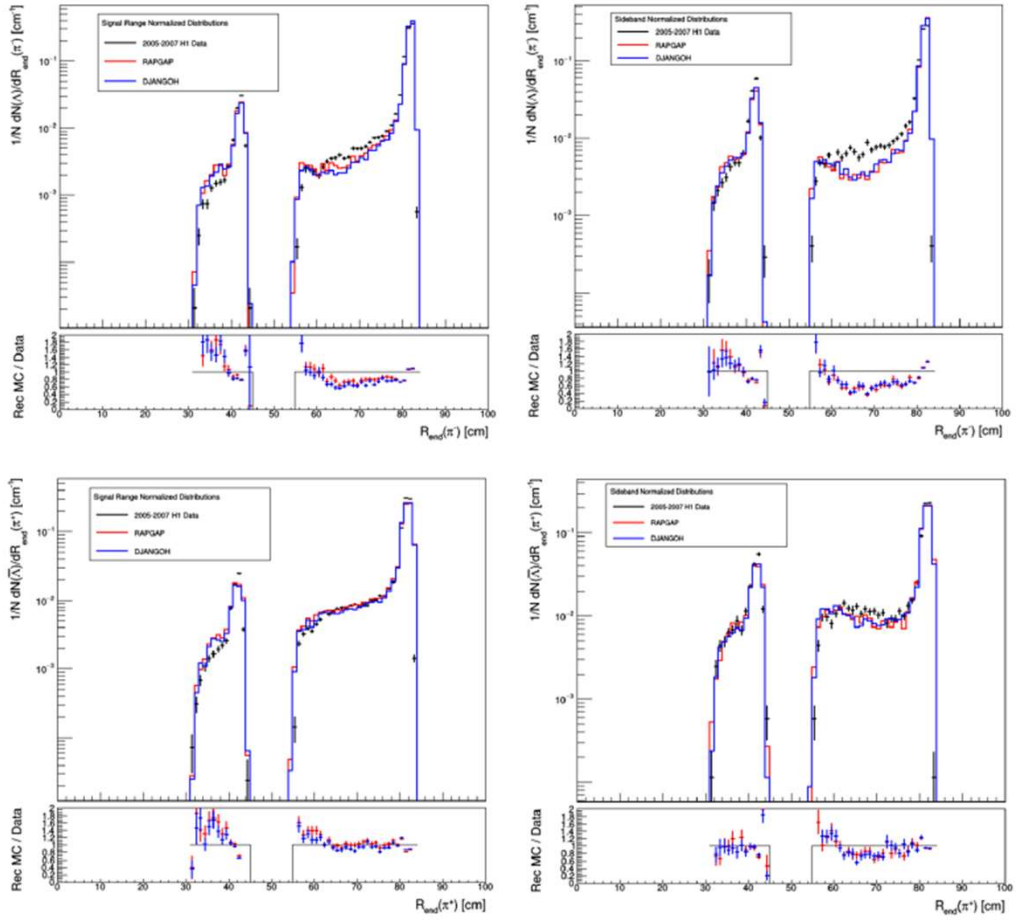

Figure 5.27: Normalized pion track radius end distributions of Λ (top) and $\bar{\Lambda}$ (bottom) candidates in the signal (left) and sideband (right) ranges for Data and MC. These are the distributions following the DIS event selections and all selective cuts.

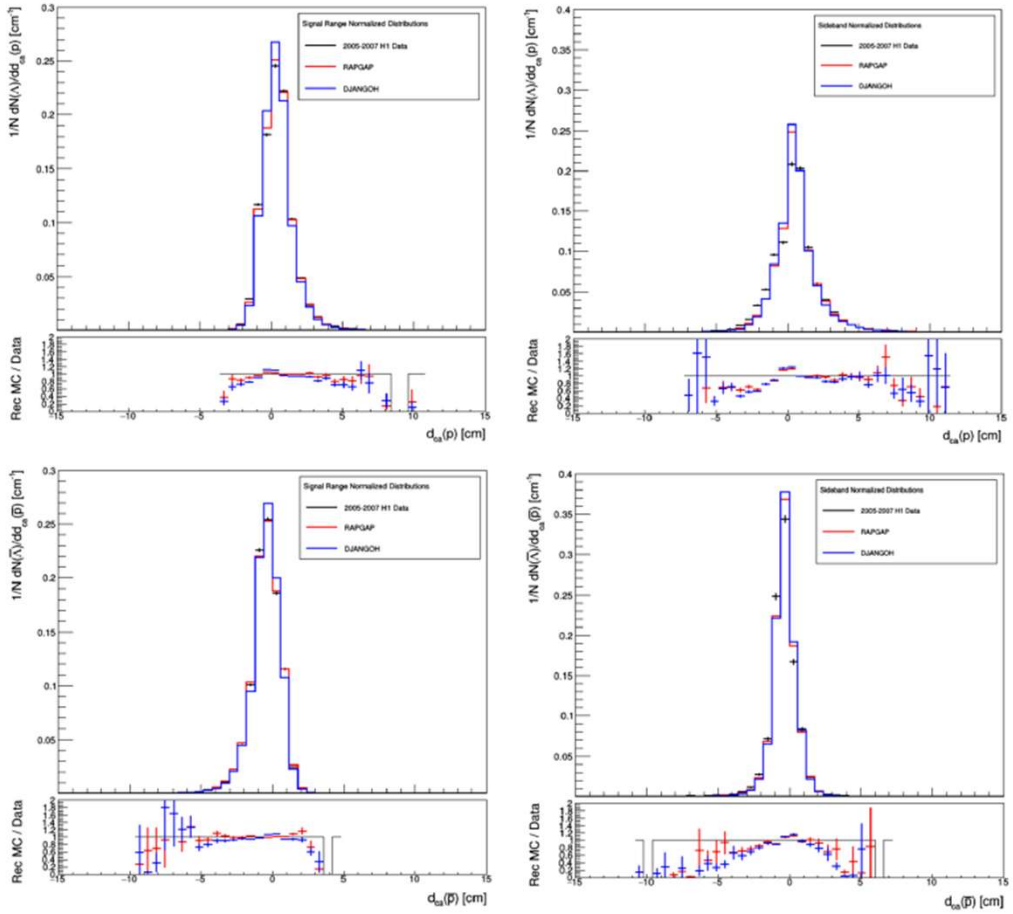

Figure 5.28: Normalized proton track distance of closest approach distributions of Λ (top) and $\bar{\Lambda}$ (bottom) candidates in the signal (left) and sideband (right) ranges for Data and MC. These are the distributions following the DIS event selections and all selective cuts.

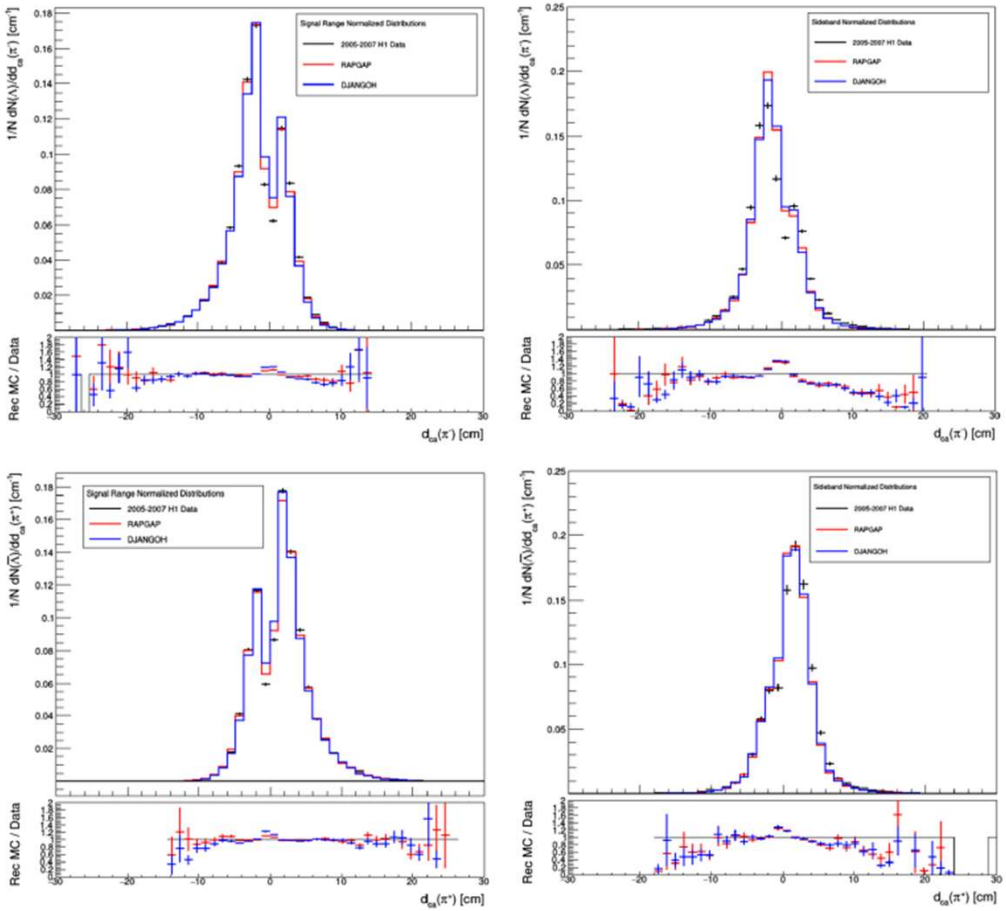

Figure 5.29: Normalized pion track distance of closest approach distributions of Λ (top) and $\bar{\Lambda}$ (bottom) candidates in the signal (left) and sideband (right) ranges for Data and MC. These are the distributions following the DIS event selections and all selective cuts.

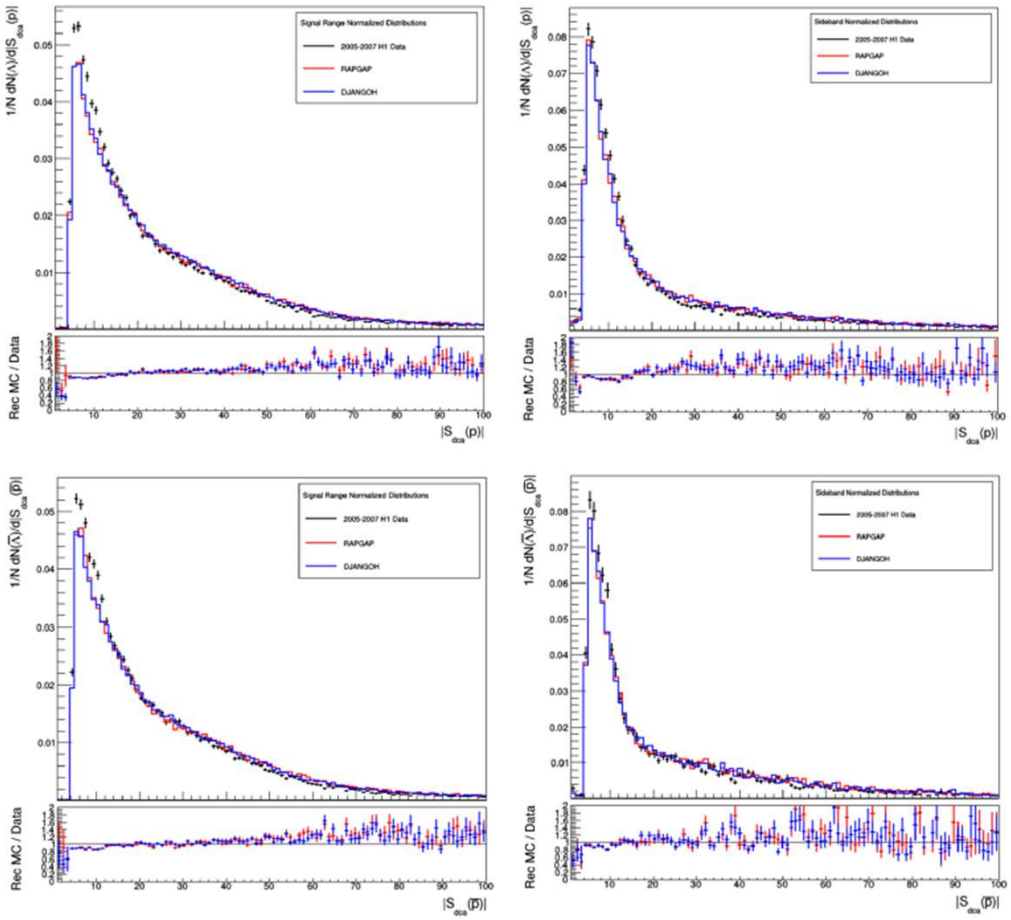

Figure 5.30: Normalized proton track distance of closest approach significance distributions of Λ (top) and $\bar{\Lambda}$ (bottom) candidates in the signal (left) and sideband (right) ranges for Data and MC. These are the distributions following the DIS event selections and all selective cuts.

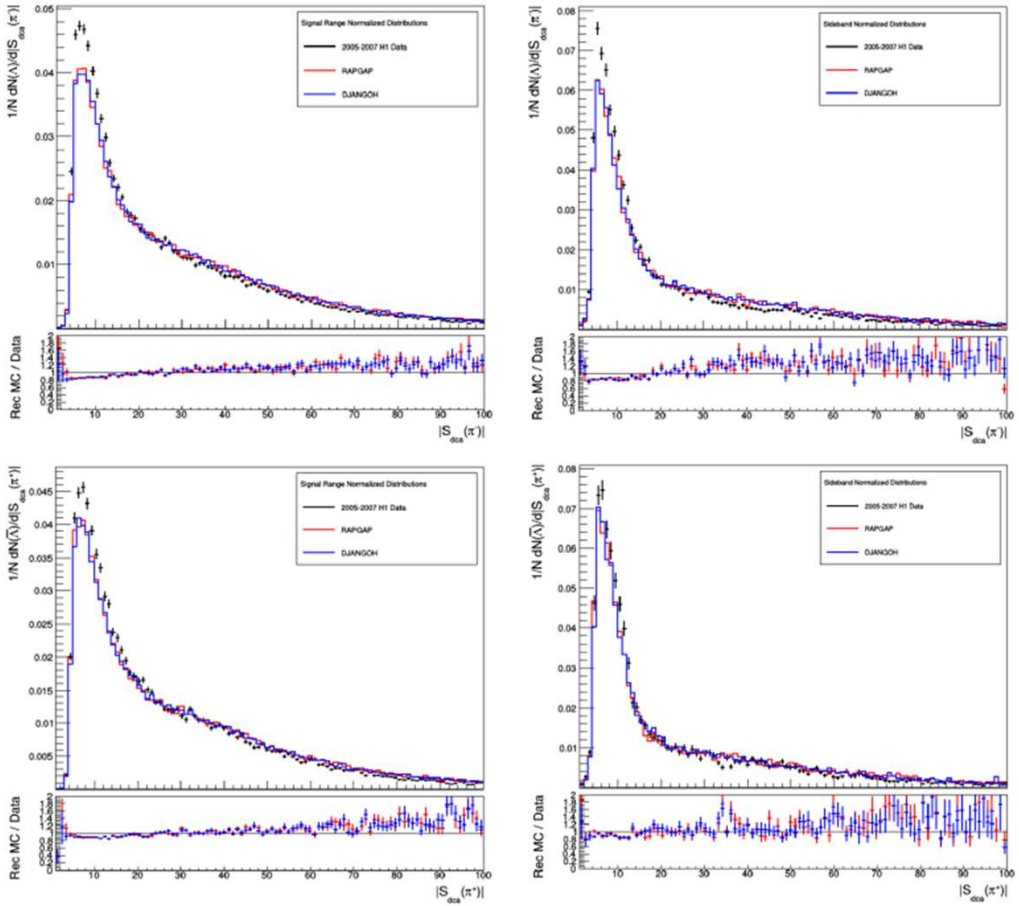

Figure 5.31: Normalized pion track distance of closest approach significance distributions of Λ (top) and $\bar{\Lambda}$ (bottom) candidates in the signal (left) and sideband (right) ranges for Data and MC. These are the distributions following the DIS event selections and all selective cuts.

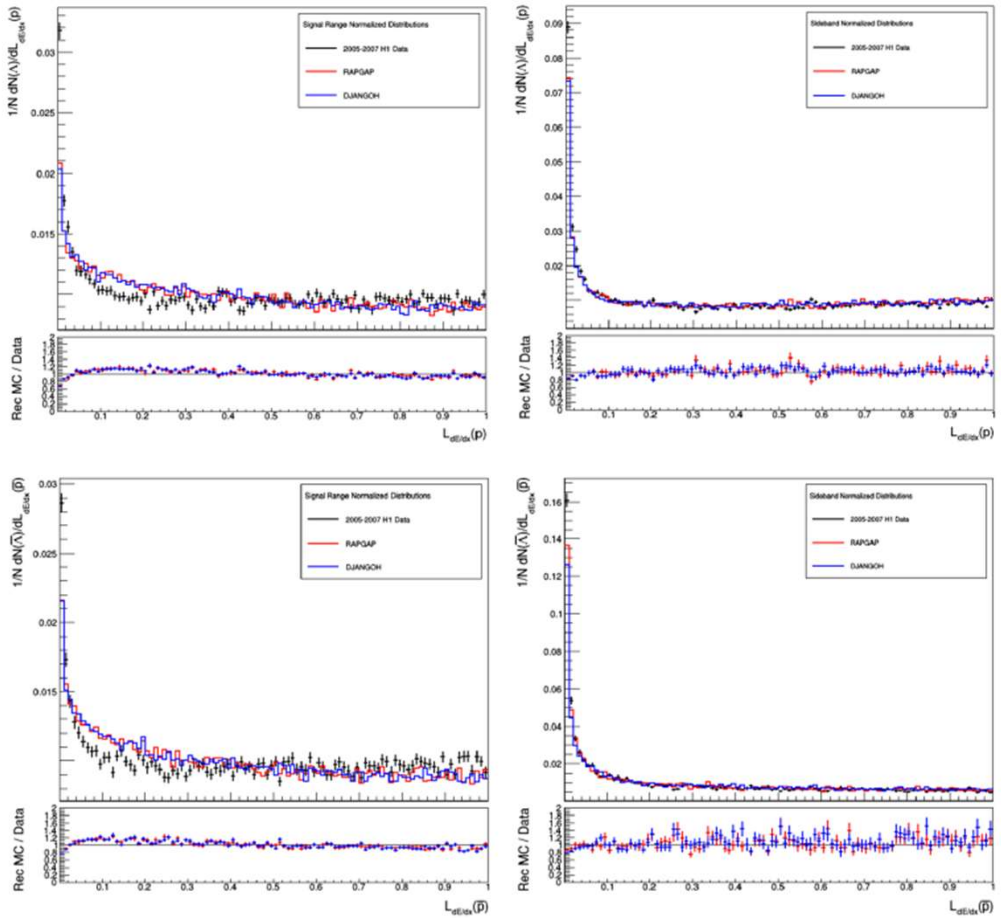

Figure 5.32: Normalized proton track dE/dx likelihood distributions of Λ (top) and $\bar{\Lambda}$ (bottom) candidates in the signal (left) and sideband (right) ranges for Data and MC. These are the distributions following the DIS event selections and all selective cuts.

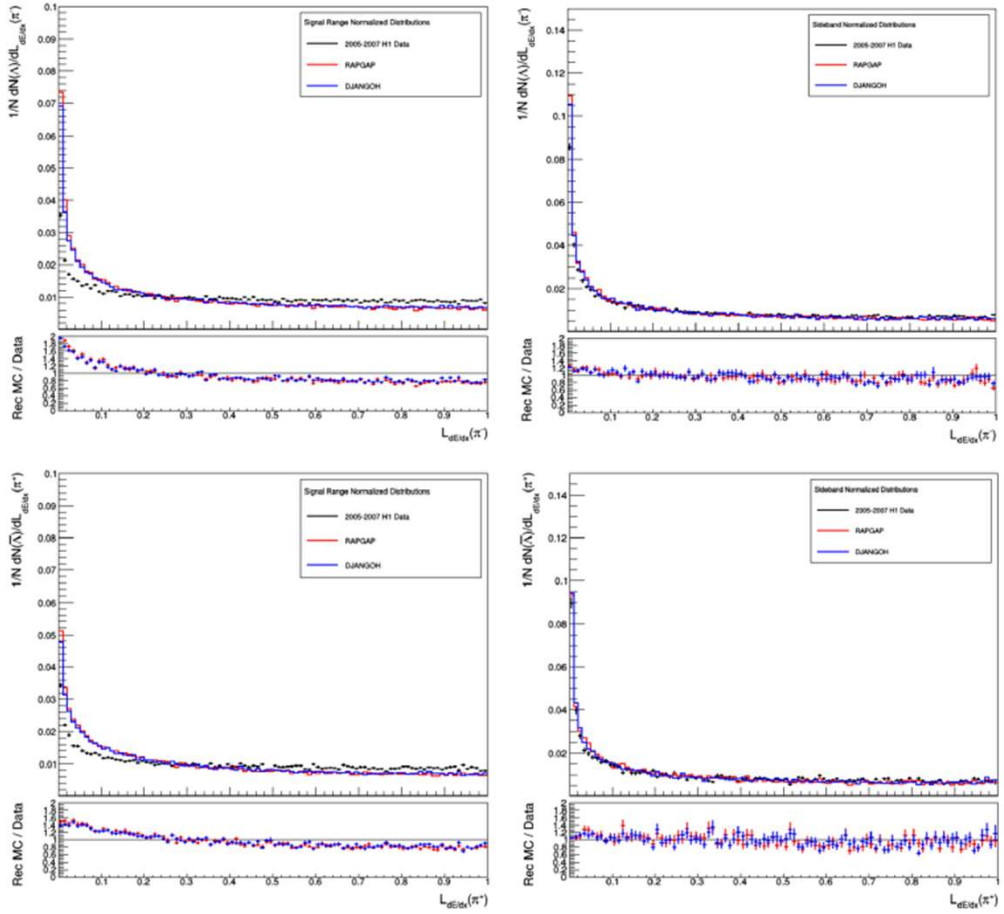

Figure 5.33: Normalized pion track dE/dx likelihood distributions of Λ (top) and $\bar{\Lambda}$ (bottom) candidates in the signal (left) and sideband (right) ranges for Data and MC. These are the distributions following the DIS event selections and all selective cuts.

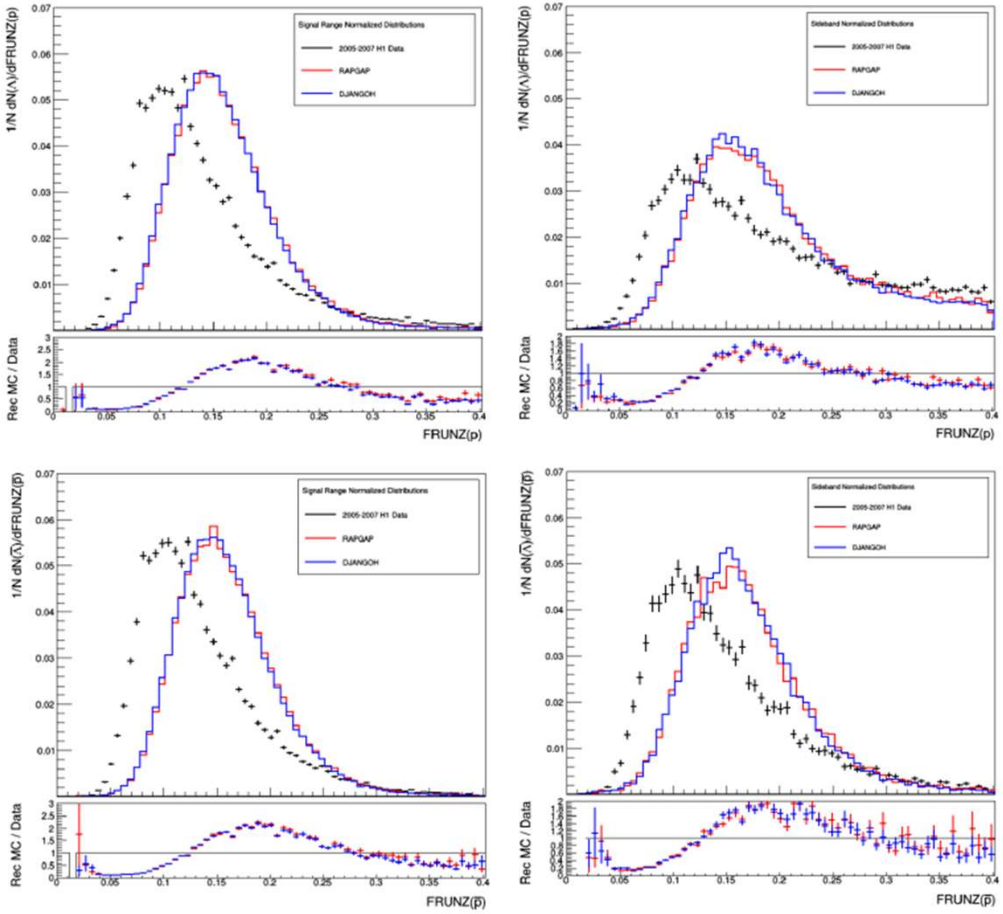

Figure 5.34: Normalized proton track fraction of rejected z hits (FRUNZ) distributions of Λ (top) and $\bar{\Lambda}$ (bottom) candidates in the signal (left) and sideband (right) ranges for Data and MC. These are the distributions following the DIS event selections and all selective cuts.

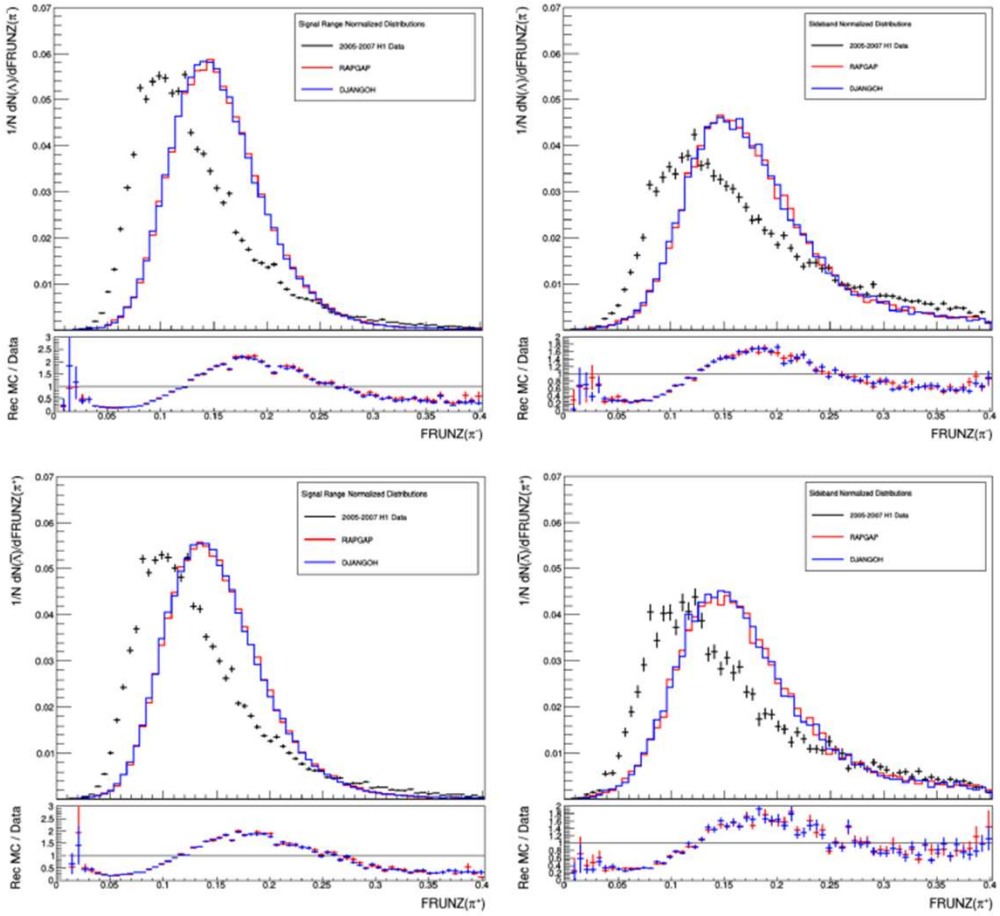

Figure 5.35: Normalized pion track fraction of rejected z hits (FRUNZ) distributions of Λ (top) and $\bar{\Lambda}$ (bottom) candidates in the signal (left) and sideband (right) ranges for Data and MC. These are the distributions following the DIS event selections and all selective cuts.

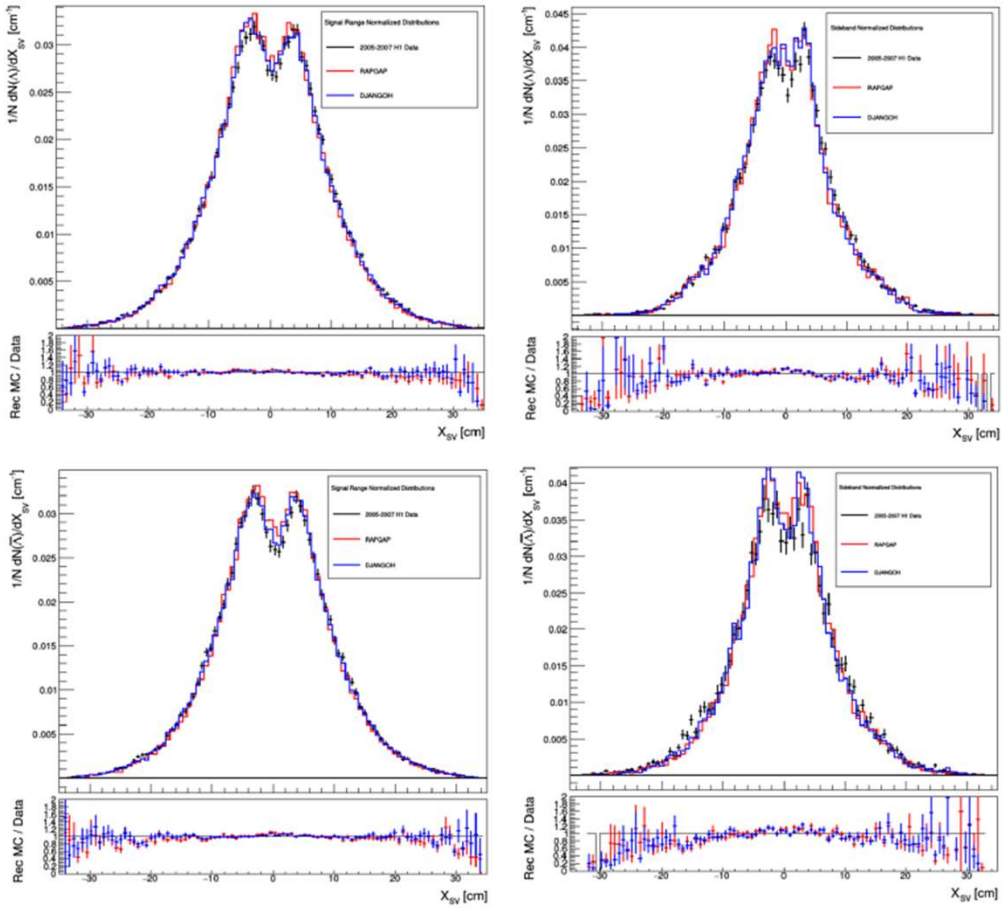

Figure 5.36: Normalized x secondary decay vertex position distributions of Λ (top) and $\bar{\Lambda}$ (bottom) candidates in the signal (left) and sideband (right) ranges for Data and MC. These are the distributions following the DIS event selections and all selective cuts.

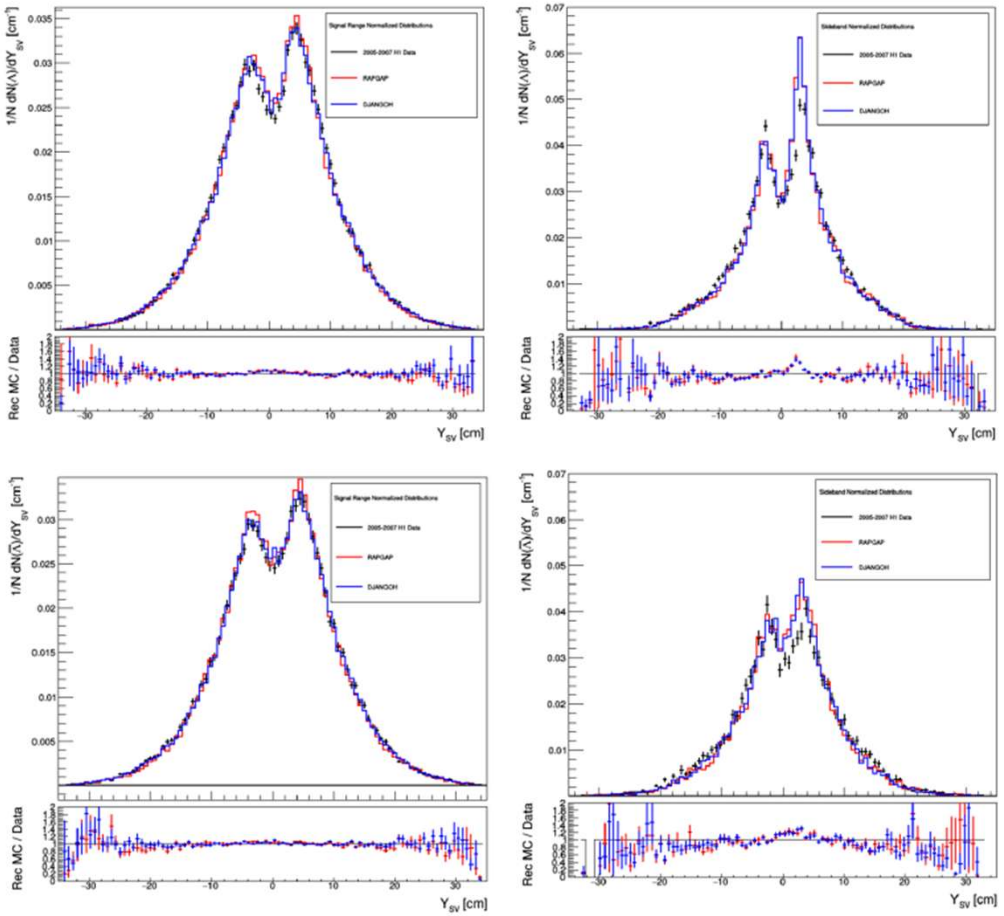

Figure 5.37: Normalized y secondary decay vertex position distributions of Λ (top) and $\bar{\Lambda}$ (bottom) candidates in the signal (left) and sideband (right) ranges for Data and MC. These are the distributions following the DIS event selections and all selective cuts.

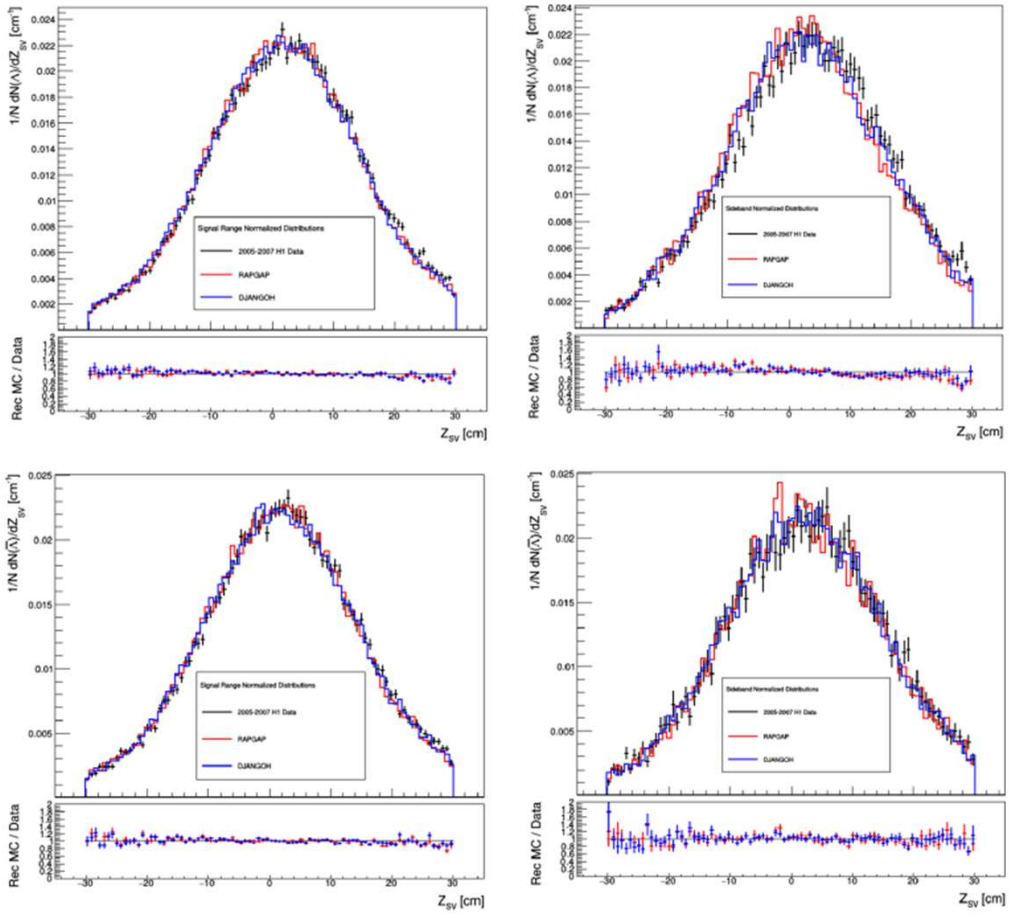

Figure 5.38: Normalized z secondary decay vertex position distributions of Λ (top) and $\bar{\Lambda}$ (bottom) candidates in the signal (left) and sideband (right) ranges for Data and MC. These are the distributions following the DIS event selections and all selective cuts.

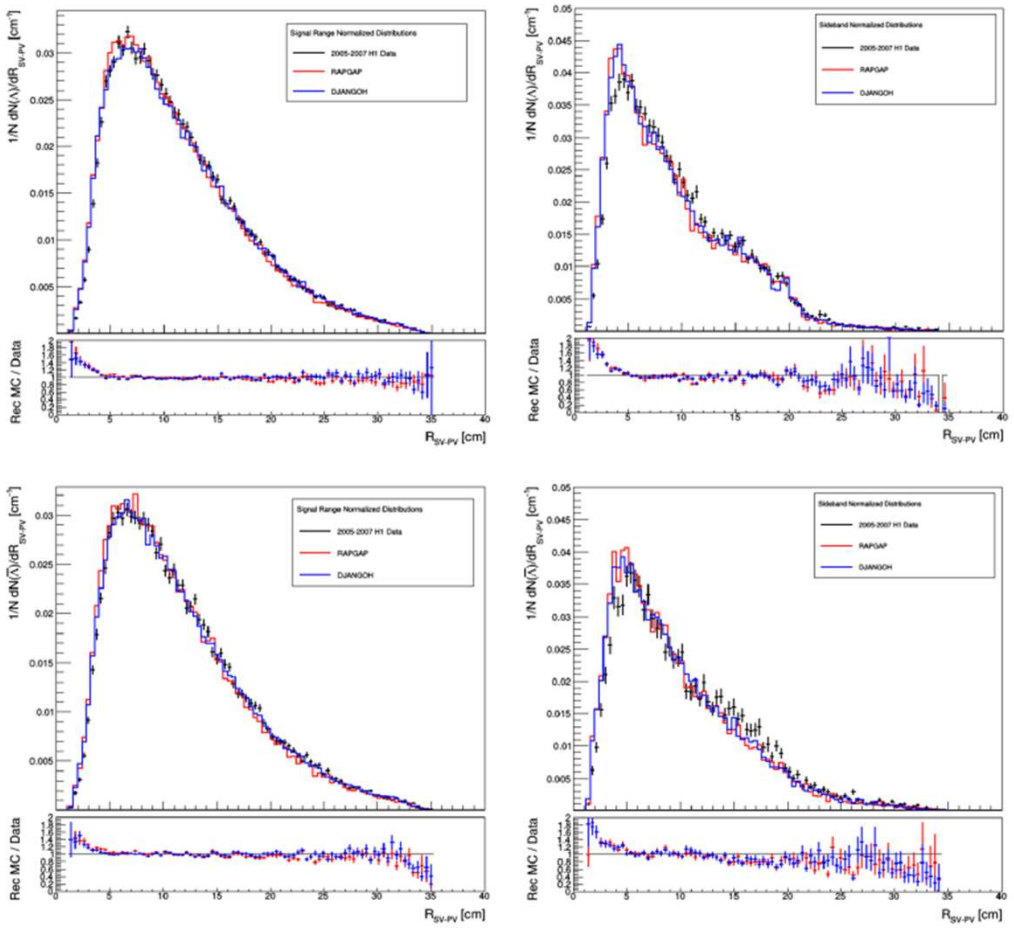

Figure 5.39: Normalized distributions of the radial distance between the primary DIS vertex and secondary decay vertex of Λ (top) and $\bar{\Lambda}$ (bottom) candidates in the signal (left) and sideband (right) ranges for Data and MC. These are the distributions following the DIS event selections and all selective cuts.

Cross Section Control Plots

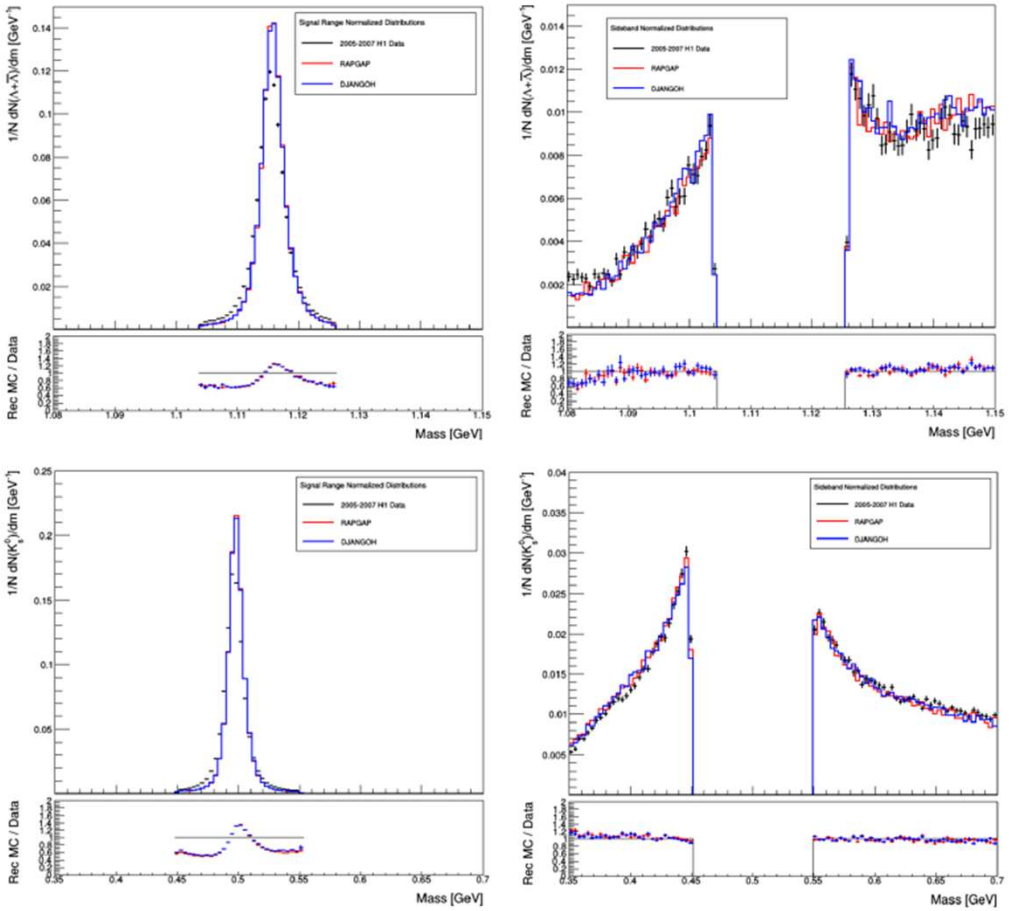

Figure 5.40: Normalized invariant mass distributions of $\Lambda + \bar{\Lambda}$ (top) and K_s^0 (bottom) candidates in the signal (left) and sideband (right) ranges for Data and MC. These are the distributions following the DIS event selections and all selective cuts. These invariant mass signal and sideband ranges are representative of the ones used in the following control plots.

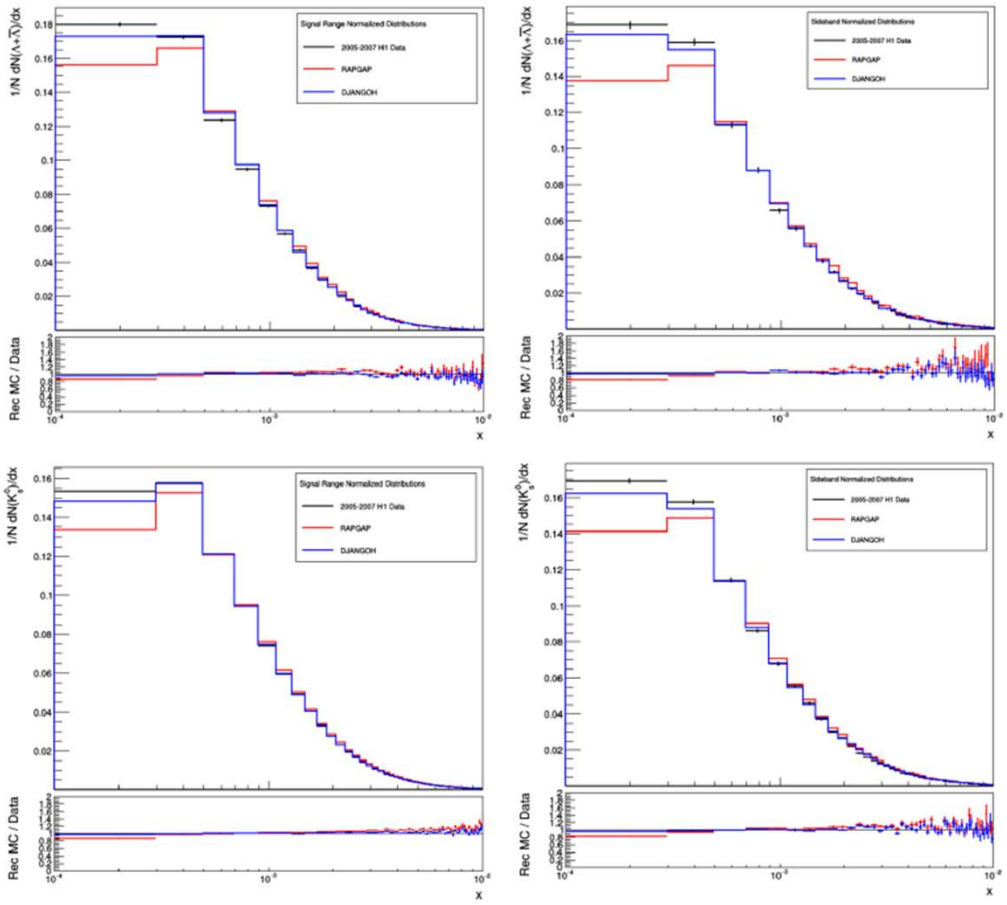

Figure 5.41: Normalized Bjorken-x distributions of $\Lambda + \bar{\Lambda}$ (top) and K_s^0 (bottom) candidates in the signal (left) and sideband (right) ranges for Data and MC. These are the distributions following the DIS event selections and all selective cuts.

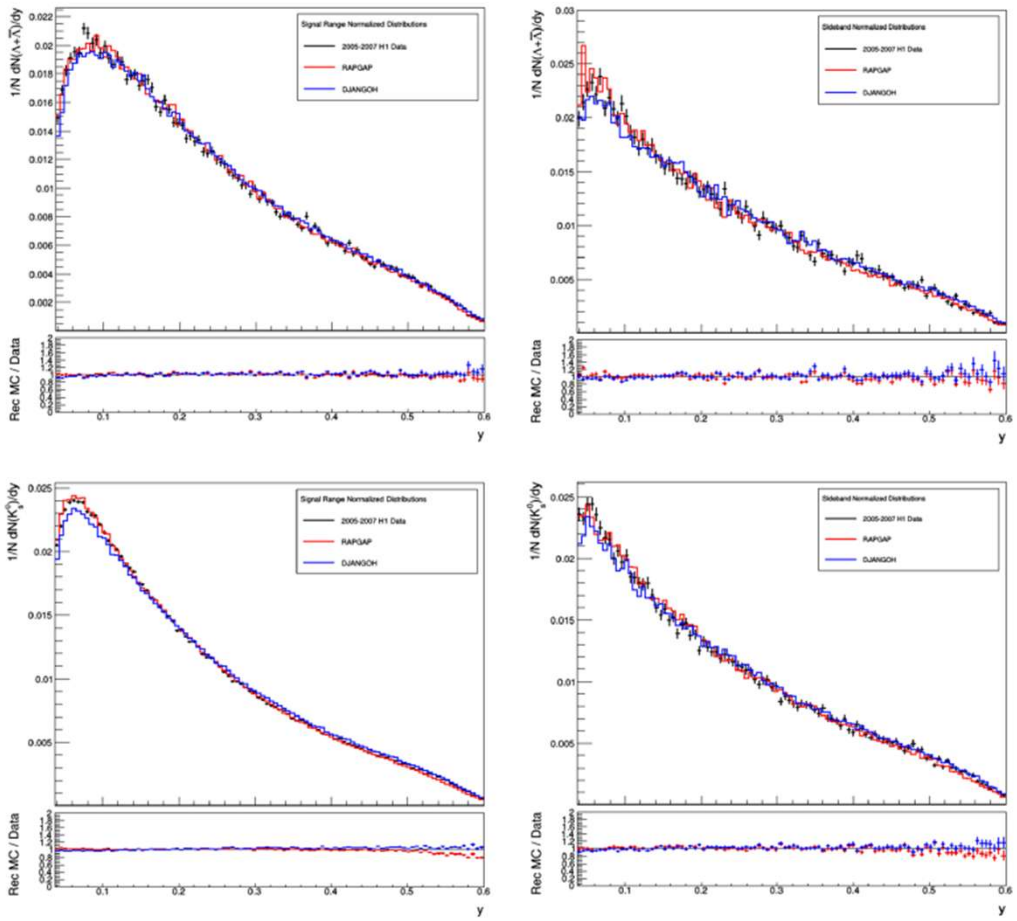

Figure 5.42: Normalized inelasticity (y) distributions of $\Lambda + \bar{\Lambda}$ (top) and K_s^0 (bottom) candidates in the signal (left) and sideband (right) ranges for Data and MC. These are the distributions following the DIS event selections and all selective cuts.

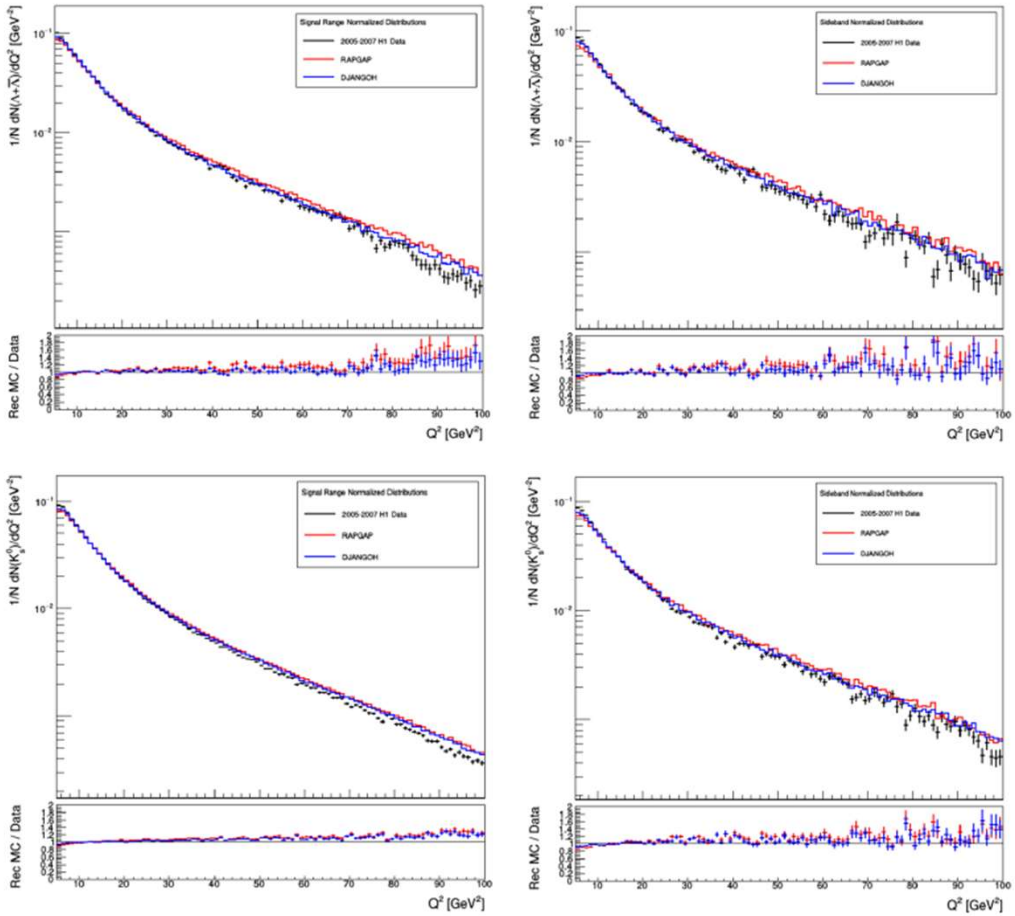

Figure 5.43: Normalized Q^2 distributions of $\Lambda + \bar{\Lambda}$ (top) and K_s^0 (bottom) candidates in the signal (left) and sideband (right) ranges for Data and MC. These are the distributions following the DIS event selections and all selective cuts.

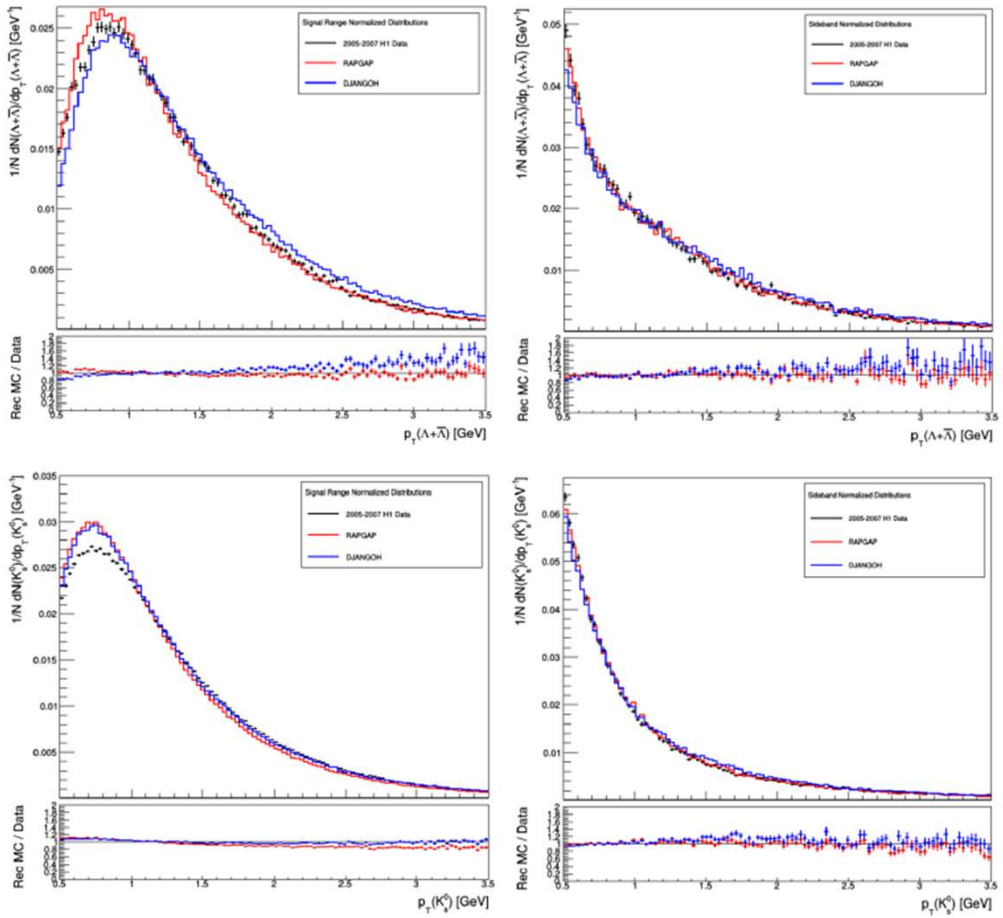

Figure 5.44: Normalized p_T distributions of $\Lambda + \bar{\Lambda}$ (top) and K_s^0 (bottom) candidates in the signal (left) and sideband (right) ranges for Data and MC. These are the distributions following the DIS event selections and all selective cuts.

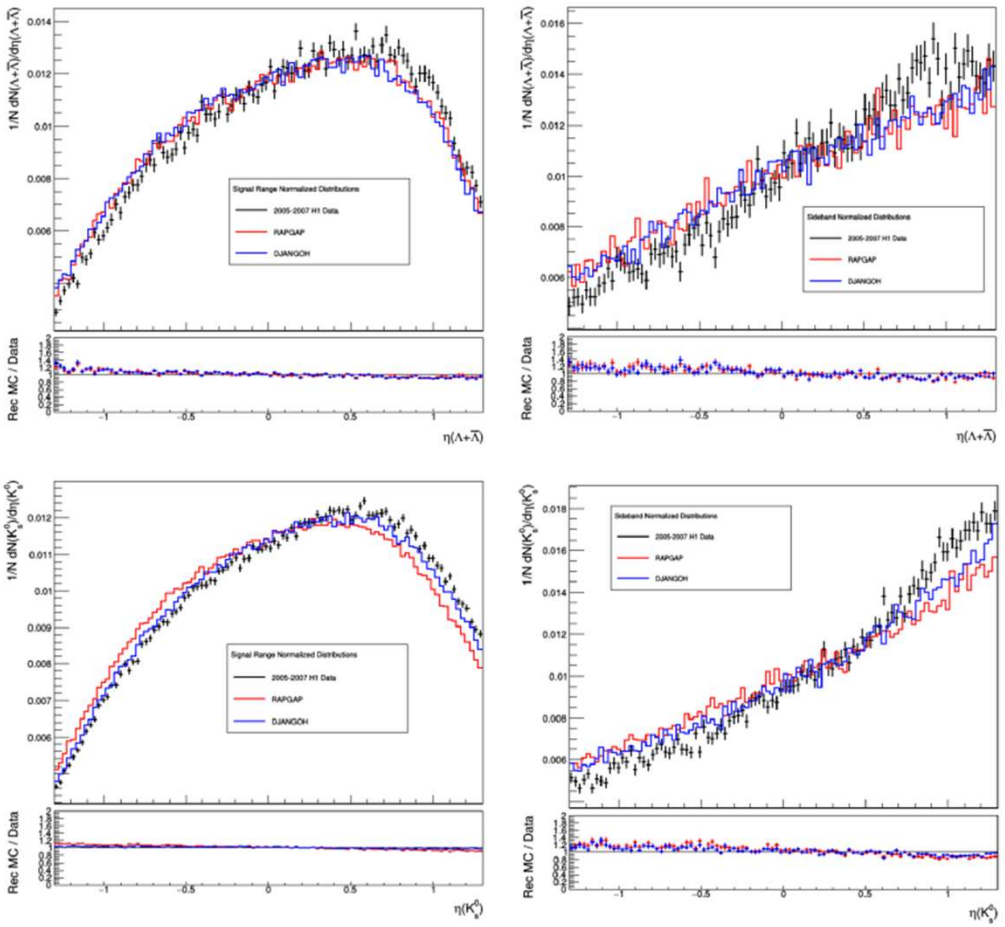

Figure 5.45: Normalized pseudorapidity (η) distributions of $\Lambda + \bar{\Lambda}$ (top) and K_s^0 (bottom) candidates in the signal (left) and sideband (right) ranges for Data and MC. These are the distributions following the DIS event selections and all selective cuts.

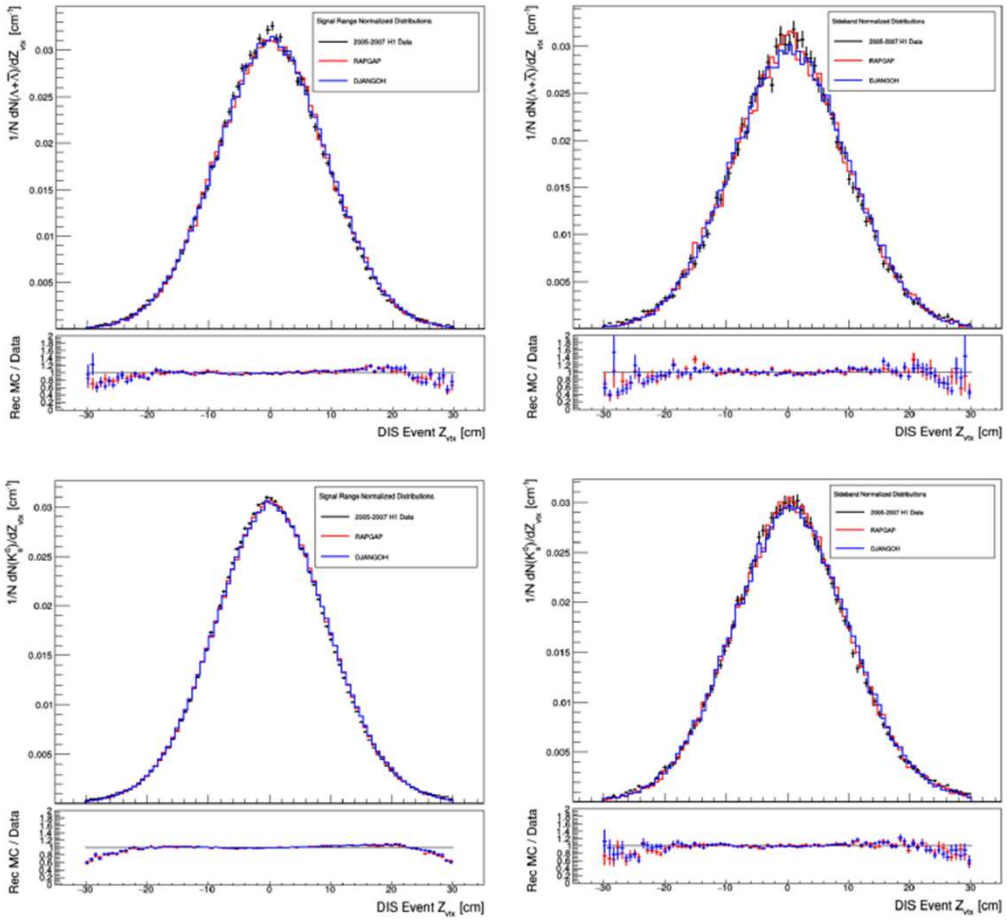

Figure 5.46: Normalized DIS event z vertex distributions of $\Lambda + \bar{\Lambda}$ (top) and K_s^0 (bottom) candidates in the signal (left) and sideband (right) ranges for Data and MC. These are the distributions following the DIS event selections and all selective cuts.

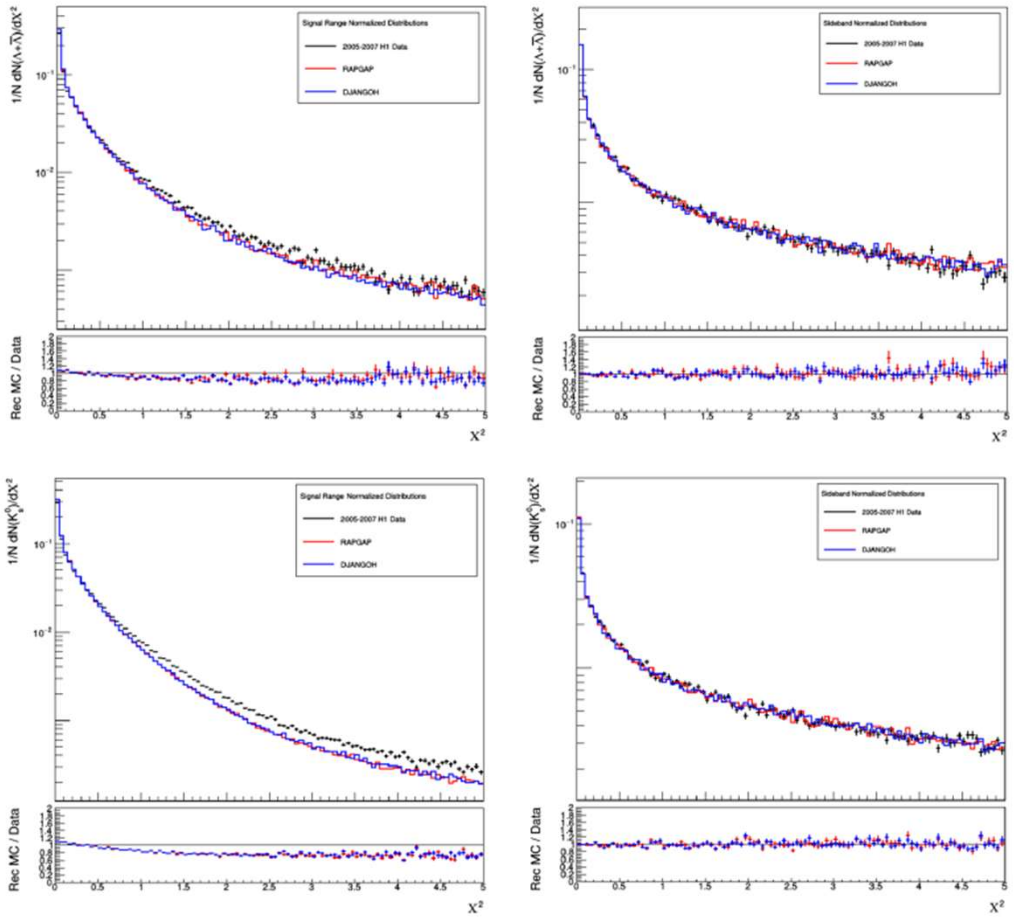

Figure 5.47: Normalized secondary vertex fit χ^2 distributions of $\Lambda + \bar{\Lambda}$ (top) and K_s^0 (bottom) candidates in the signal (left) and sideband (right) ranges for Data and MC. These are the distributions following the DIS event selections and all selective cuts.

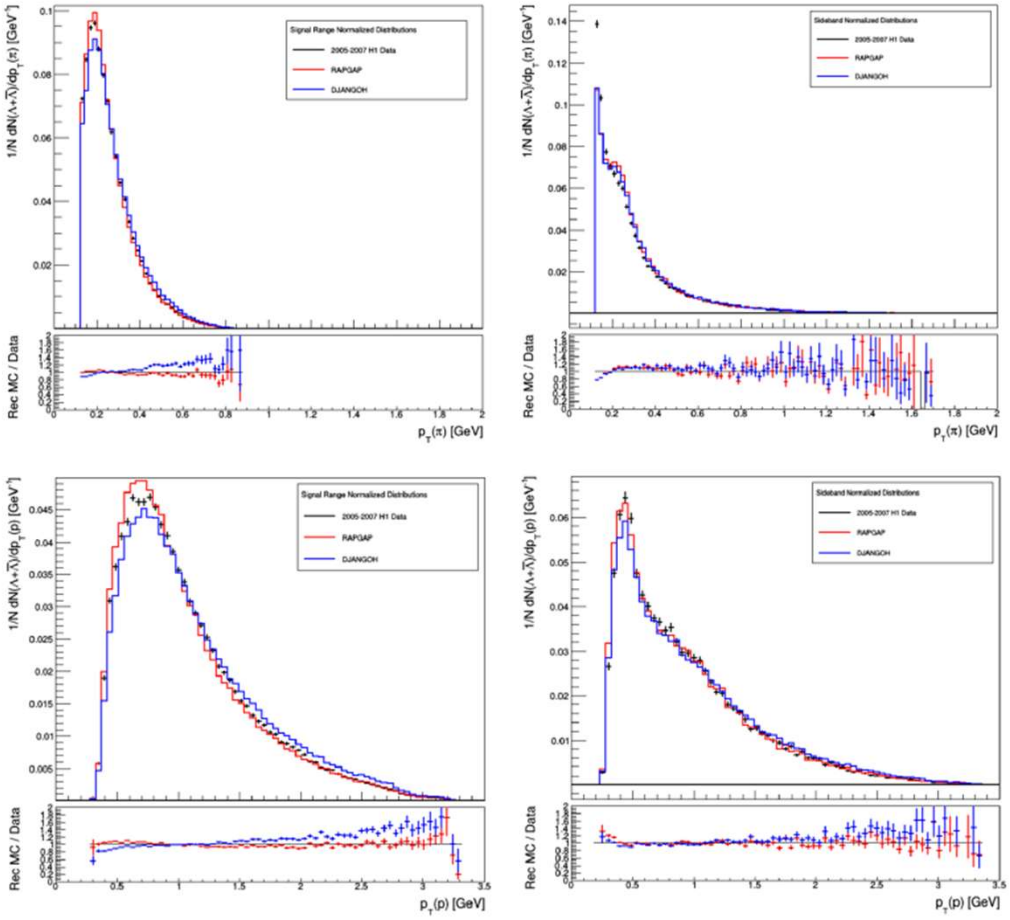

Figure 5.48: Normalized pion track p_T (top) and proton track p_T (bottom) distributions of $\Lambda + \bar{\Lambda}$ candidates in the signal (left) and sideband (right) ranges for Data and MC. These are the distributions following the DIS event selections and all selective cuts.

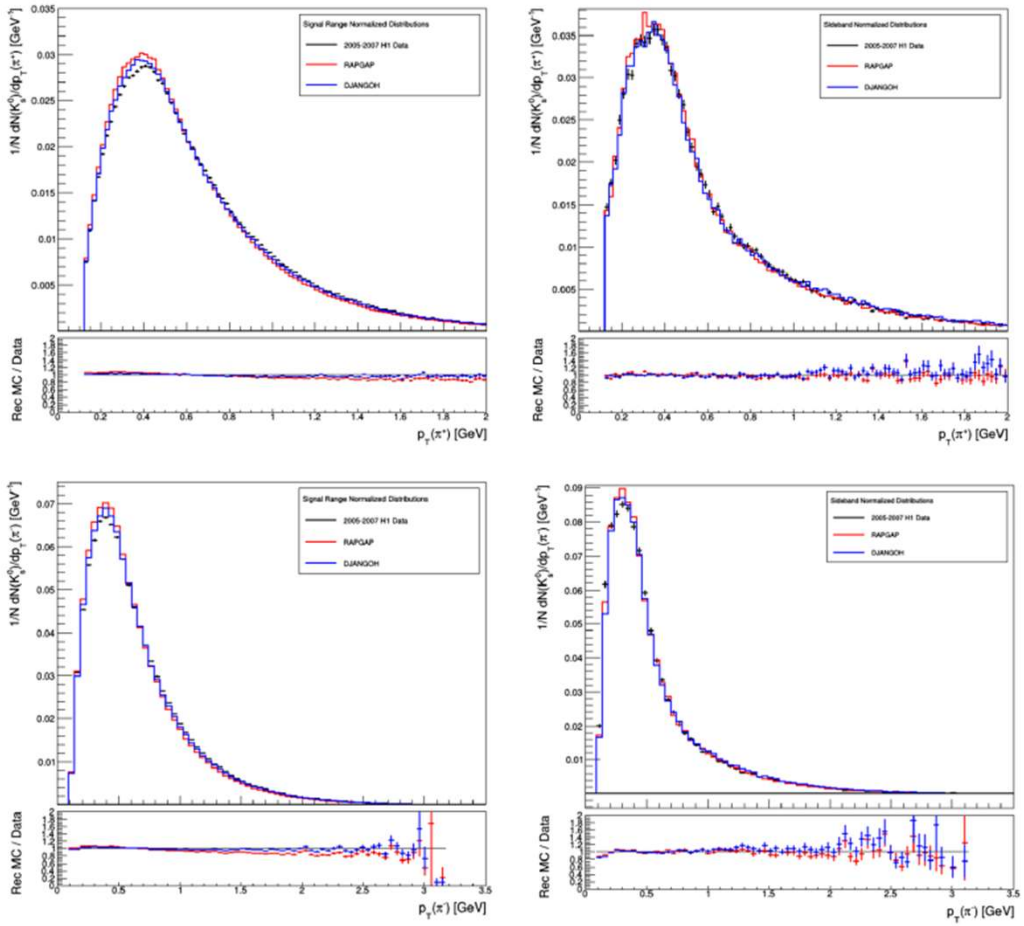

Figure 5.49: Normalized positive pion track p_T (top) and negative pion track p_T (bottom) distributions of K_s^0 candidates in the signal (left) and sideband (right) ranges for Data and MC. These are the distributions following the DIS event selections and all selective cuts.

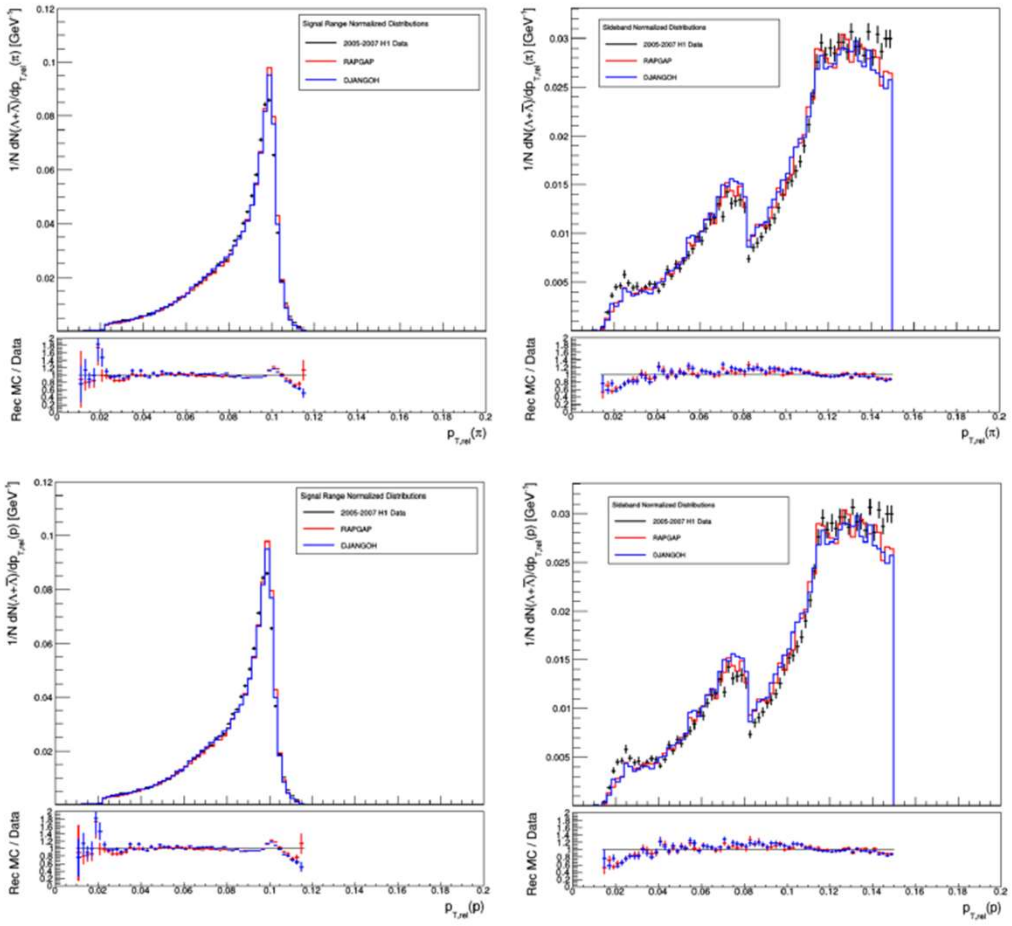

Figure 5.50: Normalized pion track $p_{T,rel}$ (top) and proton track $p_{T,rel}$ (bottom) distributions of $\Lambda + \bar{\Lambda}$ candidates in the signal (left) and sideband (right) ranges for Data and MC. These are the distributions following the DIS event selections and all selective cuts.

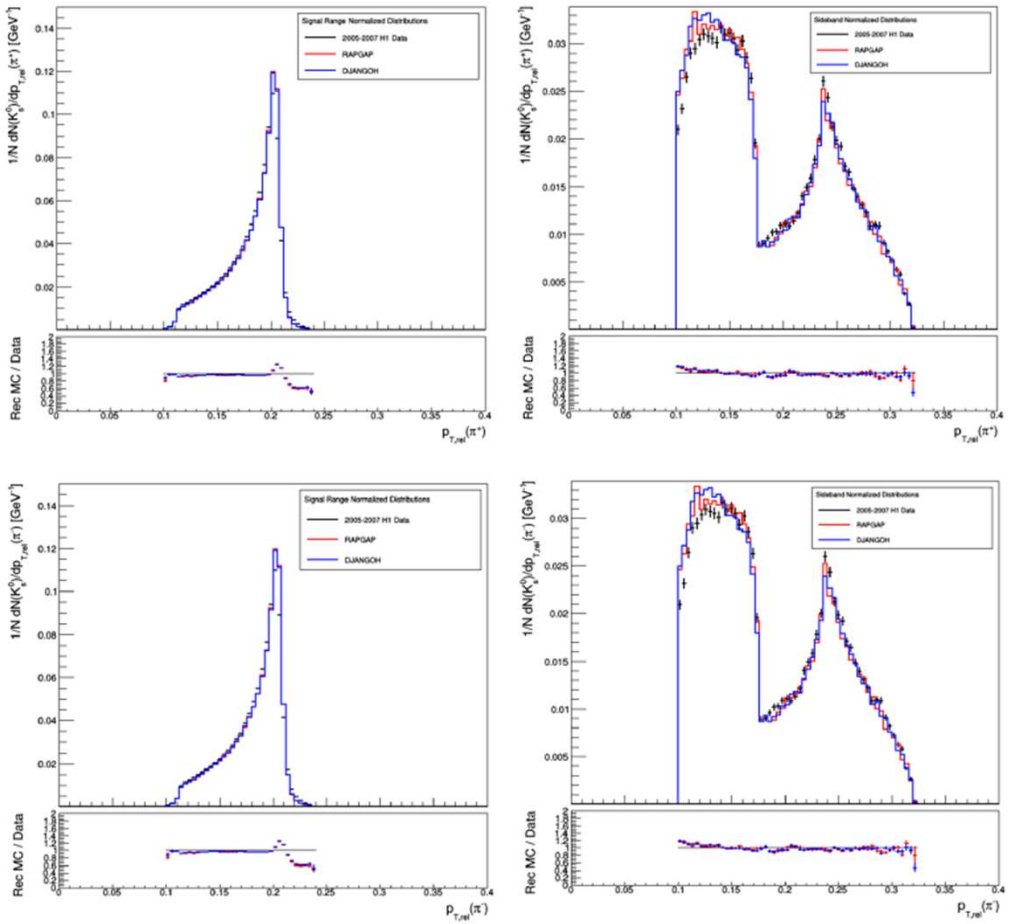

Figure 5.51: Normalized positive pion track $p_{T,rel}$ (top) and negative pion track $p_{T,rel}$ (bottom) distributions of K_s^0 candidates in the signal (left) and sideband (right) ranges for Data and MC. These are the distributions following the DIS event selections and all selective cuts.

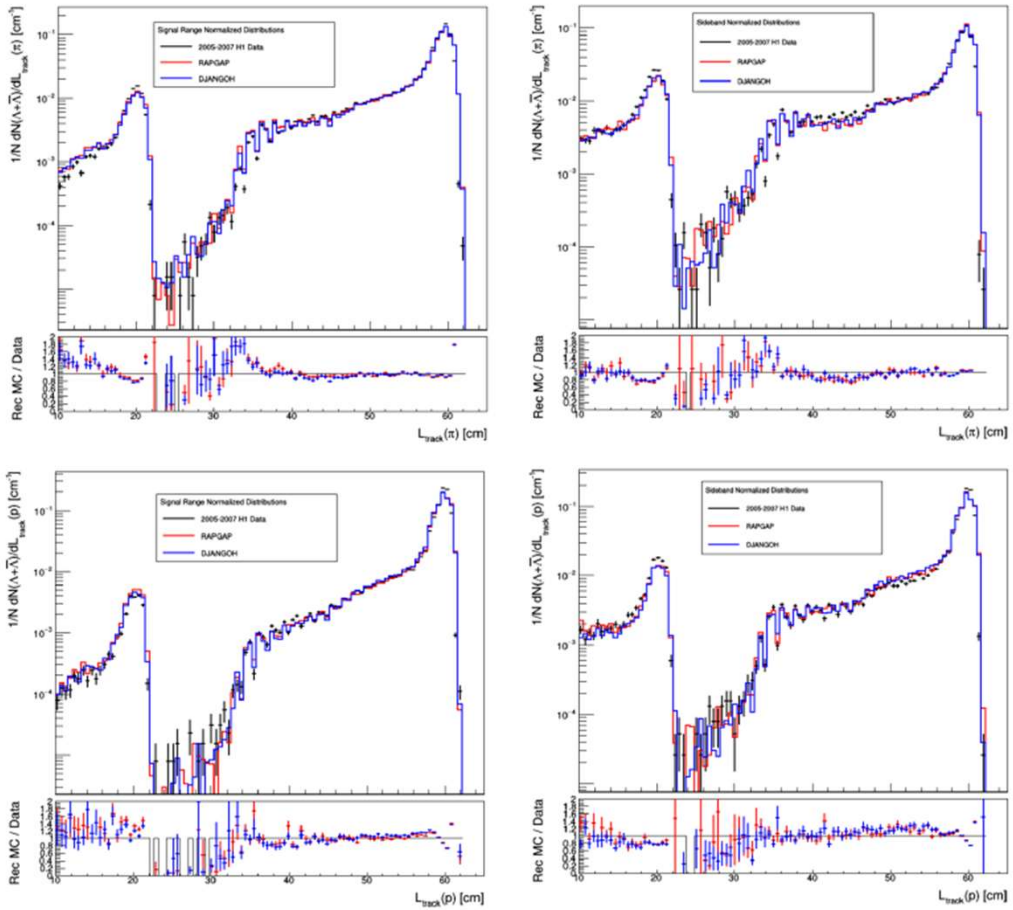

Figure 5.52: Normalized pion track length (top) and proton track length (bottom) distributions of $\Lambda + \bar{\Lambda}$ candidates in the signal (left) and sideband (right) ranges for Data and MC. These are the distributions following the DIS event selections and all selective cuts.

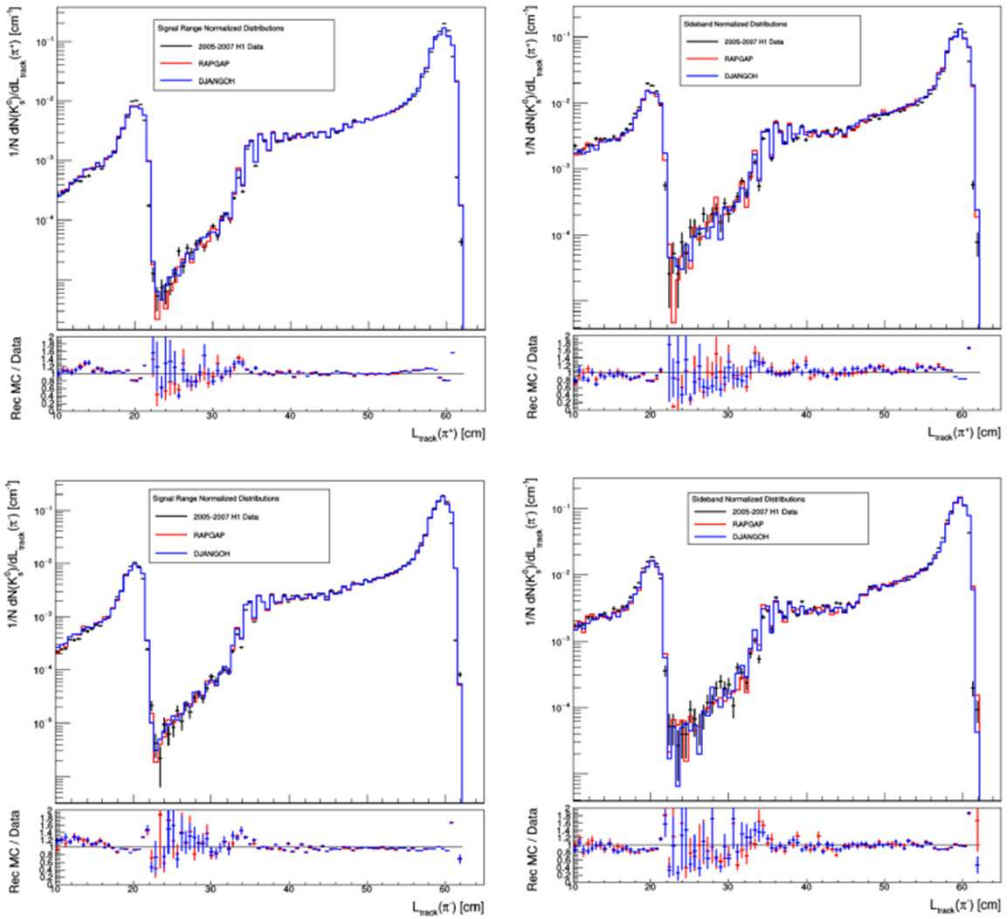

Figure 5.53: Normalized positive pion track length (top) and negative pion track length (bottom) distributions of K_s^0 candidates in the signal (left) and sideband (right) ranges for Data and MC. These are the distributions following the DIS event selections and all selective cuts.

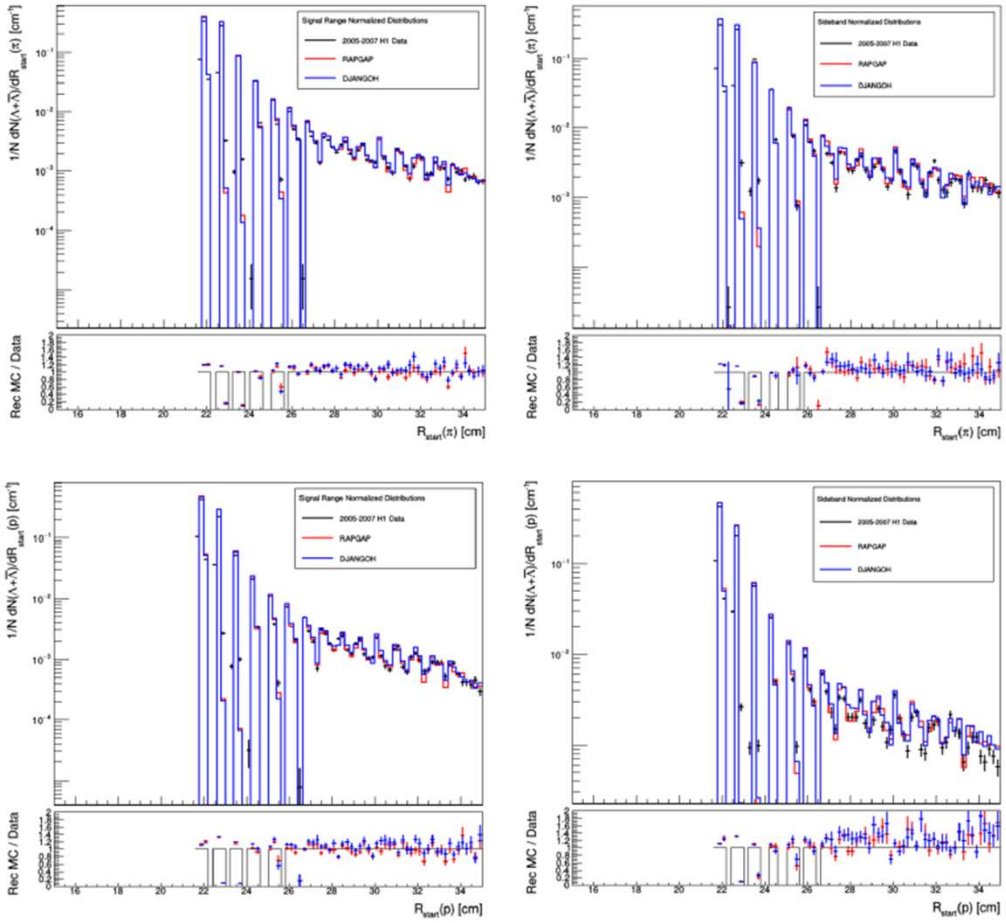

Figure 5.54: Normalized pion track start radius (top) and proton track start radius (bottom) distributions of $\Lambda + \bar{\Lambda}$ candidates in the signal (left) and sideband (right) ranges for Data and MC. These are the distributions following the DIS event selections and all selective cuts.

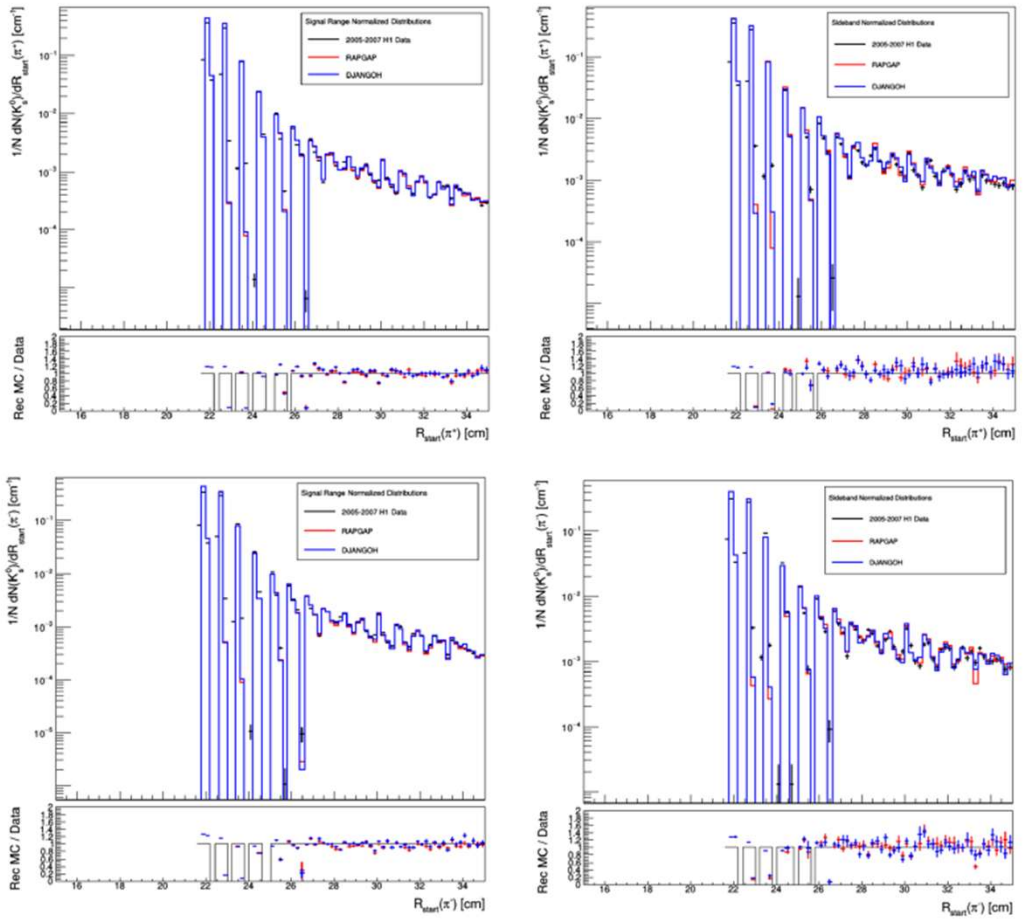

Figure 5.55: Normalized positive pion track start radius (top) and negative pion track start radius (bottom) distributions of K_s^0 candidates in the signal (left) and sideband (right) ranges for Data and MC. These are the distributions following the DIS event selections and all selective cuts.

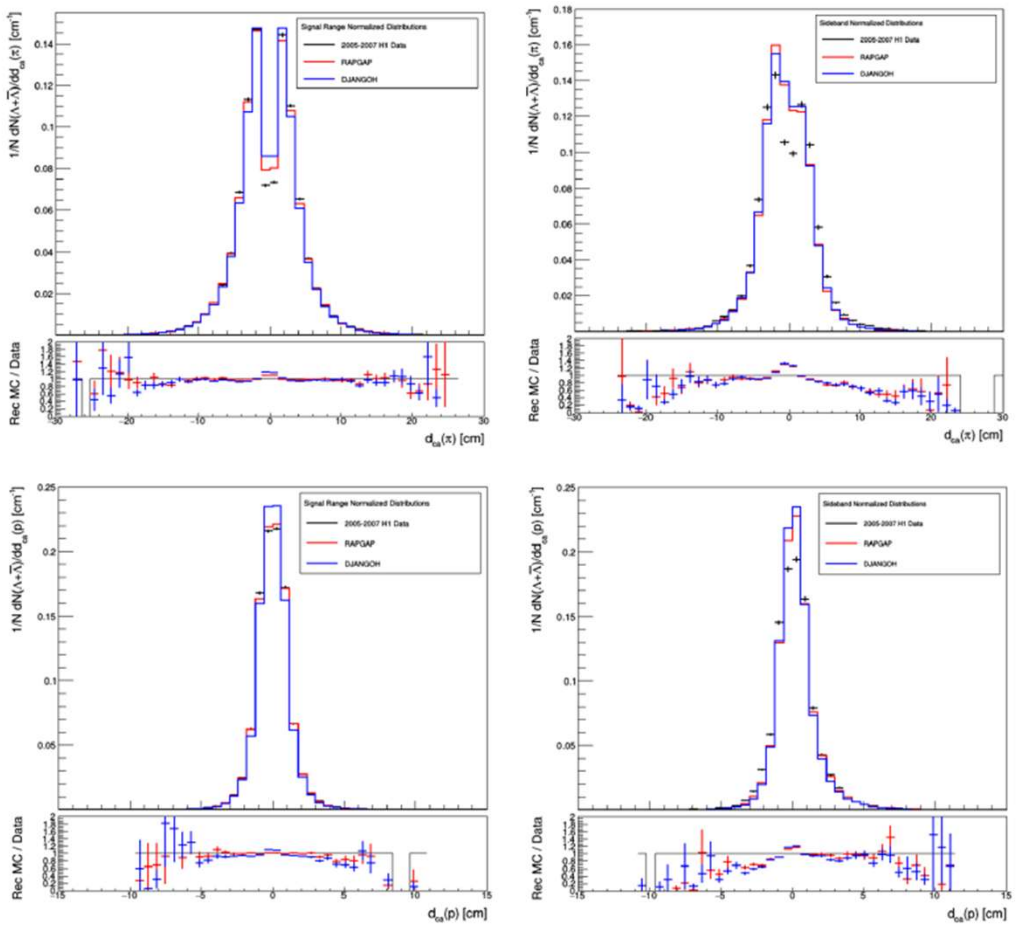

Figure 5.56: Normalized pion track distance of closest approach (top) and proton track distance of closest approach (bottom) distributions of $\Lambda + \bar{\Lambda}$ candidates in the signal (left) and sideband (right) ranges for Data and MC. These are the distributions following the DIS event selections and all selective cuts.

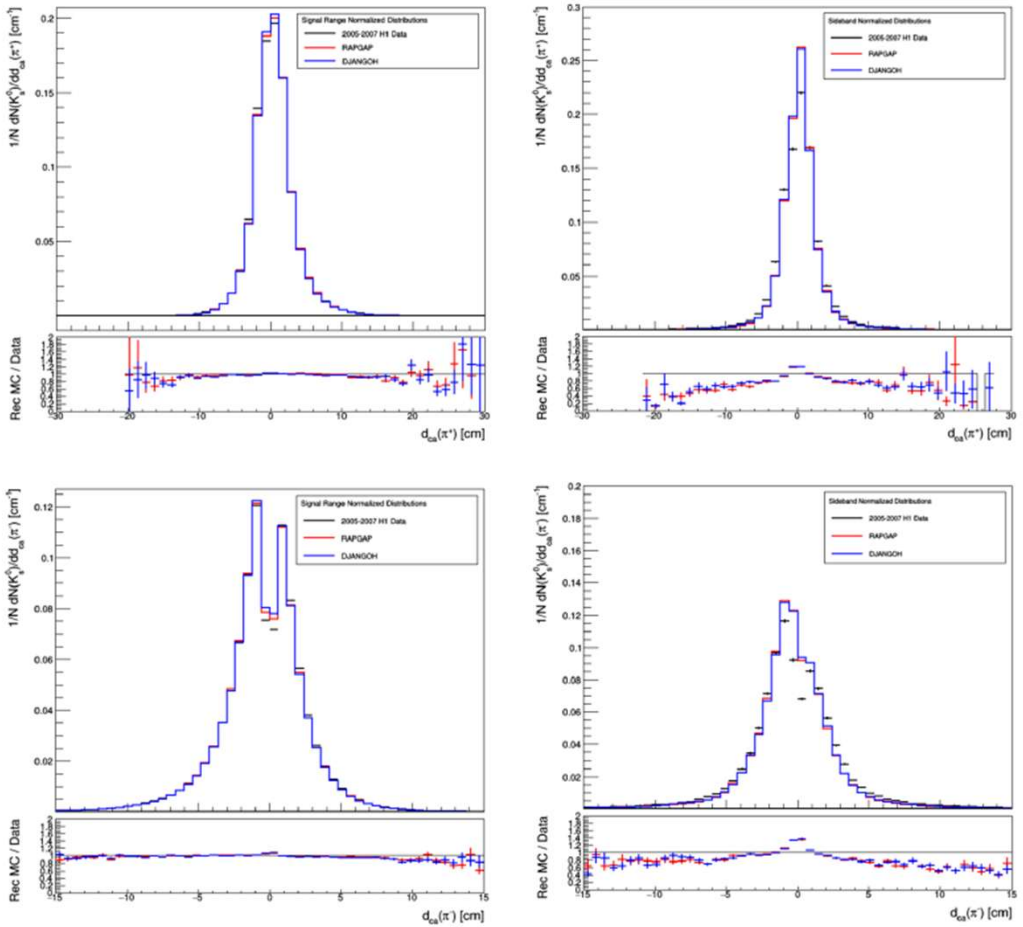

Figure 5.57: Normalized positive pion track distance of closest approach (top) and negative pion track distance of closest approach (bottom) distributions of K_s^0 candidates in the signal (left) and sideband (right) ranges for Data and MC. These are the distributions following the DIS event selections and all selective cuts.

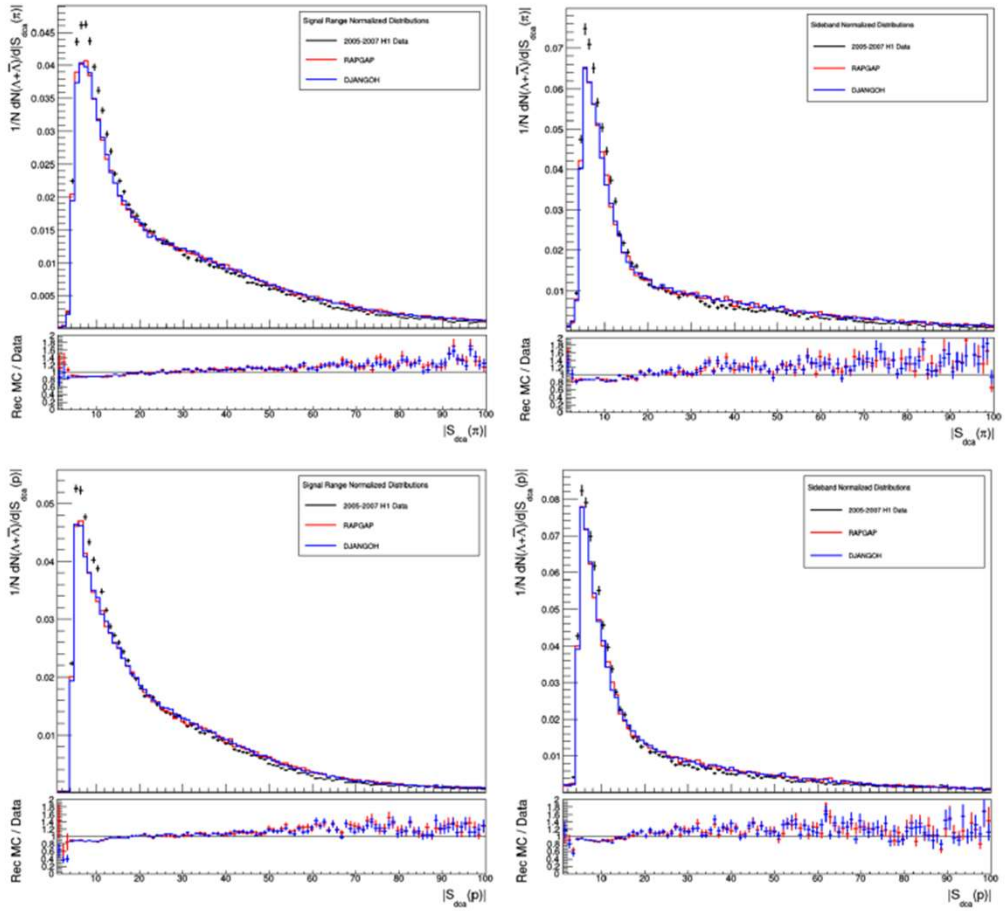

Figure 5.58: Normalized pion track distance of closest approach significance (top) and proton track distance of closest approach (bottom) distributions of $\Lambda + \bar{\Lambda}$ candidates in the signal (left) and sideband (right) ranges for Data and MC. These are the distributions following the DIS event selections and all selective cuts.

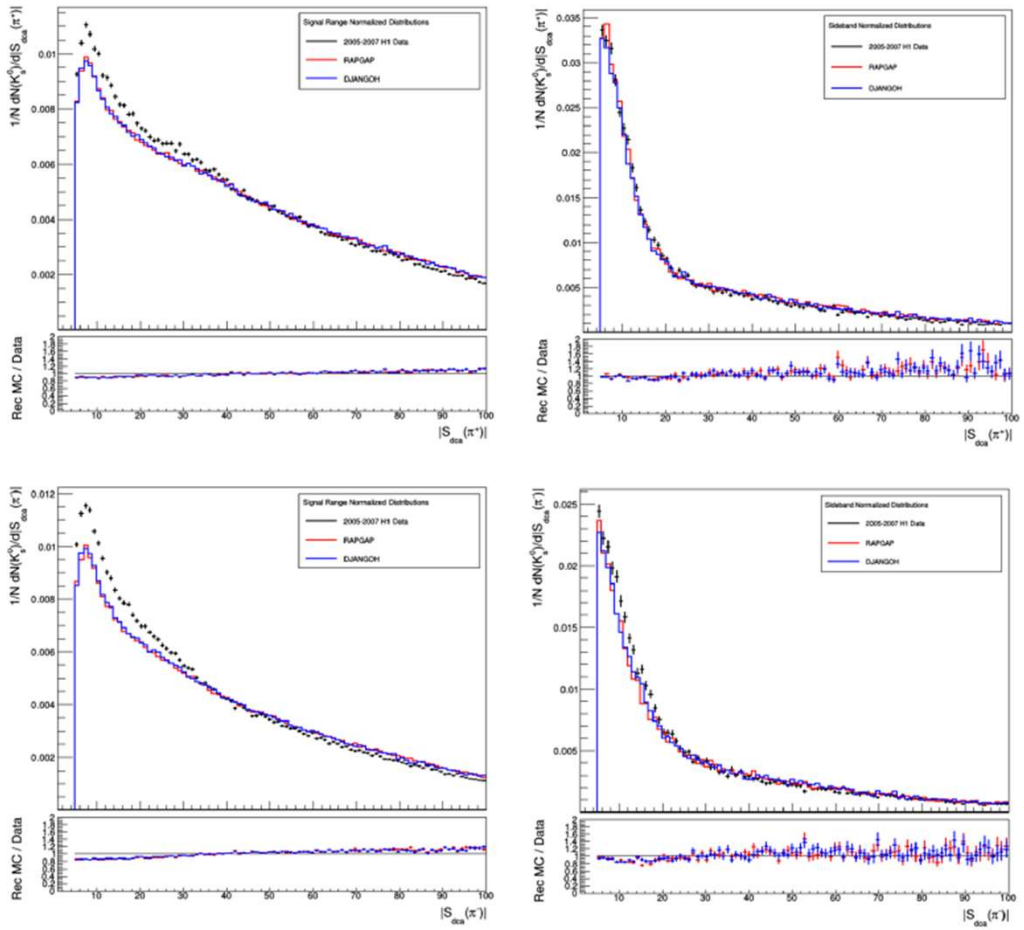

Figure 5.59: Normalized positive pion track distance of closest approach significance (top) and negative pion track distance of closest approach (bottom) distributions of K_s^0 candidates in the signal (left) and sideband (right) ranges for Data and MC. These are the distributions following the DIS event selections and all selective cuts.

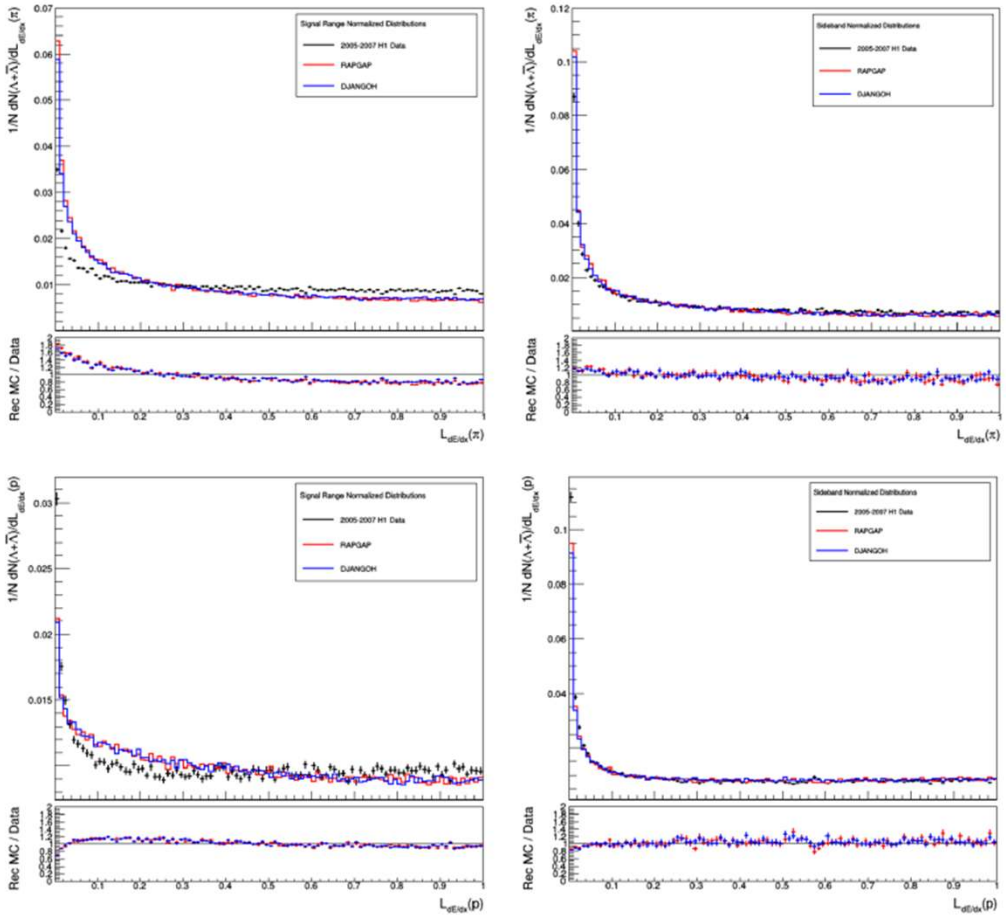

Figure 5.60: Normalized pion track dE/dx likelihood (top) and proton track dE/dx likelihood (bottom) distributions of $\Lambda + \bar{\Lambda}$ candidates in the signal (left) and sideband (right) ranges for Data and MC. These are the distributions following the DIS event selections and all selective cuts.

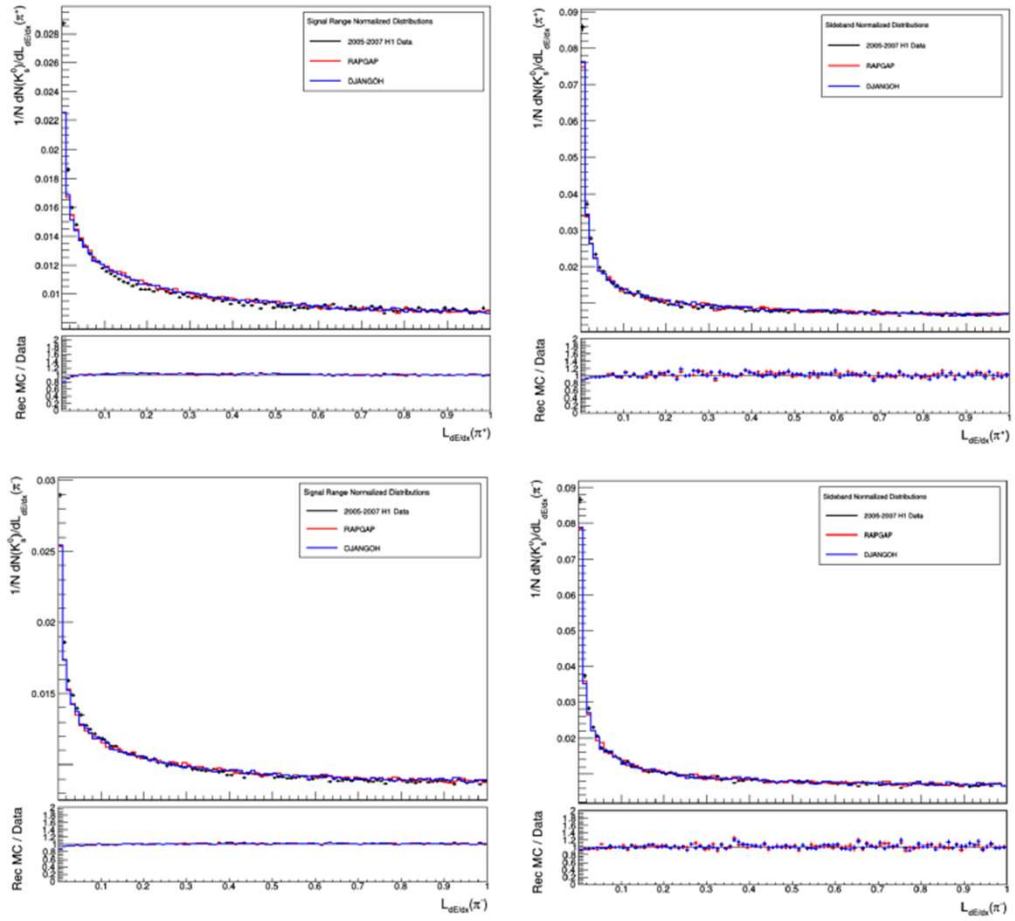

Figure 5.61: Normalized positive pion track dE/dx likelihood (top) and negative pion track dE/dx likelihood (bottom) distributions of K_s^0 candidates in the signal (left) and sideband (right) ranges for Data and MC. These are the distributions following the DIS event selections and all selective cuts.

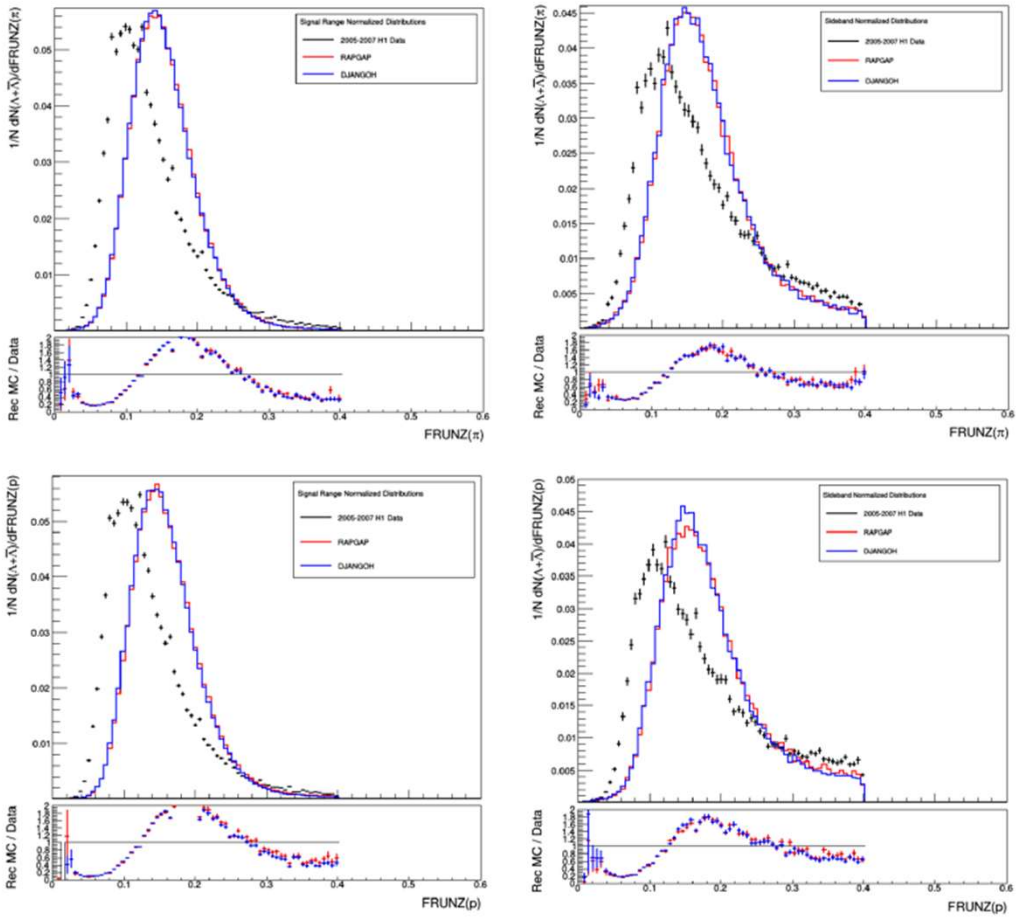

Figure 5.62: Normalized pion track fraction of rejected z hits (top) and proton track fraction of rejected z hits (bottom) distributions of $\Lambda + \bar{\Lambda}$ candidates in the signal (left) and sideband (right) ranges for Data and MC. These are the distributions following the DIS event selections and all selective cuts.

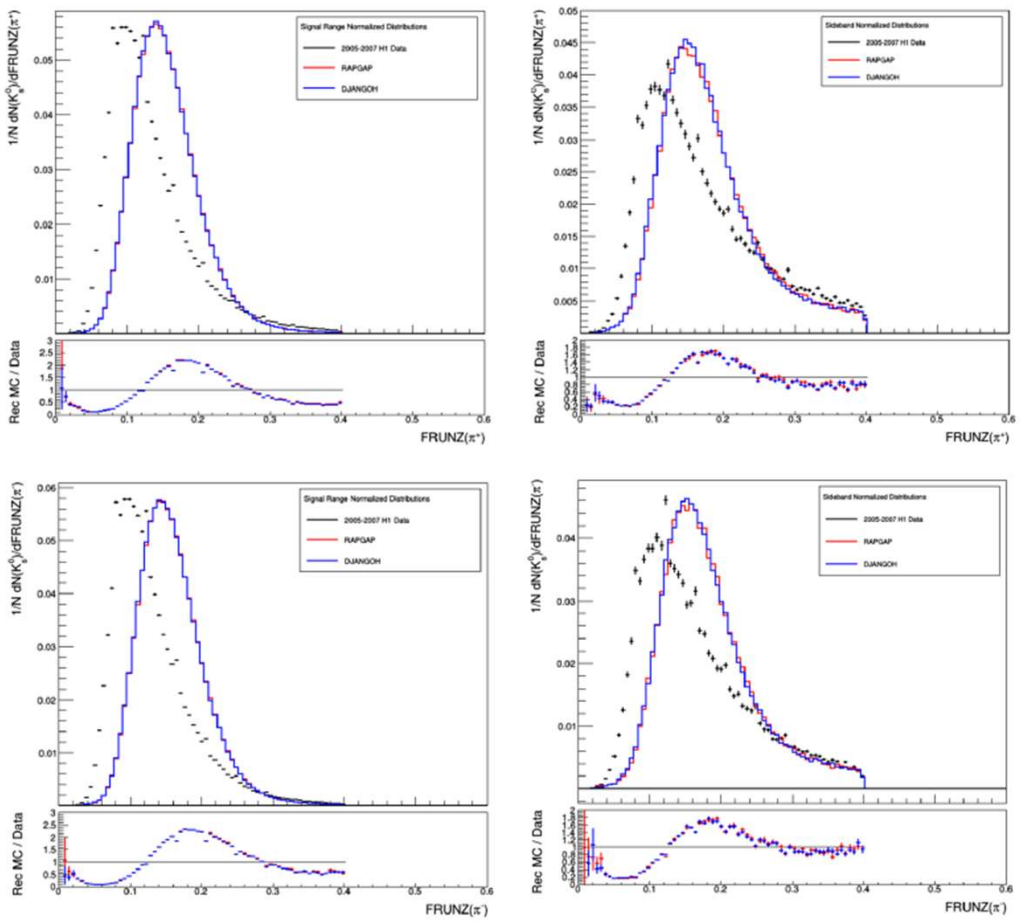

Figure 5.63: Normalized positive pion track fraction of rejected z hits (top) and negative pion track fraction of rejected z hits (bottom) distributions of K_s^0 candidates in the signal (left) and sideband (right) ranges for Data and MC. These are the distributions following the DIS event selections and all selective cuts.

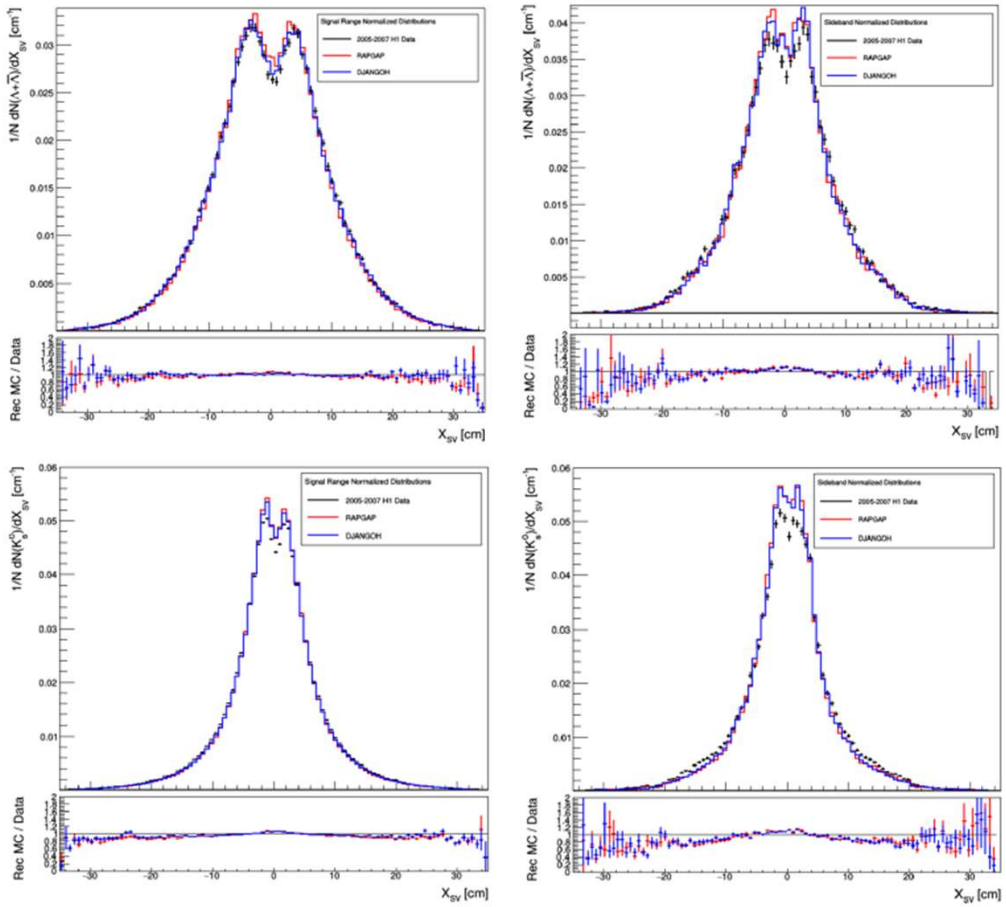

Figure 5.64: Normalized x secondary decay vertex position distributions of $\Lambda + \bar{\Lambda}$ (top) and K_s^0 (bottom) candidates in the signal (left) and sideband (right) ranges for Data and MC. These are the distributions following the DIS event selections and all selective cuts.

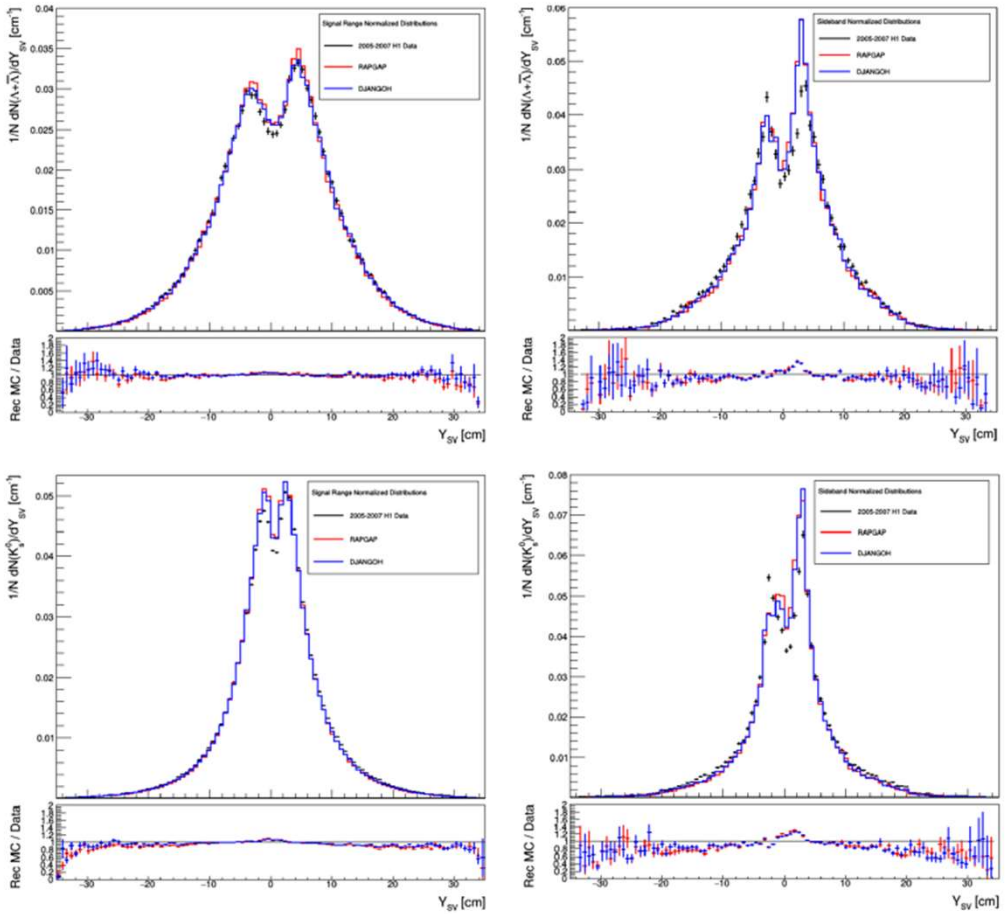

Figure 5.65: Normalized y secondary decay vertex position distributions of $\Lambda + \bar{\Lambda}$ (top) and K_s^0 (bottom) candidates in the signal (left) and sideband (right) ranges for Data and MC. These are the distributions following the DIS event selections and all selective cuts.

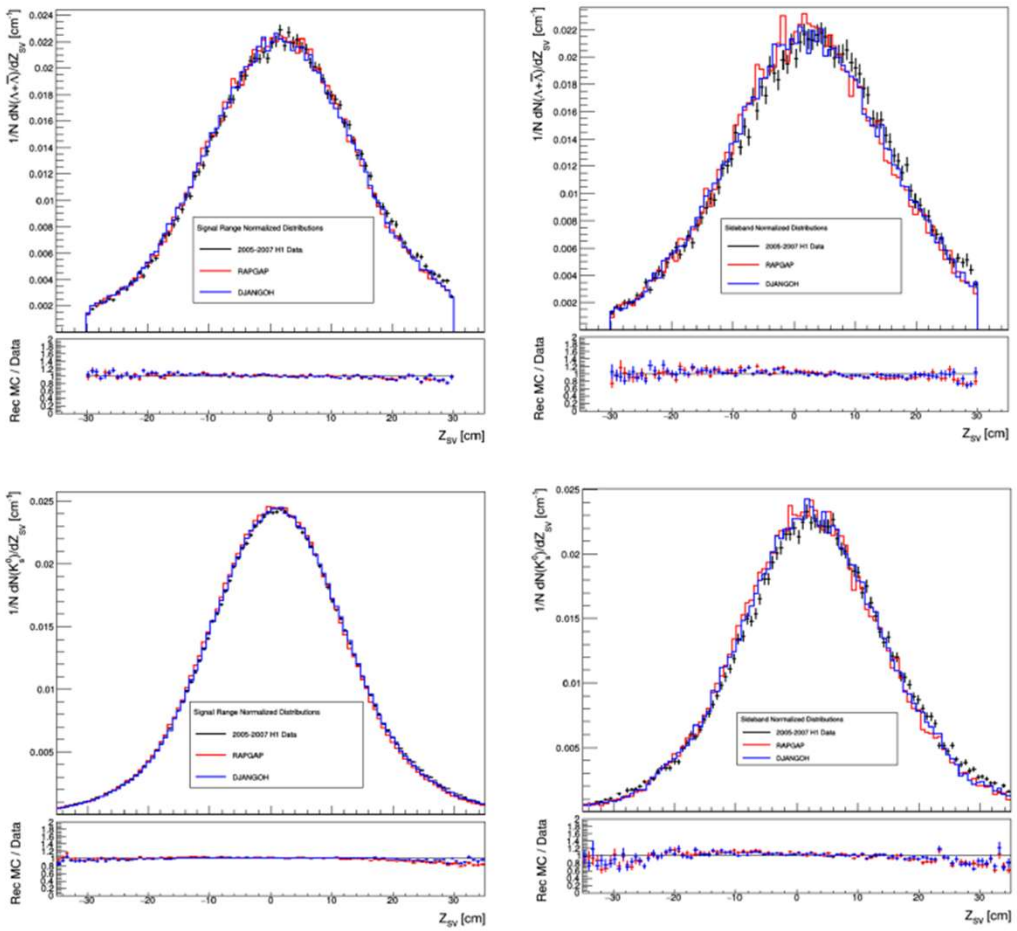

Figure 5.66: Normalized z secondary decay vertex position distributions of $\Lambda + \bar{\Lambda}$ (top) and K_s^0 (bottom) candidates in the signal (left) and sideband (right) ranges for Data and MC. These are the distributions following the DIS event selections and all selective cuts.

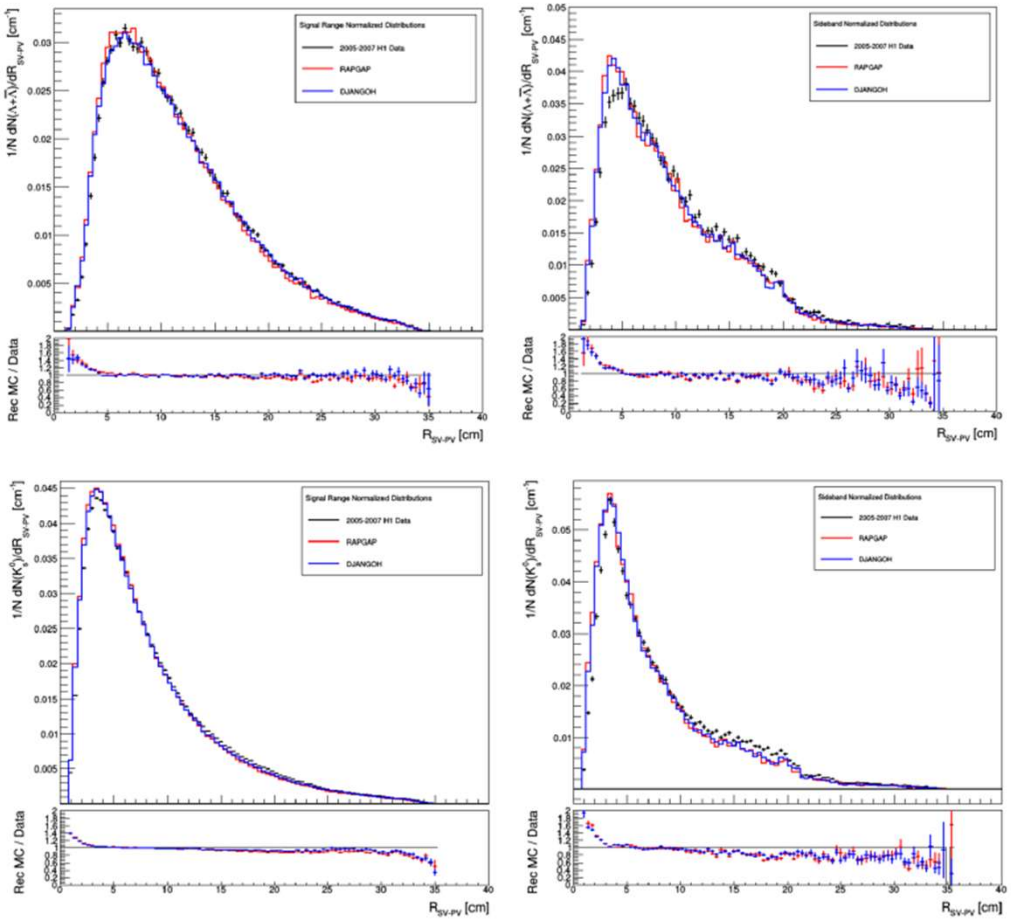

Figure 5.67: Normalized distributions of the radial distance between the primary DIS vertex and secondary decay vertex of $\Lambda+\bar{\Lambda}$ (top) and K_s^0 (bottom) candidates in the signal (left) and sideband (right) ranges for Data and MC. These are the distributions following the DIS event selections and all selective cuts.